Shape and size optimization of a wind turbine transport structure

Structural optimization with a compliant ship foundation

MT54035: Masters Thesis

F.A. Boer

Delft University of Technology

TU Delft

Shape and size optimization of a wind turbine transport structure

Structural optimization with a compliant ship foundation

by

F.A. Boer

to obtain the degree of Master of Science
at the Delft University of Technology,
to be defended publicly on Monday November 7, 2022 at 16:15.

Document number:	MT.22/23.010.M	
Student number:	4721470	
Project duration:	November 25, 2021 – November 7, 2022	
Thesis committee:	Dr. C.L. Walters,	TU Delft, supervisor
	Prof. dr. ir. A. van Keulen,	TU Delft
	Dr. ir. J.H. den Besten	TU Delft
Daily supervisors:	Ir. W.K. van der Leeden,	Vuyk Engineering
	Ir. H.W. Vuijk,	Vuyk Engineering

Image source frontpage: iStock/janssenkruseproductions [29]

TU Delft

Preface

This thesis is written as a final part of the master Maritime Technology at Delft University of Technology. It is carried out at Vuyk Engineering Rotterdam.

I want to thank Willem van der Leeden and Wouter Vuijk for helping me by guiding the research with their experience in shipbuilding and optimization. Also their support in solving the problems in Ansys was very helpful. I also would like to thank Carey Walters for sharing his view on the research perspective and for giving detailed comments on the reports. Also the extensive knowledge of optimization of Fred van Keulen supported me by setting up the optimization and by getting a better understanding of the many aspects of an optimization problem. I also want to thank Henk den Besten for taking place in the graduation committee and for sharing his view on this thesis.

Last, but certainly not least, I want to thank my parents for mentally supporting me in the tough moments during this thesis. They helped me to keep the right perspective. Also my friends helped me to take a step back after a week of hard work.

F.A. Boer
Delft, November 2022

Summary

Due to the growing quest for renewable energy, wind turbines grow in size. This means that higher demands are posed on the transporting structures, also called tower grillages, which brings its challenges for their design. The fact that the structures considered in this thesis are placed on a ship makes the design even more complicated. Therefore, a procedure is developed in this thesis that is able to optimize a tower grillage, while keeping the underlying ship intact. This tool is based on a combination of size and shape optimization.

The optimization is performed with the dual annealing algorithm. The objective is mass reduction, with the stress in the grillage, and stress and buckling in the ship as constraints. These constraints are taken into account by a penalty function. The design variables are the angles at which the radial supports attach and the thicknesses of the radial supports and the other elements of the grillage. The main question that is answered in this thesis is how this optimization procedure can help in the design of a tower grillage, where the underlying ship structure is implemented as a boundary condition.

First, a single layout is optimized with the ship modelled as a rigid boundary condition. Next, a model of a section of the ship is made and used as the boundary condition on the tower grillage. A comparison between these models showed that the main differences in stress between the two optimization results are seen in the largest parts of the grillage: the sides, the flanges and the can. The maximum stress in the latter two elements is larger, which also results in larger thicknesses in the optimization with the ship. This affects the average mass in the ship, which is increased with 5.7% when compared to the grillage on the rigid constraint.

After that, a full grillage is optimized. A first attempt demonstrated that the stress in the ship could only be decreased a little with the initial settings of the optimization. That required a slightly different model, to make sure that the stress in the ship remains acceptable. With that model, a mass decrease of 32 tons could be obtained, which is a decrease of 9.1 % compared to the original design by Vuyk Engineering.

From the different optimization steps became clear that the main factors influencing the optimal distribution of radial supports are the lengths of the supports, and the location of the outer brackets. The compliance of the ship changes the stresses in the grillage, and therefore the optimization result. The stress in the ship can be reduced only to some extent, so the effect of a stress violation in the initial design is that a new bracket design needs to be made. The results show that the stress is governing for the current optimization, and buckling is not.

The conclusion is that the current procedure can help in the design by providing a global image of lighter layouts which avoid stress and buckling constraint violations in the ship. However, the limitation of the research is that the result is only a global image. It is therefore considered not worth the effort and time to apply the current method in an engineering environment. It does however show the potential of this method, so future enhancements can make the procedure suitable for engineering.

Contents

1

Introduction

Offshore wind has gained a lot of attention over the past years due to the quest for renewable energy sources. Many developments in this area have taken place in recent years, which increased the economical attractiveness of the turbines. As a result, new offshore wind farms are installed, and even more will be installed in the near future. Ships play a vital role in the installation of these wind farms, both for transporting and the installation of the turbines and their foundations. An example of an installation and transportation ship is shown at the front page. What stands out in this image is that the towers are mounted vertically instead of horizontally. Benefits of transporting the towers vertically are reducing installation time and using the deck space more efficiently. The downside is that much larger forces are exerted on the ship due to the higher accelerations on the towers.

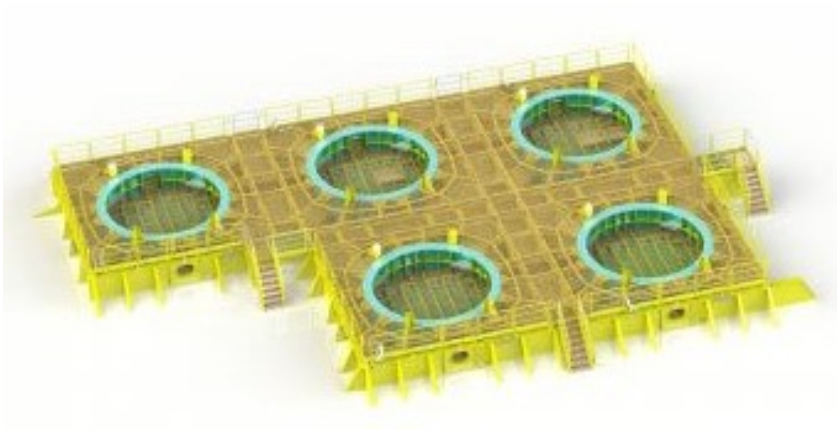

Figure 1.1: Example of a tower grillage [21]. These structures are used on a ship to transport wind turbine towers. A similar structure will be optimized in this thesis.

A special structure is needed to transport these towers vertically, which is called a tower grillage. An example is shown in Figure 1.1. Most often, several of these structures are designed over the lifetime of a ship. The first cause is that the tower diameters differ per project due to different sizes per manufacturer, but also due to the increase in turbine capacity over the years. The other cause is the high load on these grillages due to the vertical transport of the towers. This results in a much shorter fatigue life, and they need therefore to be replaced after some years.

The design of these grillages involves several challenges when they are designed for an existing ship. The tower grillage needs to transfer its loads in such a manner that the ship remains intact. Often several iterations are required before the design is accepted. This problem is also encountered by Vuyk Engineering, and they want to find a better and faster way of designing these grillages. This led to this thesis, which aims at developing an algorithm that can be applied in the design of a tower grillage. This should give more insight into the best way of connecting the tower grillage to the ship structure with accounting for the weak parts in the ship. The algorithm will be based on structural

optimization techniques. These techniques are an active research field because it allows people to gain new insight into the parameters in the design, which helps them by building better and often also lighter structures. Before the computer era, only relatively simple optimization problems could be solved by hand, which was often not useful in engineering practice. Currently, computers are available to everyone, and their power keeps increasing, allowing companies to optimize larger problems within a reasonable timeframe.

1.1. Structure definition

A schematic view of a tower grillage is shown in Figure 1.2. The 'can' in the middle of the grillage is a circular structure on top of which the tower is bolted. The load from the tower is transferred via the can and the radial supports to the ship. The brackets are placed on both sides of the surrounding plate of the grillage, and they are used to distribute a part of the load from the outer plate to the ship structure. The plates on top and at the bottom of the grillage serve as flanges for the radial supports to make them more similar to I-beams, and thus increase their stiffness.

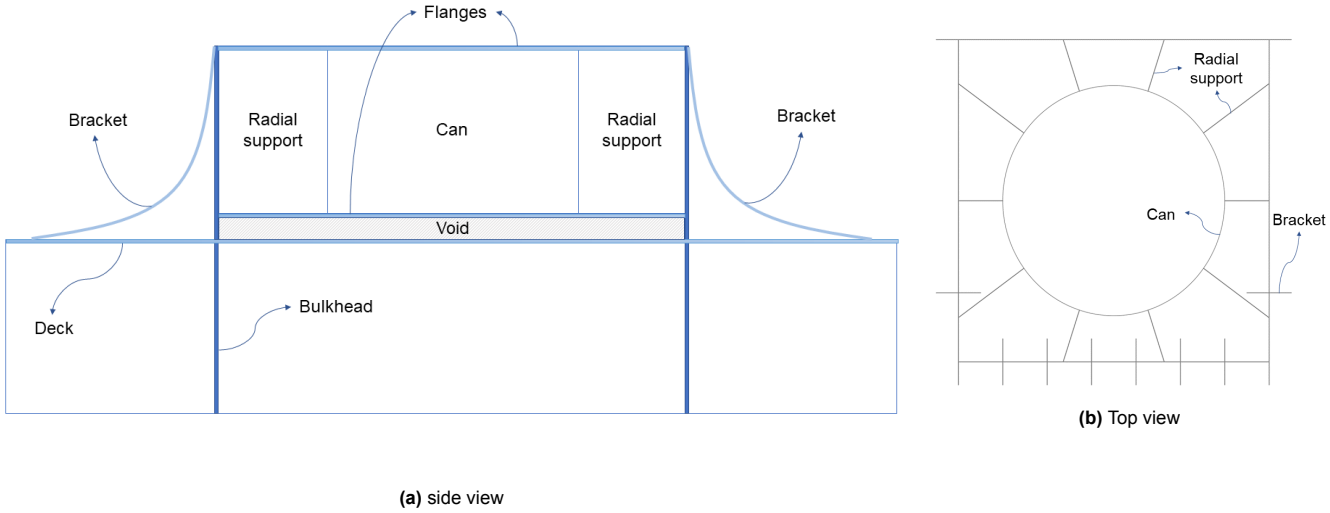

(a) side view

(b) Top view

Figure 1.2: Schematic representation of a single layout in a tower grillage with the names and locations for the relevant structural members. A real tower grillage often consists of multiple layouts, as shown in Figure 1.1

Figure 1.2a shows that the structure is free from the deck, which means that the can is only supported by the radial supports and the flanges. This is necessary since the deck is not strong enough to withstand the applied loads. Another reason is that high peak stresses will occur at the locations where the circular can and the (linear) stiffeners under the deck intersect, resulting in failure of the stiffeners. These problems are avoided by transferring the loads to the stronger parts of the ship, like bulkheads.

1.2. Problem description

As mentioned before, the biggest challenge in the design of tower grillages is that it needs to be connected to an existing ship. It is often assumed in standard design practice that the boundaries cannot fail. This assumption does however not hold for a tower grillage, because the boundaries are described by the ship, which can fail due to the loads exerted from a tower grillage. That means that yielding and buckling failure in the ship structure also need to be considered, instead of only failure in the tower grillage itself.

The easiest solution seems to be strengthen the ship structure, but that is not the case. It is inefficient and costly to stiffen an existing ship structure because of other components under the deck, such as cables, tanks and equipment. Welding in the ship should therefore be avoided as much as possible. It is in some cases inevitable because the loads are too large to handle, but still the amount of work should be limited.

The loads on a tower grillage are different from most other stiffened structures. The most important loads are the moments induced by the ship motions, but the shear force from the weight also plays a role. Loads often considered in literature are in-plane and lateral distributed loads which gives a structure like a stiffened panel. For the radial supports in a tower grillage however, the most important loads are moments and shear forces and another type of stiffening needs used.

To properly transfer the load from the tower grillage to the ship structure, the tower grillage is generally connected to bulkheads and web frames. The bulkheads are mainly stiffened panels, and they are therefore sensitive to buckling. On top of that, several holes are cut in these bulkheads, which decrease their strength. These can be quite large, like funnel holes, and they therefore result in a significant decrease in stiffness.

How the loads are transferred to the ship mainly depends on the locations, the amount, and the size of brackets and radial supports. The latter ones are the main focus in this thesis. The distribution and size of these items will be optimized for a given ship using a computer program. Manufacturability aspects, such as accessibility and weldability, should also be taken into account. A welder should for instance be able to weld a structure, which is not possible if the optimizer comes up with a result where two brackets are very close to each other.

1.3. Significance

From the literature research became clear that available research mainly focuses on stiffened plates, and the underlying structure is not taken into account. This thesis differs from that, because the tower grillage is optimized while taking the underlying structure into account. Most often, the connection of the optimized structure to the outer world is assumed to be infinitely strong. So the results in the thesis are not only useful for a tower grillage, but also for other structures which are placed on a non-rigid base. Another difference is that the considered type of stiffening is different from most other stiffened structures, as explained in Section 1.1. Analyzing these structures will give more insight into stiffening in radial direction.

The number of offshore wind farms is still growing, so tower grillages will remain important in the future. Because the demands on these structures will increase, it is important to find an improved way of designing these structures. This research is now focused on a tower grillage, but it can also be extended to be useful for other structures. The application of the theory to a real-world example will show the potential for further developments in the (shipbuilding) industry.

1.4. Research question

As explained in the previous sections, there is a desire for an algorithm that is able to find an optimized layout for a tower grillage with a compliant ship below it. This research will address this problem, and will give at the same time more insight into optimization with external constraints. The problem and the study that need to be conducted are summarized in the following research question:

How can the combination of size and shape optimization help in the design of a tower grillage where buckling and stresses in the underlying compliant ship structure are implemented as constraints?

When answering this question, manufacturability of the design should be taken into account, and the design should be analysed for multiple loading conditions. To answer the research question, 3 subquestions are defined:

1. *What determines the optimal distribution of the radial supports in the grillage?*
2. *How does the behaviour of the underlying ship structure influence the optimization result?*
3. *How does the result compare to an initial manual design considering mass and stresses?*

These questions will be answered in three different substeps, with increasing complexity. These steps will be explained in more detail in Chapter 4.

2

Literature review

This chapter will give an introduction to the relevant literature for the thesis. First, different structural optimization techniques are discussed in Section 2.1. The different loads on a tower grillage are taken into account by using different load cases. Relevant research for including that into an optimization is presented in Section 2.2. Methods to implement and check constraints on the ship and grillage are described in Section 2.3. Then, an overview of optimization algorithms is given in Section 2.4. Lastly, a more in-depth study in the chosen algorithm is presented in Section 2.5.

The general mathematical form of an optimization problem is expressed as:

$$\begin{aligned} & \min f(\mathbf{x}) \\ \text{subject to:} \quad & g(\mathbf{x}) \leq 0 \\ & h(\mathbf{x}) = 0 \end{aligned} \tag{2.1}$$

This equation means that objective function $f(\mathbf{x})$ is minimized with respect to the design variables $\mathbf{x}$. The function $g(\mathbf{x})$ is generally used to express an inequality constraint, so the value of the function should be smaller than or equal to the specified value. The other function $h(\mathbf{x})$ is an equality constraint, so this function is only allowed to take the required value. Equation 2.1 is only a general form, so the actual form differs per problem. It is possible to have multiple objective functions, and also to have a different number of constraints.

2.1. Structural optimization techniques

Structural optimization techniques are often used to improve certain aspects of the structure, such as the stiffness, weight or the eigenfrequencies. Before the computer era, problems could only be solved by hand with a mathematical formulation. That means that only relatively simple and academic structures could be optimized in practice. An example of such an early paper is the work of Michell [48]. Most realistic structures consist of a lot of different elements, and it is therefore not possible to solve them by hand in a reasonable amount of time. Because the availability of computational power is increasing, structural optimization has become available for more complicated problems. It allows researchers and designers to obtain better insight in structures, and thus enhance their designs. It is therefore a popular research area and many advances are made in recent years.

Structural optimization techniques are generally divided into three types: size, shape, and topology optimization, as shown in Figure 2.1. This division is made based on the type of design variables in the optimization. The choice of these design variables influences also the form of the optimization result. A structural optimization technique does however not solve the defined problem itself, it is only a description of the problem and design variables. For the actual solution, an optimization algorithm is needed, which will be described in Section 2.4.

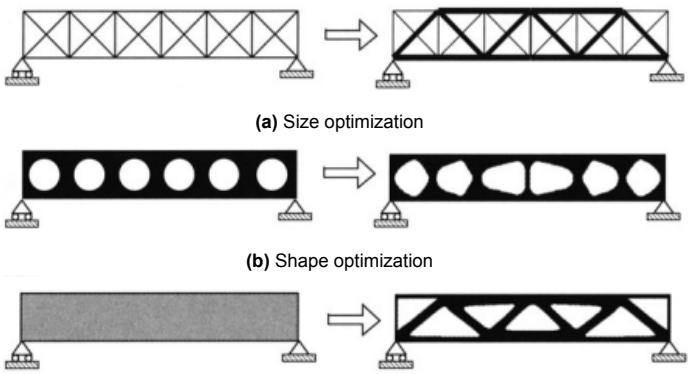

(a) Size optimization

(b) Shape optimization

(c) Topology optimization

Figure 2.1: Different optimization techniques that can be used in structural optimization [6]. The design freedom and complexity increase from the top to the bottom.

Figure 2.1 shows that the design freedom increases from *a* to *c*. In Figure 2.1a, the geometry is already defined, and only the thickness of the different structural members is allowed to change. Figure 2.1b shows already more design freedom, but the shape is still quite constrained to the predefined structure. When looking at Figure 2.1c, a design space and boundary conditions are defined. During the optimization, any structure within these restrictions can be created. The disadvantage of the increasing design freedom is the increasing number of design variables. This generally leads to increased computing times. Also, increasing design freedom means in general more post-processing, because the resulting shapes are often less manufacturable.

2.1.1. Size optimization

The first optimization type in Figure 2.1a is size optimization. In this type only the dimensions of structural elements can be optimized, such as the thickness or the diameter. This means that only the cross-sections of the different elements are optimized, but the overall geometry remains the same. As a result, an initial design is required before the optimization could start. The most general objective for this type of optimization is minimizing the mass of the structure.

Some research is performed where only size optimization is used, but these applications are limited. Examples are optimizations in spatial structures such as trusses and cable-strut systems [36, 53]. Size optimization is often used in combination with the other two optimization techniques, either simultaneously [50] or as the last step in multilevel optimization [43, 64]. Simultaneous optimization leads to better results, because the design variables are not linearly independent, so they should be taken into account together [50].

This type of optimization is also used in the shipbuilding industry. In this field generally a combination with other optimization techniques such as layout or shape optimization is used (see for instance Refs. [45, 64]). Research in the maritime field for these combinations will be discussed in the next paragraphs.

2.1.2. Shape optimization

The second optimization type is shape optimization. For this type of optimization, like for size optimization, an initial design is needed. The difference is however that the geometry of the structure can also be changed within certain boundaries. Shape optimization is often used for two types of structures: solid structures and spatial structures, like trusses. The first type is shown in Figure 2.1b. In such an optimization, the surface of the design is discretized with nodes, which control the geometry of the design [32]. Examples of relevant structures are tools or bent plates. Examples for the optimization objectives are reducing peak stresses or optimizing flow characteristics [20, 47].

The second type of structures are the spatial structures, where the locations of the different nodes are to be optimized [31, 50]. This is often used in combination with size optimization, which is used to optimize the cross-section of the bars. Recent research in this field mainly consists of finding new and improved algorithms for the optimization of these trusses. The reader is referred to the review paper of Hare, Nutini, and Tesfamariam [26] and its references for an overview of research.

The combination of size and shape optimization is gaining interest in the shipbuilding industry. Size optimization is then used for the size of the stiffeners and shape optimization for the locations [61, 69]. In literature, this is also called layout optimization, but in this thesis, a distinction will be made between the two names. 'Size and shape optimization' will be used when the location of the stiffeners is allowed to change, like in the thesis of Vuijk [69] and 'layout optimization' will be used when possible locations of the stiffeners are predefined, like in the research of Sleesongsom and Bureerat [67]. Further elaboration about layout optimization will be given in the next section.

One of the first who applied a large scale size and shape optimization in the maritime world was Sekulski [64]. He optimized the layout and scantlings of a midship section of a catamaran. More recent research is done by Lin, Yang, and Guan [45] and Yang and Guan [75], who optimized turret scantlings for an FPSO. These papers are of particular interest for this thesis, because they also included a part of the surrounding structure in the optimization. They did however not account for the stresses in that structure but they only used the surrounding structure to account for the effects of global loads.

2.1.3. Topology optimization

The last optimization technique is topology optimization (TO). This optimization technique differs from the other two in the sense that the design space is not limited by a predefined structure, but only the boundaries of the design space are defined. The structural shape is therefore much less dependent on the input of the designer. The resulting designs from size and topology optimization in Figure 2.1 are quite similar, but the difference can be much larger for other structures.

The first one to formulate a TO problem was Michell in 1904 [48]. After that, very few papers were presented about the topic until Bendsøe and Kikuchi [5] presented their paper in 1988. From that moment, much research was done in the field of TO. During the development, different methods are developed to solve the optimization problem. Many of these methods are used to solve the density-based topology optimization problem. This problem starts with a full design space, and then redundant material is removed until the optimized condition is reached. Not all these methods will be discussed in this literature review, so the reader is referred to the review papers of Rozvany [58] and Sigmund and Maute [66].

Topology optimization has a large variety of applications. It is already studied extensively in the aerospace and automotive industry (see for instance Refs. [38, 43]), but it is not applied at a large scale yet in the maritime industry. The reason for this is that in the first two industries, the parts are much smaller, and therefore other manufacturing techniques like casting and additive manufacturing can be used. In shipbuilding however, most structures are large, and they consist of plates and stiffeners which need to be welded together. Therefore, the manufacturability aspect can be an issue in the maritime industry, especially when using density based topology optimization. Density based topology optimization is applied to optimize a transverse web frame [69, 81] and to find a stiffening pattern for a yacht [42]. The research in this area is however limited, which is expected to be a result of the manufacturability issues as mentioned before.

Another topology optimization method is the ground structure approach [17]. This method uses a predefined distribution of nodes in the design space. Between these nodes, connections are made, which are optimized by changing the thickness. That means that it is actually a size optimization problem, but with much more connections, and usually many of the connections disappear during the optimization. An example of such an optimization for a 2D structure is shown in Figure 2.2.

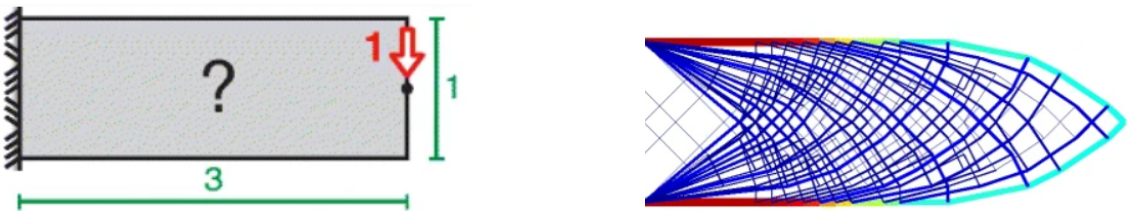

(a) Design definition **(b)** Solution

Figure 2.2: Design definition and result for the ground structure approach [78]. This approach predefines a ground structure of connections and optimizes the thicknesses of these connections.

This method often results in truss-like structures, as shown in Figure 2.2b [78, 79]. This figure shows that the results can be hard to interpret and manufacture. This method is therefore mainly used to give the designer some design intuition about the structural behaviour and load paths of the design. The results can be improved by using filtering techniques, but still the interpretation of the designer is needed [56, 60]. Issues can for instance be that the filtering removes too much connections, resulting in mechanisms in the final solution.

An application of the ground structure approach is layout optimization, which aims at optimizing the location of stiffeners on a panel. For layout optimization, again an initial ground structure of stiffeners is made, but it is defined such that it looks already like a stiffened panel. In that way, a better manufacturable stiffening pattern can be obtained [67, 77]. A recent improvement in layout optimization can be found in the paper of Bakker et al. [4]. They coupled layout optimization and density based topology optimization to optimize both the shape and the layout of the stiffeners. An application of layout optimization on a real ship structure can be found in the research of Liu et al., [46]. They first identified the best locations for the stiffeners. After that, the sizes of these stiffeners are optimized. The advantage of this method is that the location of the stiffeners is better defined.

A relatively new type of topology optimization is the method of Moving Morphable Components (MMC's), which can be called an 'adaptive ground structure approach' according to Guo, Zhang, and Zhong [25]. This method makes use of a set of predefined components (often bars) that can change their size and move through the design space to find the optimal structure. The basic idea is shown in Figure 2.3. A lot of developments are taking place in this field of topology optimization, such as the use of hollow components and the extension to 3D structures [3, 80]. The advantage of this method is that it allows designers to have more control over the design elements, while still keeping a large design freedom. Although the method seems promising for certain applications, no literature is found with applications outside the academic world, and it is therefore not considered further in this thesis.

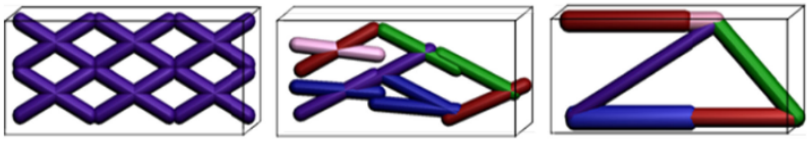

Figure 2.3: Basic idea of the method of Moving Morphable Components [80]. This method uses a number of predefined components that can change shape and location during the optimization process to form an optimized structure.

2.2. Optimizing for multiple load cases

On a real structure, such as a tower grillage, many different loads are exerted. These cannot be taken into account by applying a single load case, because the loads can act in opposite directions and in different combinations. For example, in a design of Vuyk Engineering, 96 load cases were examined. These load cases mainly consist of combinations of forces and moments in the main axes, but also in axes under a 45°-angle. These forces are caused by wind and ship motions. It is not feasible to use all these load cases within the thesis, but at least a limited number of load cases should be considered in order to have a useful design.

In literature, different methods are presented that can be used to take multiple load cases into account. The first method is the weighted sum approach. This approach can also be used when optimizing for multiple objectives. So for this approach, a separate objective function $f_i(\mathbf{x})$ is defined for each of the M load cases, whereafter a weighted sum of these objective functions is optimized (see for instance ref [27]):

$$f(\mathbf{x}) = \sum_{i=1}^{M} w_i f_i(\mathbf{x}) \tag{2.2}$$

The factors w_i determine the relative importance of the different objective functions. If one wants to optimize for objectives with different physical meaning, these factors can be different [27]. For multiple

load cases, the physical meaning can however be the same. Some authors state that for multiple load cases the factors are equal for all the load cases [27], but others (for instance Krog et al. [38]) state that they are not always equal, because of similarities between the load cases. An example of such a similarity is the weight of the structure. This is present in each of the load cases, and can thus dominate the results. Each of the load cases adds another factor to this weight and its relative importance increases. So, the factors can in general only be equal if the physical meaning is the same and if the load cases do not have similarities.

A disadvantage of this method is that it can be difficult to obtain the factors for the different load cases, because of similarities in the load cases or the differences in the physical meaning. Often no clear relation between the different objectives can be found, and it is therefore hard to find a reasonable factor for each objective.

Another option is to use a min-max formulation. With this formulation, the maximum of all the objective functions is minimized. That results in the following objective function [30]:

$$\min_{\mathbf{x}}: \quad \max f_i(\mathbf{x}) \quad i = 1, \ldots, M \tag{2.3}$$

Optimizing this function is easier than the weighted sum method, because no weights need to be determined for multiple load cases. A problem with this method can be that it is not differentiable. This function is therefore often rewritten to another optimization problem, called the bound formulation. That means that the objective function is rewritten to a combination of a single objective and a constraint [44]:

$$\begin{aligned} \text{min:} \quad & y \\ \text{Subject to:} \quad & f_i(\mathbf{x}) \leq y, \quad i = 1, \ldots, M \end{aligned} \tag{2.4}$$

The third method is a Kreisselmeier-Steinhauser function. This function is also used in other aspects of optimization such as multiobjective problems and problems with local stress constraints [30]. The aim of this method is to overcome possible numerical problems with non-smoothness of the max-formulation. This function uses the objectives of each of the load cases to construct an aggregate objective function, which approximates the max-formulation [37]:

$$\begin{aligned} f_{\mathsf{KS}} &= \frac{1}{\eta} \ln \sum_{i=1}^{m} \mathrm{e}^{\eta \bar{f}_i} \\ \text{With:} \qquad \bar{f}_i &= \frac{f_i}{f_{0_{\max}}} - 1 \end{aligned} \tag{2.5}$$

In this equation, η is a parameter that describes how close the KS-function is to the max-formulation. Taking the limit of this parameter to infinity gives the initial min-max function. In reality, this value is much smaller, again to avoid numerical issues in the optimizer. A problem with the KS-function is however that the result is dependent on the choice of η. Solutions are proposed for this problem, but these will not be considered in this thesis [30, 54].

Another option is to search for a single objective that is independent of the different load cases. An example of this is the minimization of mass or volume [38]. This has the advantage that no additional parameters need to be determined, like for the KS-function or the weighted sum approach. These parameters have influence on the quality of the result, and wrong values can therefore result in less optimal results. This can be avoided by optimizing for a single objective, because no assumptions for certain parameters need to be made. Krog et al. applied this method to a large scale design problem and they concluded that this is the preferred option, because it also allows designers to use realistic design targets.

2.3. Structural limitations

Another important aspect in the thesis are the yield stresses and buckling limits in the tower grillage and the ship structure. In the optimization, a finite element model will be used to calculate the stress. The response of this model should be analyzed by the optimizer to check if it complies with the given

constraints. This section gives first an overview of the possibilities of the implementation, after which possibilities for the two constraints on the external structure are presented.

2.3.1. Implementation

The most intuitive way of including the stresses and buckling loads is by using inequality constraints. These constraints state that the stresses and buckling loads in the ship should stay below certain thresholds. The advantage of this method is that it is relatively simple to check the constraints. A disadvantage is however that for the stresses a constraint needs to be set for every element in the FEA-model, which results in a high number of constraints. This can be amongst others a problem for the computational effort, depending on the optimization algorithm that is used. The reason is that for some optimizers, sensitivities or gradients need to be calculated for each of the responses (in this case the stress). This can however be solved by using the Kreisselmeier-Steinhauser function as described in Equation 2.5 [37]. Then instead of the objective function value, the stress value in each of the elements should be used. That results in the end in a single constraint function. But again the choice of the parameter η influences the result, which is a disadvantage of using this method.

Because the ship is an external structure, also other methods can be used to couple the ship structure and the tower grillage. Some research is performed into finding the optimum support location for an optimization. Buhl [10] presented a method that is able to optimize the boundaries and the topology of the structure simultaneously. Some more recent research is performed on finding the optimal boundaries [41, 70], but these papers address the support only from the viewpoint of the structure. No papers are found that consider stresses in the supporting structure.

2.3.2. Stress

A constraint on the stress can be set by using the Von-Mises stress criterion:

$$\sigma_{VM} = \sqrt{\sigma_{xx}^2 + \sigma_{yy}^2 - \sigma_{xx}\sigma_{yy} + 3\tau_{xy}^2} \tag{2.6}$$

This criterion is used, because a structure will generally not fail due to uni-axial stresses, but due to a combination of stresses in all directions. Because plates are considered in this thesis, the stresses are assumed to be in-plane, so only a 2D case needs to be considered. This stress can be compared to the maximum allowable stresses in the ship to check if they comply.

2.3.3. Buckling

The bulkheads in the ship consist mainly of large plates, and they are therefore sensitive to buckling. Consequently, a buckling check is needed in the optimization to make sure that the bulkheads stay intact. The buckling check for a plate is however more complicated than a stress check. The different stress parameters that should be considered for buckling are shown in Figure 2.4. This figure shows that in total five parameters are considered: The stresses in x- and y-direction, the corresponding stress ratios ζ_x and ζ_y and the shear stress.

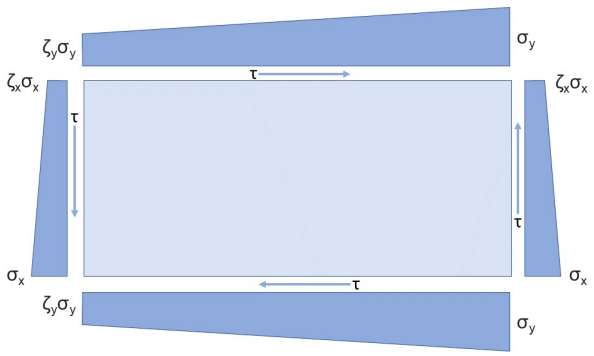

Figure 2.4: Important buckling loads on a plate, consisting of the in-plane stresses σ_x and σ_y with their corresponding ratios ζ_i, and the shear stress τ.

In finite element analyses, two approaches can be used to calculate the buckling load: a non-linear and a linear approach. In the first method, the applied load is increased until the structure collapses. At every load increment, the structure is analyzed, and the results are used in the next increment. This approach is generally used to obtain a more accurate result for the buckling load, but it requires much longer computing times. This is especially an issue for an optimization problem because such a problem requires multiple iterations. As a result, the computing times increase dramatically, so a non-linear approach is not feasible in this setting.

The other method that can be applied in FEA is the linear or eigenvalue buckling approach. Here, eigenvalues and eigenmodes of the model are calculated for a certain load as expressed in Equation 2.7 [1]:

$$(K + \lambda_i K_g)\,\Psi_i = 0 \tag{2.7}$$

In this equation is K the stiffness matrix, K_g the geometric stiffness matrix, computed for the applied load, and λ_i and Ψ_i are the ith eigenvalue and eigenvector. The first positive eigenvalue is used as a load multiplier for the design. This eigenvalue should be above 1, otherwise the panel fails. This method generally overestimates the allowable buckling load, and one should thus be careful by using this method. It is however expected to be sufficiently accurate for the optimization as considered in this thesis.

Another option is to calculate the buckling strength with an analytical formulation instead of directly from the finite element analysis. In literature about shape optimization of truss structures is buckling taken into account by using Euler buckling (see for instance Schwarz et al. [62]). Euler buckling is however intended for beams, whereas in this thesis plates are considered. In the theory of Euler, the shape is assumed to be a sine, with the number of half sine waves dependent on the boundary conditions. For a plate however, buckling can also occur in the transverse direction. An example for a simply supported plate on all edges is shown in Figure 2.5

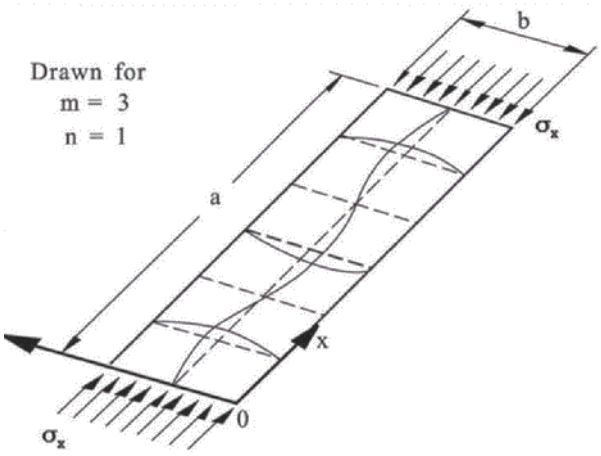

Figure 2.5: Example of a plate buckling shape with three half sine waves in longitudinal direction and one in transverse direction [28]. The number of half sine waves is dependent on the dimensions of the plate.

This shape can be described with:.

$$w = \sum_m \sum_n w_{mn} = \sum_m \sum_n C_{mn} \sin\frac{m\pi x}{a} \sin\frac{n\pi y}{b} \tag{2.8}$$

In this equation is m the number of half sine-waves in longitudinal direction of the plate and n the number of half sine waves in transverse direction. Buckling of such a plate is determined by four loads: Normal stresses in x- and y-direction, in-plane shear stress and lateral pressure. For this thesis, only the first three are of importance, because we are inside the ship. A representation of the interaction between the stresses is shown in Equation 2.9 [13]:

$$\begin{gathered}\left(\frac{\gamma_{c1}\sigma_x^S}{\sigma_{cx}}\right)^{e_0} - B\left(\frac{\gamma_{c1}\sigma_x^S}{\sigma_{cx}}\right)^{\frac{e_0}{2}}\left(\frac{\gamma_{c1}\sigma_y^S}{\sigma_{cy}}\right)^{\frac{e_0}{2}} + \left(\frac{\gamma_{c1}\sigma_y^S}{\sigma_{cy}}\right)^{e_0} + \left(\frac{\gamma_{c1}|\tau|^S}{\tau_c}\right)^{e_0} = 1 \\ \left(\frac{\gamma_{c2}\sigma_x^S}{\sigma_{cx}^S}\right)^{e_0} + \left(\frac{\gamma_{c2}|\tau|^S}{\tau_c}\right)^{e_0} = 1 \qquad \text{for } \sigma_x \geq 0 \\ \left(\frac{\gamma_{c3}\sigma_y^S}{\sigma_{cy}}\right)^{e_0} + \left(\frac{\gamma_{c3}|\tau|^S}{\tau_c'}\right)^{e_0} = 1 \qquad \text{for } \sigma_y \geq 0 \\ \frac{\gamma_{c4}|\tau|^S}{\tau_c} = 1 \\ \text{with} \qquad \gamma_c = \min\left(\gamma_{c1}, \gamma_{c2}, \gamma_{c3}, \gamma_{c4}\right) \qquad \text{and } \eta = \frac{1}{\gamma_c}\end{gathered} \tag{2.9}$$

This equation is written in the Class Guidelines of the classification Society DNV. The approach has similarities to the approach of Hughes and Paik [28], but only the Class Guidelines are considered for this thesis because these are already used by Vuyk Engineering. In this equation, σ_x, σ_y and τ are the applied normal and shear stresses in the coordinate system of the plate. σ_{cx}, σ_{cy} and τ_c are the ultimate buckling stresses in the given directions which are dependent on the boundary conditions of the plate. e_0 and B are parameters dependent on a plate slenderness parameter and S is a safety factor dependent on the loading and the ship type. γ_{ci} are multiplication factors, which are determined by solving the above equations. The smallest of these values is used to determine the maximum utilization factor η, which should be below 1 to have a safe structure.

An important difference between the two methods is that linearized buckling overestimates the allowable buckling load, so it is well possible that the structure collapses before this load is actually reached. On the other hand, the Class Guidelines state that dynamic load effects are not considered in their approach, which is a conservative assumption [13]. So this approach has a higher degree of certainty that the structure will not collapse under the estimated load, but that also means that the structure is overdesigned.

2.4. Optimization algorithms

The optimization techniques as described in Section 2.1 do not solve the problem itself, but they only describe the problem and the corresponding design variables. To perform the actual optimization, an algorithm is needed. These algorithms are not only used in structural optimization, but also other fields, such as economics and geophysics. As a result, many different algorithms are developed, each with its advantages and disadvantages for given problems. Examples of optimization algorithms can be found in the books of Bozorg-Haddad, Solgi, and Loiciga [9] and Antoniou and Lu [2]. When choosing the most appropriate method for the considered problem, different aspects of the problem should be taken care of, such as linearity and convexity of the objective function and the availability of gradient information. Optimization algorithms can be subdivided in two categories: gradient-free and gradient-based algorithms. In this setting, the gradients are used to express the sensitivity of the design variables with respect to the responses.

2.4.1. Gradient-free methods

The first category does not require any gradient information. These methods are solely based on function evaluations and elements from artificial intelligence to converge to a solution [9]. The most popular methods in structural optimization are the (meta)heuristic algorithms such as swarm algorithms and genetic algorithms. An extensive overview of most general methods is given by Bozorg-Haddad, Solgi, and Loiciga [9].

The strength of gradient-free methods is that they can handle many difficulties, such as non-convexity and non-linearity. These algorithms are often applied in areas where it is hard or computationally expensive to calculate gradients. An example of such a problem is a black-box model. That means that an input is fed into a model, which gives a result without any information about the processes going on within this model. Examples of such problems are simulations, such as CFD or FEA [26]. Another advantage is that heuristic algorithms are generally well suited for parallel computing [33, 74]. That

means that multiple branches of the algorithm are optimizing at the same time, which can significantly reduce the computational time.

This might be a part of the solution for one of the disadvantages of this model. That is that these algorithms often require many function evaluations. Cao et al. [11] compared several algorithms to their own algorithm, and they reported numbers of structural analyses in the order of 5,000 up to 25,000 for a problem with 10 design variables. These numbers even increase for a larger problem of 59 design variables to values between 35,000 and 150,000 analyses. Similar values are reported by Mortazavi and Toğan [50]. The earlier mentioned simulations are however often computationally expensive, with computational times from minutes up to hours or even days, which means that the optimization will take very long. This is also the case for maritime structures, because ships are generally large. There are however possibilities to reduce the complexity of the model [12, 45], which will be explained in more detail in Section 2.4.3.

Another disadvantage is that no mathematical proof of the convergence to the optimum can be given (unless all possible solutions are examined). However, they seem produce good results in certain areas of structural optimization (see for instance Refs. [50, 65]). There are however also algorithms that do have (some) proof of convergence, which will be described in the next section.

2.4.2. Gradient-based methods

The second category of algorithms uses gradient information to determine the best direction in which to optimize. Also for this category, many different algorithms exist. The book of Rao [57] gives an explanation for the most general methods. The strength of gradient-based methods is that they converge to an optimum within relatively few function evaluations. An example is the research of Schwarz et al. [62] who solved a combination of size and shape optimization with sequential linear programming. They reported convergence after 267 iterations for 16,288 design variables and 11 iterations for 464 design variables. They did not report the quality of their solutions compared to the solutions of other papers, but Lamberti and Pappalettere [40] reported values in the same order of magnitude for the number of iterations. These values are much lower than the values reported for gradient-free algorithms. It is therefore generally better to choose gradient-based methods if reliable gradient information can be obtained easily.

Only a limited amount of research to mathematical programming in the relevant field for this thesis is available. One of the reasons is that the search space is generally non-convex and non-linear, and the optimizer is therefore sensitive to getting stuck in a local minimum [22, 51]. The problem can be linearized to overcome problems with non-linearity. Schwarz et al. [62] showed that this is more efficient than a non-linear approach. This approach was possible because they formulated the problem such that the functions, and thus gradient information were available. In many cases, these functions are however not known. Another problem is that often the number of responses and variables is large, and calculating the sensitivities can therefore be computationally expensive [59]. Methods that do not have this problem, but which can to handle expensive problems in a reasonable amount of time are presented in the next section.

2.4.3. Approximation techniques

Foregoing showed that the complexity of the problem is an important aspect of the feasibility of the optimization. A too complex problem cannot be solved in a reasonable amount of time. Therefore, some solutions are proposed in literature, which aim to simplify the problem such that it can be solved more easily. Three of the most important methods will be discussed. The first solution is linearization, which can be a good solution for non-linear functions. Schwarz et al. [62] showed that this can improve the convergence significantly. This is however only possible if the functions are available, which is often not the case.

Another option is to use a metamodel. This is a mathematical model that is built from several samples from this design space. Such models can for instance be a good solution if a black-box function needs to be optimized. A black-box model can normally only be solved with a gradient-free optimization technique, which has the disadvantage of many function evaluations. A metamodel can however be solved with a more efficient gradient-based algorithm. Such a model is often used when the analyses are expensive like a non-linear FEA-model [45, 76] or a CFD-calculation [8, 12]. An additional advantage of a metamodel is that it filters some of the computational noise that may exist in the solution

[19].

Building the metamodel can be done with many different approaches, such as least-squares fitting, radial basis functions and kriging [19, 45, 52]. The choice of the method is important for the reliability of the model. Also the number of required function evaluations is dependent on the chosen model. For instance, a radial basis function approximation needs at least 2N+1 datapoints, with N the number of design variables. That means that for a large number of design variables also many function evaluations are needed to obtain a model. It is important to note that the number of required function evaluations for a reliable model is often much higher. For instance, a highly non-convex function needs much more sample points to capture the right behaviour of the design variables. As a result, this method is only useful if the number of design variables is relatively small, because otherwise the number of function evaluations will be large, which one wants to avoid by using this method. This is also shown by the presented literature, because the numbers of design variables is in the order of 20 [45, 52]

The last method that will be discussed is Sequential Approximate Optimization (SAO). This method is a variant of the metamodeling technique. The difference is that with SAO only a part of the design space is modeled, in contrary with the whole design space as in standard metamodeling. The algorithm starts in a so-called trust region or region of interest (ROI), as presented in Figure 2.6. Within this region, a number of samples is generated to create a response function. This function is optimized, and new sample points are generated around the optimum, but also the ones from the previous step that lie in the new region are used. This procedure repeats until the termination criterion is met [35]. The advantage of this method is that a local approximation is made, so only a part of the whole design space needs to be covered. That means that the sample points can be taken closer to each other, resulting in a more reliable estimate of the response function and thus less sample points are required. This is also directly a disadvantage of the method, because not the whole design space is covered, and one can therefore not be sure that the found optimum is the true optimum.

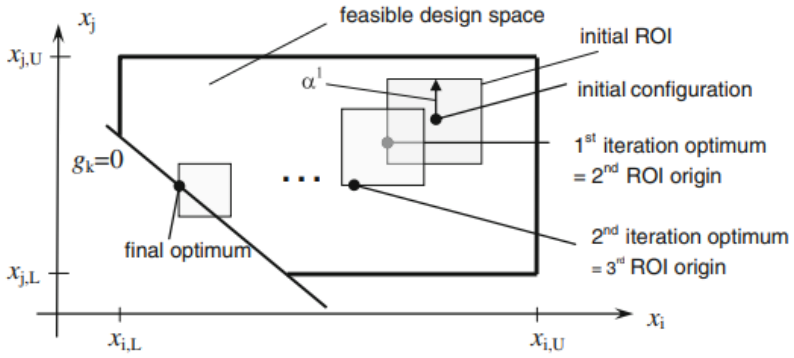

Figure 2.6: Example of sequential approximate optimization in 2D [52]. The optimization start in an initial trust region (ROI). The optimum of each iteration is the origin of the next ROI.

An maritime application of this method is shown by Pajunen and Heinonen [52]. They developed a method to automate the design of plate structures, which is based on the principles of sequential approximate optimization. They found that the automated process is significantly faster than a traditional design process, while also having a slightly lighter design.

2.5. Used algorithm

The optimization in this research depends on stresses that are calculated with a finite element program. This is an external program, and therefore no gradient information can be obtained, which means that a gradient-free method or an approximation method needs to be chosen. One disadvantage of the latter method is however that a larger number of design variables require many function evaluations, as explained in Section 2.4.3. Available research considers problems with a size in the order of 20 design variables [45, 52]. The research in this thesis does however consider 174 design variables, which is much larger. It is therefore not known if this method will decrease the computational time, and

it is therefore not be used. That means that the gradient-free methods are left.

Bozorg-Haddad, Solgi, and Loiciga show that there are many different methods to choose, with each their own advantages for certain problems. A problem with for example genetic and swarm algorithms is that they need a relatively large number of inputs, such as population size and combination parameters [39]. That means that the choices of the designer can have large influences on the result. This problem is however smaller for simulated annealing (SA), which is only dependent on an initial 'temperature' T (which determines how local the search is), an initial vector with design variables and a specified number of iterations. Another reason to choose for this method is that it is used often in the field of structural optimization (see for instance Refs. [39, 49, 69]). This showed that this method is suitable for this type of problems.

A disadvantage of classical simulated annealing (CSA) is that many structural analyses may be required to converge to the global optimum [39]. However, several authors claimed that there is an algorithm that produces good results for a relatively small number of function evaluations as shown in the benchmarks of Gubian [24] and Xiang et al. [73]. This is the generalized simulated annealing (GSA) algorithm, as implemented in the SciPy package of Python [63, 68]. This algorithm is a combination of Classical Simulated Annealing (CSA) [34] and Fast Simulated Annealing (FSA) [18]. The advantage of GSA is that it does not only converge faster for many problems, but it is also able to escape from local minima more easily than CSA and FSA [73]. This is a result of the fact that this method searches the design space more homogeneously [71]. Xiang and Gong also states that the relative efficiency of the GSA compared to the CSA and FSA algorithms increases with the number of design variables.

Simulated annealing is an algorithm that is based on the cooling process of a material, which was developed by Kirkpatrick, Gelatt, and Vecchi [34]. In the first stages of the cooling process, the atoms are moving fast and they also move larger distances. This behaviour decreases with the decrease of temperature, until the freezing point is reached. This 'freezing point' is in the simulated annealing algorithm the point where the optimum is found. The pseudocode for the general form of simulated annealing is given in Algorithm 1. This pseudocode is representative for both CSA as well as GSA.

Algorithm 1 Simulated Annealing

$\vec{x}_{best} \leftarrow \vec{x}_{initial}$
for t **in** $iterations$ **do**
  $T \leftarrow$ **calculate_temperature**(t)
  for $step$ **in** $substeps$ **do**
    $F_{current} \leftarrow F(x_{best})$
    $\Delta F = F_{current} - F_{new}$
    $\vec{x}_{new} \leftarrow$ **create_new_solution**$(\vec{x}_{best}, T)$
    $F_{new} \leftarrow F(x_{new})$
    if ΔF > 0 **then**
      $\vec{x}_{best} \leftarrow \vec{x}_{new}$
    else if $min\{1, p_x(\Delta F)\} > random(0, 1)$ **then**
      $\vec{x}_{best} \leftarrow \vec{x}_{new}$
    else
      $\vec{x}_{best} \leftarrow \vec{x}_{best}$
    end if
  end for
end for
return $\vec{x}_{best}$

The algorithm starts with defining a design vector $\vec{x}_{best}$, which contains the optimized combination of design variables at the given time step. This vector is at the start of the optimization initialized by either predefined or randomly generated values. After that, the optimization process starts. This process is divided into two loops. In the outer loop, the temperature is decreased with [68]:

$$T_{q_v}(t) = T_{q_v}(1)\frac{2^{q_v-1}-1}{(1+t)^{q_v-1}-1} \tag{2.10}$$

This temperature controls the shape of the visiting distribution. The higher the temperature, the wider the distribution. The parameter q_v is the so-called visiting parameter, which controls the cooling rate and the width of the visiting distribution, which will be shown in Figure 2.8. Because the temperature is decreased only in the outer loop, the temperature is constant for the number of specified substeps, also called an iteration. An example of the temperature decrease is shown in Figure 2.7.

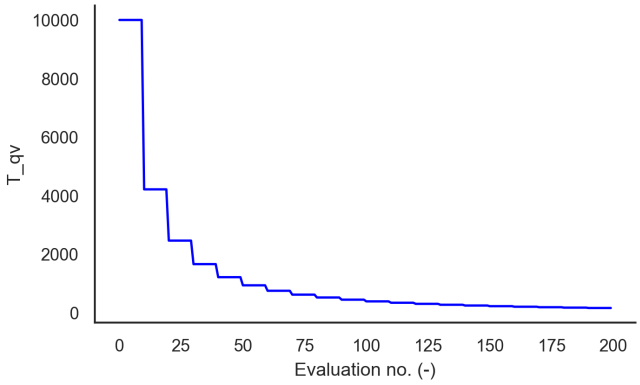

Figure 2.7: Example of the temperature decrease over the evaluations

In the implementation of the algorithm used in this study, the number of substeps in an iteration is twice the number of design variables or dimension D of the problem. This a result of using two search methods during each iteration: global and local search [7, 12]. Global search means that all variables are changed at once, whereas local search means that the variables are changed one-by-one. Lamberti [39] concludes that the overall performance of SA may be improved if a combination of the two methods is applied. This is also done in the GSA algorithm [68]. For the first D substeps, all design variables are changed at the same time, but for the second set, the variables are changed one by one. So, in every iteration, each design variable is changed $D + 1$ times.

The next step in the loop is the calculation of the function value F for the best solution. After that, a new design vector $\vec{x}_{new}$ is made, which is a random draw of values around the design vector $\vec{x}_{best}$, which is described in line 7 of Algorithm 1. For the classical simulated annealing algorithm, these values are drawn from a Gaussian distribution [71]. For the generalized simulated annealing algorithm however, another distribution is used: a distorted Cauchy-Lorentz distribution:

$$g_{q_v}(\Delta x) \propto \frac{[T_{q_v}(t)]^{-\frac{D}{3-q_v}}}{\left[1 + (q_v - 1)\dfrac{(\Delta x)^2}{[T_{q_v}(t)]^{\frac{2}{3-q_v}}}\right]^{\frac{1}{q_v-1}+\frac{D-1}{2}}} \tag{2.11}$$

This distribution is a combination of a normal distribution and a Cauchy-Lorentz distribution, as described by Tsallis and Stariolo [68]. In this equation describes Δx the distance between the new design vector and the current design vector.

A comparison between the shape of a normal distribution and a distorted Cauchy-Lorentz distribution is given in Figure 2.8. Both distributions are shown for a one-dimensional case. This figure shows that the tails of the distorted Cauchy-Lorentz distribution are heavier than those of the normal distribution. It becomes clear that the visiting parameter q_v has a large influence on these tails. The distribution is the same as a normal distribution if this value is set to 1 and the same as a Cauchy-Lorentz distribution when $q_v = 2$. The larger the value, the heavier the tails. That means that there is still a probability of long jumps at low temperature, meaning that it is easier for the algorithm to escape from local optima [71].

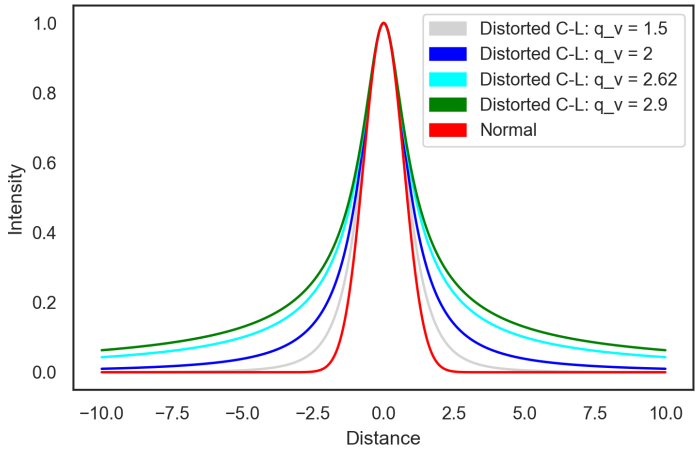

Figure 2.8: Comparison between the distorted Cauchy-Lorentz distribution for different values of q_v, and the normal distribution. The graphs are scaled to 1 to compare the behaviour.

With the generated design vector, a new function value F_{new} is calculated. If this function value is smaller than the current function value, the best design vector will be updated with the new one. If this is not the case, still two options are open. The first option is that the new function value is accepted, although it is higher than the current value. This is described in line 9 of Algorithm 1. This step is made to decrease the probability of getting stuck in a local optimum. The probability of acceptance is determined by:

$$p_{x,CSA} = \exp\left(\frac{\Delta F}{T}\right) \tag{2.12a}$$

$$p_{x,GSA} = \left[1 - (1 - q_a)\frac{\Delta F}{T_{q_a}}\right]^{1/1-q_a} \tag{2.12b}$$

The acceptance parameter q_a is a value to control the acceptance probability, which is a parameter defined by the designer. The value T_{q_a} is the acceptance temperature, which can be determined by $T_{q_a} = T_{q_v}/t$ [72]. These equations show that the probability of acceptance will be small when the difference between the current function value and the new function value is large. The same holds for a low temperature. That means that in the first steps, the probability of acceptance is larger. Whether the value is accepted depends again on a randomly generated number between 0 and 1.

The other option when the new function value is higher than the old one is that the new solution is rejected and the old optimum solution is kept. The new best solution is used again in the new function evaluation and the calculation starts again. If the maximum number of function evaluations is reached, the best solution is returned as the optimum solution.

3

Numerical model

This chapter will describe how the optimization is set up. First, Section 3.1 will describe the how the problem will be approached. Next, Section 3.2 will describe the settings of the algorithm. After that, Section 3.3 will explain the optimization objective and the constraints. Then, three important functions in the optimization will be explained in more detail. First, the penalty function, which accounts for the constraints will be described in Section 3.4. Next, a function that considers peak stresses in the solution will be explained in Section 3.5, and lastly, the implementation of the buckling constraint is shown in Section 3.6.

3.1. Optimization procedure

Section 2.1 showed that many approaches are developed to solve optimization problems, but there is generally not a single best technique for a given problem. Every option has its advantages and disadvantages. For this thesis, the combination of size and shape optimization is used, because the expectation is that this method can give a solution, while keeping the complexity of both the implementation and the result on a reasonable level.

The problem as presented in Chapter 1 will be solved with a 2.5D approach. That means that the optimization will take place in the 2D space, where only the layout and the thicknesses of the radial supports are optimized. The responses are however calculated with a 3D finite element model. This results in a lower complexity, but still realistic model.

In order to study the different aspects of the problem, three different optimization steps will be performed. The size and complexity of the problem are increased throughout the different stages. In the first two steps, a small optimization model is used, and in the last step, a full grillage will be modelled. The optimization steps that are followed in this thesis are:

1. *Single layout on a rigid foundation*
   In this step, the ship is modelled with fully rigid boundary conditions. That means that the only constraints on this optimization are the stresses in the grillage. The results of this step are used to gain knowledge about the behaviour of the optimization, but also to make a comparison to the results with the ship as a foundation as calculated in the next step.
2. *Single layout on a (flexible) ship foundation*
   In this stage, still a single grillage is optimized, but a part of the ship is included as the boundary condition. That means that stress and buckling in the ship are considered in the optimization. This step will, in combination with the previous step give an answer to the second sub-question, as presented in Section 1.4. This step also partly gives an answer to the first research question.
3. *Full problem*
   In the last step, again a part of the ship is used as the boundary condition, with a block of four layouts on top. This is the solution that is needed to show the actual performance of the algorithm. The result of this optimization step is compared to an existing grillage design to see if the optimization indeed finds a feasible and improved design. With this step finished, an answer can be given to the first and third sub-question, and with that the main research question.

The first two steps will mainly focus on the optimization problem and a comparison between the rigid and the ship foundation: how does the algorithm behave and what are the most important differences between the two boundary conditions. The last step will pay more attention to a comparison to the original design.

The optimization procedure that is used in these steps is shown in Figure 3.1. This figure shows two main blocks, which each describe a different program. The left main block is the Python code that is developed during this thesis. The block on the right is the finite element analysis (FEA) program that is used to calculate the responses of the model. The communication between the two blocks is handled with the Python package PyAnsys [55]. This package allows the user to create and analyze a model in Ansys with Python code. Also the responses of the model can be retrieved from Ansys so that they can be handled within Python.

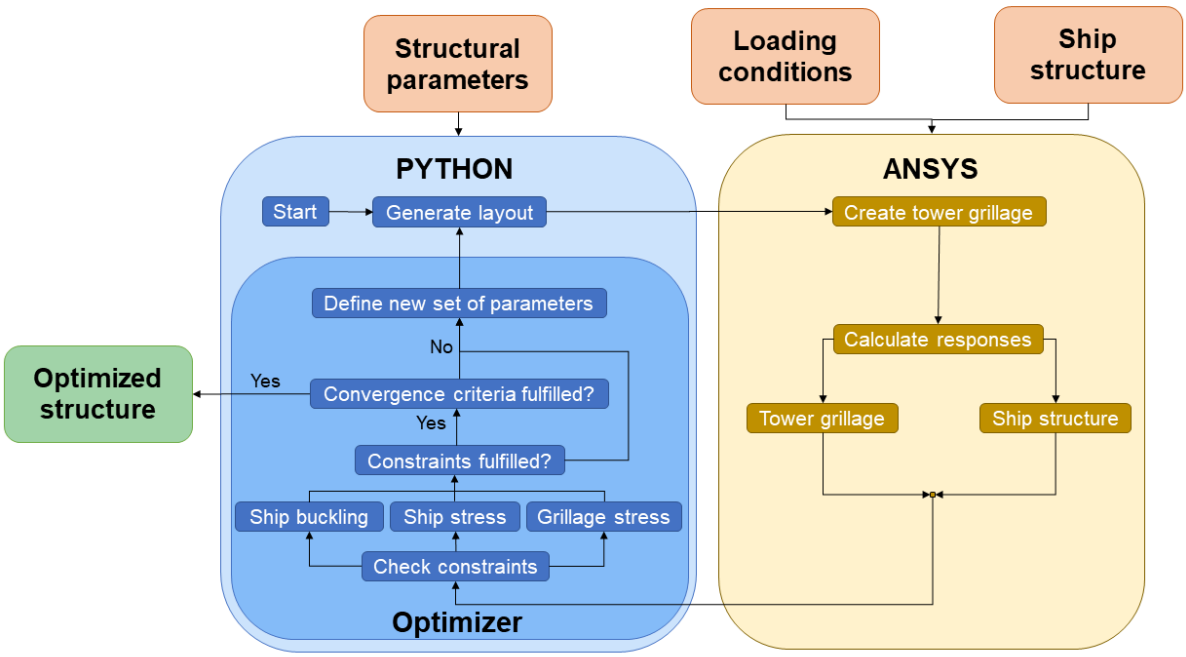

Figure 3.1: Workflow of the optimization explaining the coherence between Python and Ansys. The connection between the two programs is made with the Python package PyAnsys.

The first step in the Python block is the generation of a parametric initial layout. This is fed into the Ansys program, which creates a geometrical model. The responses of this model are analyzed for the given loading conditions. These responses are returned to the Python model, where these responses are fed into the optimizer. This optimizer is a combination of the generalized simulated annealing (GSA) algorithm in the SciPy package [63] as explained in Section 2.5 and a penalty function. This penalty function is used to include the constraints, which will be explained in more detail in Section 3.4. This penalty function checks whether the constraints are fulfilled, and then the GSA algorithm checks whether the convergence criteria are fulfilled. If not, a new set of parameters is defined and the loop starts again until the convergence criteria are met.

3.2. Optimization algorithm settings

The optimization algorithm does need some settings in order to run properly. As explained in Section 2.5, three inputs are needed for a simulated annealing algorithm: an initial temperature (defining how local the search is), an initial vector with design variables and a specified number of function evaluations.

Two temperatures are used in this thesis: 10,000 and 5,000. These temperatures are selected based on the default temperature of the SciPy implementation, which is 5,230. No explanation of this temperature could be found, but this temperature is used in several benchmarks [23, 24]. From

that, the assumption is made that the temperature should be chosen in the same order of magnitude. Because no evidence is found for the default temperature, a rounded value of 5,000 is chosen. A higher temperature means a larger search space, which might be favourable for the optimization result. For that reason, the temperature of 10,000 is selected. Another temperature with a lower value would have been desirable, but that is not implemented due to a lack of time. These temperatures are used in the first two steps, to see which of the two yields the best results. The best results depend on the weights that are found, but also on the variability between the results of the different runs. The temperature that gives the best results is used in the third step of the optimization.

At every temperature, two different runs are done to verify if these results are in the same order of magnitude. These results are produced with so-called seeds, which are sets of random numbers that are the same every time this seed is called (under the restriction that the model and the other optimization settings are equal). That means that the results are reproducible, which is an issue with this type of optimizers, as mentioned in Section 2.4. The seed numbers that are used in this thesis are 0 and 365. These numbers will be referred to as run 1 and 2, respectively.

The initial design vector that will be used will be described in more detail in Section 4.5, after the different variable groups are explained. Then, only the number of function evaluations needs to be determined. This value is a trade-off between the convergence and the run time of the optimization. The longer the run, the lower the optimized value (if the optimizer is not converged earlier), but that does also mean that it takes longer before the result can be processed. The number of function evaluations in this thesis is set to 14,000. With this setting, the run time for the full grillage is two weeks. For this amount of function evaluations, a good image of the results can be obtained.

The GSA algorithm requires two additional parameters q_a and q_v, as shown in Section 2.5. The default values for these parameters in the SciPy implementation are 2.62 and -5 respectively. These values are based on the experience of Xiang et al. [73], which is in accordance with the findings of Tsallis and Stariolo [68], who reported values in the order of 2.7 for the acceptance parameter q_a. These parameters are therefore kept at the default values.

3.3. Objective and constraints

The objective for the optimization is the mass m of the tower grillage. This objective is taken because it allows for optimizing for multiple load cases, as explained in Section 2.2. For the current optimization, the mass m is defined as the sum of the masses of the N_c different components i of the grillage. This is combined with the allowable stresses in the grillage and ship, $\sigma_{vm,g,i}$ and $\sigma_{vm,s,j}$, respectively and the buckling unity checks η_l as constraints:

$$\begin{aligned} &\text{min } m = \sum_{i=1}^{N_c} m_i \\ \text{subject to:} \quad &\frac{\sigma_{vm,g,j}}{\sigma_{a,g}} - 1 \leq 0 \text{ for } j \in [1, 2, ..., N_g] \\ &\frac{\sigma_{vm,s,k}}{\sigma_{a,s,k}} - 1 \leq 0 \text{ for } k \in [1, 2, ..., N_s] \\ &\eta_l - 1 \leq 0 \text{ for } l \in [1, 2, ..., N_p] \end{aligned} \tag{3.1}$$

In this equation describes N_c the number of components in the grillage, such as the brackets and the flanges; N_b is the number of elements on the grillage and N_s the number of elements in the ship. The constraints on the stress are normalized to 1 with the maximum allowable stress σ_a. The allowable stress is not everywhere the same in the ship, because the webframes have a higher allowable stress than the rest of the ship model, which explains the index to the allowable stress in the ship. The last constraint, buckling in the ship, is calculated with the DNV code [13] as given in Equation 2.9. This value is normalized by the definition of the equation, so no normalization is necessary.

A contingency factor of 0.66 is applied to the three constraints, in accordance with the working stress design (WSD) factors as given by DNV [15]. These factors are used to cover unfavourable changes in applied forces, but also to cover modelling errors, which are present in a finite element model. Examples of these errors are constraints that are not exactly representing reality, but also the

stresses, which will in reality not develop exactly as calculated in FEA. This factor reduces the maximum allowable stress in both the grillage and a large part of the ship from 355 MPa to 234 MPa. The web frames in the ship are made from a steel with a specified yield stress of 390 MPa. That means that the maximum allowable stress for these locations is 257 MPa. A summary of the values is presented in Table 3.1. This contingency factor is also applied to the buckling factor, but that is incorporated in the buckling calculation, as described before.

Table 3.1: Constraint values as used in the optimization. The reduced values are calculated with a contingency factor of 0.66

Constraint	Symbol	Nominal value	Reduced value	Unit
Maximum allowable stress	σ_a	355	234	MPa
Maximum allowable stress 2	$\sigma_{a,2}$	390	257	MPa

3.4. Penalty function

The constraints as presented in Section 3.3 can be coupled to the optimization in different ways. Bozorg-Haddad, Solgi, and Loiciga present three different methods to deal with them: removal, refinement and penalty functions [9]. Removal means that infeasible solutions are removed from the optimization model; refinement means that the infeasible solution is refined such that a feasible solution is found and penalty functions are used to give a penalty to the objective function when an infeasible solution is encountered.

From these methods, the penalty function is applied in this thesis. The advantage of this method is that the optimization is also able to find solutions outside the feasible design space, which can contain information for the final result, so this method can enhance the convergence or the quality of the solution. Another advantage is that with such a constraint function, the optimizer is able to find a solution even if the forces on the ship are too large to handle. That means that the optimizer is able to find an optimum, even if no feasible solution can be found. A penalty function ϕ can be described with [9]:

$$\begin{aligned} \phi &= \alpha \times (G(X) - \delta)^{\beta} + \gamma \\ \vartheta(G(X)) &= \begin{cases} 1 & \text{if } G(X) < \delta \\ 0 & \text{if } G(X) \geq \delta \end{cases} \\ F(X) &= f(X) + \phi \cdot \vartheta(G(X)) \end{aligned} \tag{3.2}$$

The violation is in this equation described by the difference between the value $G(X)$ and the corresponding constraint value δ. This violation is multiplied with a constant α, which is used to scale the order of magnitude of the constraint violation. The power β describes the shape of the constraint, and γ is a constant that can be added to this constraint. The parameter ϑ is 1 if the constraint is violated and 0 otherwise. Then, the new function value $F(X)$ is calculated as the sum of the objective function $f(X)$ and the value as calculated with the penalty function.

These values also show a disadvantage of this method, because they can influence the optimization result. If the penalty is too small, the constraints are likely to be violated severely. However, if the constraint value is set too high, then the optimizer is moving away from the boundaries. An optimum solution is however often found at or close to one or more boundaries. For example, if the stress is close to the maximum allowable stress, then the material is used in an optimal sense.

The choice for these numbers is based on tests with some optimization runs with different values for the different parameters. The best of these runs is used for the rest of this thesis. These results are shown in Table 3.2. γ is kept zero, because no clear explanation for an advantage of this constant could be found. The combination of the presented values shows that the optimizer is able to find results with a small violation of the constraint during early iterations, but in later stages, these violations decrease towards zero.

Table 3.2: Values for the different parameters in the penalty function, as described in Equation 3.2

Constraint	Sign	α	β	γ
Maximum allowable stress	σ_a	100	2	0
Buckling unity check	η_a	100	2	0

3.5. Peak stress evaluation

The stresses in the ship and the grillage are calculated with a finite element model. One of the problems that can occur during the optimization is the presence of local peak stresses in this model. This can be a problem for the optimizer, because a penalty will be given to these stresses, while they are not a problem in reality. In engineering practice, these locations are checked visually, but that is not feasible in an optimization procedure. Therefore, a Python function is written that examines if a high stress is a local peak stress or that the stress is high over a larger area. The pseudocode of this function is shown in Algorithm 2. The stresses that are put into this function are ordered in descending order, which means that the element with the highest stress is treated first. Also, the stress in the elements is not examined if an element with a higher stress is in the neighbourhood, which is expressed in line 2 of Algorithm 2. In every loop, the elements are selected that surround the main element and these are stored in memory to see whether they are visited or not.

Algorithm 2 Peak stress evaluation

```
1:  for every element do
2:      if element not visited then
3:          Select neighbouring elements
4:          if σ[element] > σ_peak then
5:              Go to next element
6:          end if
7:          Calculate average stresses
8:          if (#selected elements with σ > σ_a) > threshold then
9:              Go to next element
10:         else if average stress > allowable stress then
11:             Go to next element
12:         else
13:             stress[elements] ← allowable
14:         end if
15:     end if
16: end for
```

The first statement in this function analyzes whether the stress in each element exceeds a certain peak stress or not. This peak stress is determined as 1.5 the allowable stress, according to the class rules of DNV [14]. If this peak stress is exceeded, then the stress constraint is violated.

After that, another statement is examined to see whether the number of elements in the selection with a stress higher than allowable is below a threshold, specified by the designer. If more elements have a higher stress, then it will be considered as a problematic stress. If this statement is not violated, the stresses in the neighbouring elements will be averaged, which is necessary for the next step. If this average is lower than the allowable stress, then the stress in the surrounding elements is sufficiently low, which means that this location is a peak stress, and therefore not problematic.

The previous two statements are closely related, but they can not be separated. It is therefore necessary to use an if-statement twice, instead of an if-else statement. The reason is that the first statement will filter on elements with a low stress compared to the other. If in that case the stresses are averaged, a stress lower than the allowable stress might be calculated. These stresses may cause the second check to pass, while it is a problematic stress location. On the other hand, the second statement checks the value of the stresses in the selection, which is not in the first statement. If the stress in the elements is not analyzed, then the average might still be above the allowable stress, which is what should be avoided by this function.

If all these checks are passed, then the stresses of the elements are replaced by the allowable stress, so that they are not taken into account for the constraints. An example of a peak stress that is selected by this function as not problematic is shown in Figure 3.2. The red element has a stress higher than the allowable stress of 234 MPa, but lower than the peak stress of 351 MPa. The surrounding elements have a sufficiently low stress, so this element will be ignored in the penalty function.

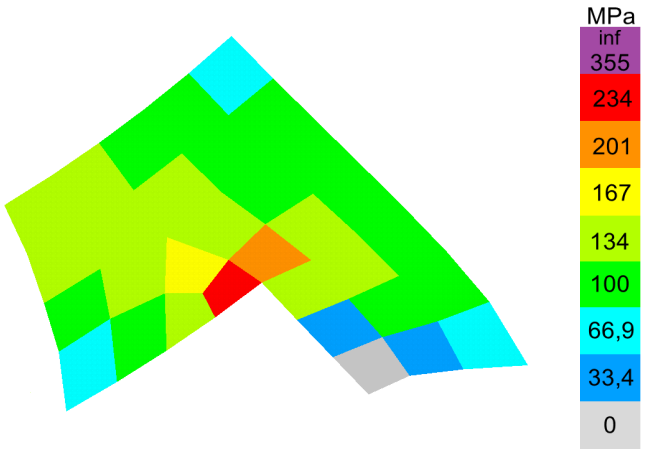

Figure 3.2: Example of a peak stress location. The red elements have a stress higher than the allowable stress, but lower than the peak stress. The surrounding elements have sufficiently small stress to ensure that the stress can redistribute.

3.6. Buckling

The last constraint considers the buckling in specified panels in the ship, which is checked with the functions as presented in Equation 2.9. These functions are applied to the panels in the ship that are most sensitive to buckling, such as the frames and bulkheads. Horizontal plates are not considered, because the loads from the tower grillage on these structural elements are much smaller than the loads in the bulkheads.

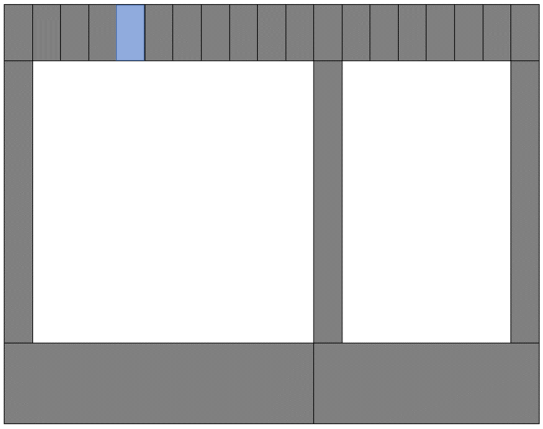

Figure 3.3: Example of a buckling panel in a frame of the ship. The highlighted area shows a typical panel.

A buckling panel is defined as a panel between two stiffeners, as shown in Figure 3.3. These panels are defined at the start of the optimization. The DNV-code accounts for linearly changing stresses with a constant factor ζ, as explained in Section 2.3.3. This is however not used in practice, because it is hard to define this factor. The reason for that is that the stresses at a panel are defined by several elements, which means that the stresses are also calculated away from the edges. These stresses may be different from the stresses at the edges, meaning that it would be complicated to account for all these stresses. Therefore, the elements in these panels are selected and an average per stress direction (x, y and shear) is calculated. In a conversation with ir. W.K. van der Leeden and ir W.H. Vuijk (oral communication, April 20, 2022), it became clear that this is common practice in the maritime industry and it is allowed by the classification society DNV, the author of the guidelines. The edges of the panel are considered simply supported. This is a conservative approach, because the panels are in reality not fully clamped. That means that the severity of the buckling load is overestimated.

With this, the numerical model is discussed. The next chapter will give an overview of the geometrical models of the grillage and the ship.

4

Model

This chapter gives an explanation of the model that will be used in the optimization. First, the geometries of the ship and grillage models will be shown in Sections 4.1 and 4.2. After that, Section 4.3 will explain the boundary conditions on the grillage and the ship. Then, the loads on the tower grillage will be considered in Section 4.4 and lastly, Section 4.5 will give a description of the design variables that will be used in the optimization.

4.1. Ship geometry

The ship model is made after the drawings of an existing ship, for which Vuyk Engineering had to design a tower grillage recently. This design will be used to compare the results of the optimization to. For the different steps in the optimization, two modelled sections of the ship are used: one for the single grillage and one for the full grillage. A 3D model of the ship section for the optimization with the single grillage is shown in Figure 4.1. A 3D model of the ship section for the optimization with the full ship is shown in Appendix A.

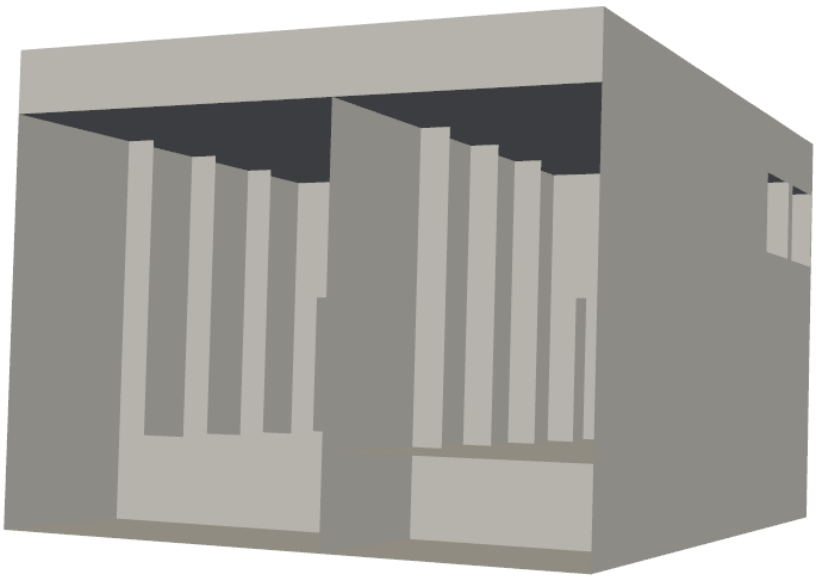

Figure 4.1: Model of the ship section that is used in the optimization of the single grillage.

Both models are kept as small as possible in order to reduce the computational effort of the optimization. At the front and aft of the grillages, the sections are extended 6 times the frame spacing. This distance is used to reduce the direct influence of the boundary conditions. On the inside, the section is extended to the first available longitudinal bulkhead. The reason for that is that such a bulkhead carries a significant

amount of load from the grillage, and it can therefore be of importance for the final result. The locations of the sections and their sizes are shown in Figure 4.2.

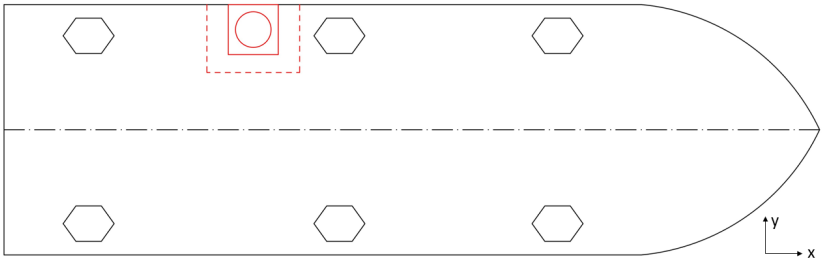

(a) Schematic view of the location and the size of the model for the single grillage

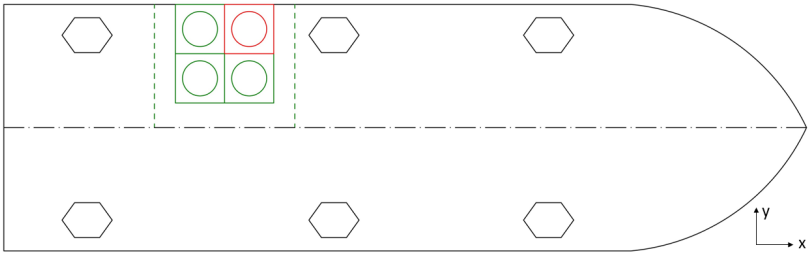

(b) Schematic view of the location and the size of the model for the full grillage. The red lines represent the location of the single grillage

Figure 4.2: Schematic overview of the location and size of the two sections that are used in the optimization. The dash-dotted line is the centerline of the ship. The dashed lines represent the modelled section of the ship.

4.2. Grillage geometry

A 3D model of the grillage that will be used in the first two steps in the optimization is shown in Figure 4.3. This figure shows clearly the orientation of the radial supports over the circumference and the location of the outer brackets.

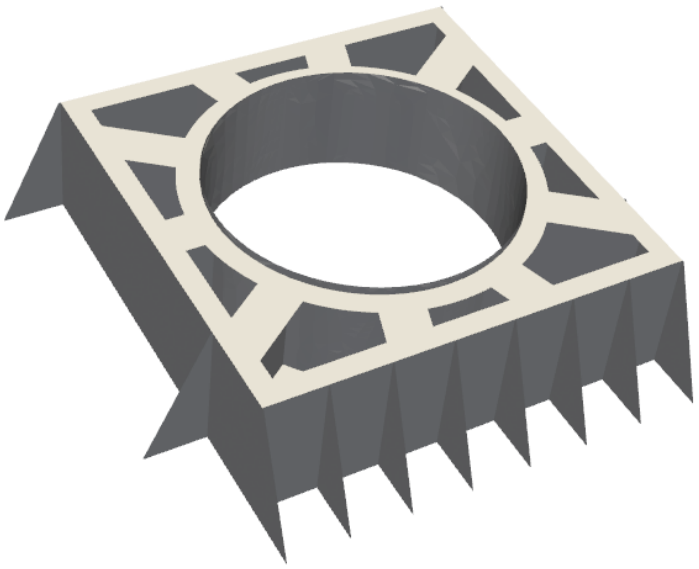

Figure 4.3: 3D model of the initial grillage model that will be used in the first two optimization steps in this thesis. The hull of the ship is located at the side of the grillage on the top of the figure.

At the top and bottom of the grillage, a flange is located. The width of these flanges extends 0.5 meter to one side of a plate. That means that the flanges around the can and at the sides of the grillage are

0.5 meter and the flanges at the radial supports are in total 1 meter. This figure shows also the outer brackets at the sides of the grillage. Only the brackets on the outside are visible, but they are also placed on the inside of the grillage, on the opposite side of the brackets on the outside. These brackets are used to transfer the stress from the grillage to the ship. Figure 1.2 showed that these brackets were rounded, but they are in the finite element model simplified to triangles, as shown in Figure 4.4.

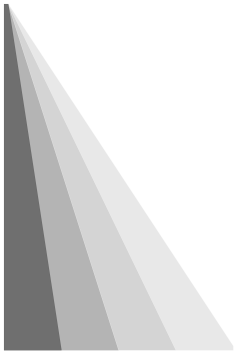

Figure 4.4: Bracket shape that is used on the boundary of the grillage. The brackets on the inside of the grillage can be changed if a radial supports is too close. The available shapes are shown by the different colors

This figure shows four different colors, which each describe a different bracket shape. The bracket on the outside of the grillage have the maximum shape, but the brackets on the inside can change their shape. The reason for this is that it is possible during the optimization that the radial supports and the brackets on the inside of the grillage intersect. If this happens, a smaller bracket shape is used, or the whole bracket is removed, such that this intersection is not present anymore. The size of the brackets is divided in four values, to ensure that not too much different bracket shapes will be used. This size reduction is implemented, because Ansys is not able to handle this type of intersections. On top of that, in engineering practice, the brackets are also reduced in size or even removed, because such an intersection means that more load is transferred to the ship via the bracket, instead of distributing through the side of the grillage and the other brackets.

Another difficulty is present for the flanges. Ansys is only able to detect full intersections, so an intersection that is present over the whole height of the shell. This is not the the case for the intersection of the brackets and the flanges, so these intersections need to be made by the algorithm instead of by the FEA program. This is done by splitting the areas with an artificial plane. This does also raise problems, because it can happen that a keypoint (a point defining the geometry) is close to this intersection, which results in an error in Ansys. This is handled by adjusting the order of cutting the planes, which resolves this problem.

(a) 3D image of the most sensitive bulkhead in the ship

(b) 2D close-up of the most sensitive location in the ship

Figure 4.5: Images of the most sensitive location in the ship.

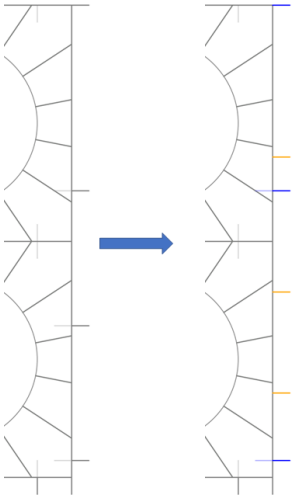

Figure 4.6: Difference in bracket location at the front side of the grillage due to holes in the bulkheads. The blue brackets are kept at the same location and the orange brackets are new.

The brackets in transverse direction are placed on the webframes in the ship, and in longitudinal direction on the bulkheads of the ship. One of the problems with the brackets in longitudinal direction is that the bulkheads on the front side of the grillage contain large holes, which are present directly below the grillage, as shown in Figure 4.5. That means that transferring the stress to these locations will lead to high stresses in the ship. For that reason, the location of the brackets on the front side is changed, to ensure that this does not happen. This change in location is shown in Figure 4.6. The brackets that have a blue color are kept the same, and the orange ones are added.

4.3. Boundary conditions

In the first optimization step, optimizing a single grillage on a rigid foundation, a boundary condition at the bottom of the grillage is used. This boundary condition is considered clamped, so all displacements and rotations are fixed. This fully rigid boundary condition is not a realistic representation of the ship, but in this way, the influence of the external boundary condition can be shown more clearly.

In the next steps, the ship sections as presented in the previous section are used. On these ship sections, three different boundary conditions are used: one on the start of the section, one on the end of the section, and one on the ship side of the section. These boundary conditions are used to represent the ship around the modelled ship section. The boundary conditions on the front and aft of the sections are applied to dummy nodes at half the height of the ship. These nodes make use of average displacements and rotations of the constrained nodes in the ship. These averages should be equal to the boundary conditions set on the distant nodes, in this case zero. Using these nodes, the constraints will be slightly relaxed, which means a more realistic representation of the ship. A summary of the applied boundary conditions on the ship sections is given in Table 4.1. The boundary conditions at the front and aft are applied to

Table 4.1: Boundary conditions for both models of the ship. 'L' represents the end of the modelled section. y=0 represents the centerline of the ship

	X	Y	Z	RX	RY	RZ
x = 0	×	×	×			
x = L		×	×	×		
y = 0		×		×		×

different parts of the ship. The boundary condition on the displacements in z-direction is applied to the longitudinal bulkheads, and on the displacement in y-direction applied to the continuous decks. The boundary condition in x-direction is applied to both the decks and the bulkheads, but only at the aft side. The consideration behind this way of constraining is that the bulkheads and decks consist of plates. Plates mainly support in-plane loads, which are also the directions that are constrained. The last boundary condition, on the ship side of the section, is regarded as a symmetry plane. The boundary conditions at this location are applied in the same way as the earlier mentioned ones. The boundary condition a the end of the ship section is shown in Figure 4.7 as an example.

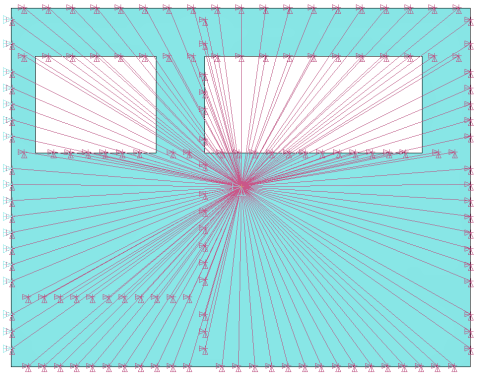

Figure 4.7: Example of the boundary condition at the end of the ship section. This figure shows that the boundary conditions are only set to the continuous components in the ship

Existing stresses in the ship, due to for instance a global bending moment are ignored. These stresses are generally not important for the design of the grillage and they are in real designs also often ignored (W.K. van der Leeden and H.W. Vuijk, personal communication, April 20, 2022). The reason why these stresses are not important is that they are typically applied in main longitudinal members, such as longitudinal bulkheads, whereas tower grillages are mainly dependent on transverse members, such as web frames.

4.4. Loads

In the optimization, four different loading conditions are used. This is not enough for a real engineering case, but including extra load cases means longer calculation times for the optimization. Therefore, only a few load cases are considered, which are however chosen such that they cover the different directions as much as possible, which is shown in Figure 4.8. In the optimization of the full grillage, one load case is applied to all four towers. That means that the forces on all towers are acting in the same direction.

The load factors for these loading conditions are presented in Table 4.2. The forces in the different directions are multiplied with these load factors to obtain the forces that will be used in that load case. The forces in the main directions are combined with forces in the perpendicular direction, as also shown in Figure 4.8. This is asked by the Class Standard of DNV [16], which was used in the design of the original tower grillage and also in the optimization. The reason for combining the forces is that the loads are generally not directed perfectly in one of the main axes. Combining does therefore give a more realistic, although conservative approach.

Table 4.2: Load factors given per loading condition for the loads on the tower grillage.

Loading condition	X	Y	Z	RX	RY	RZ
1	1	0.6	-1	-0.6	1	0
2	-1	-0.6	-1	0.6	-1	0
3	-0.6	1	-1	-1	-0.6	0
4	0.6	-1	-1	1	0.6	0

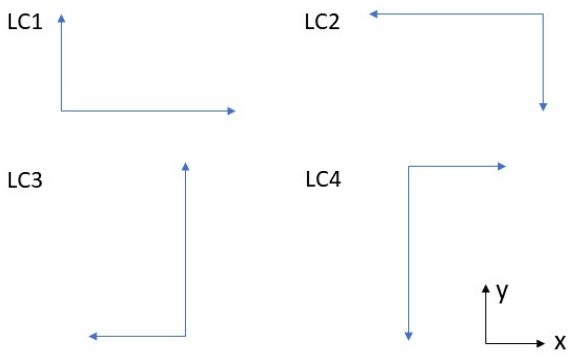

Figure 4.8: Graphical view of four load cases applied to the grillage. The directions and loads are equal for all towers

The load factors for the force in z-direction are taken downwards for all load cases. This is again a result of the fact that only a small amount of load cases can be considered within a reasonable time

frame. Only the negative force is considered, since that load is expected to be the most important case for the current analysis. This is a result of the fact that a downward force means that force from the heave motion and the weight are acting in the same direction. The downside of considering only negative heave is that no net upward force is applied in z-direction, which means a 'pulling' force in the ship. This can be of importance, because the strength of the steel in the deck might be different in through-thickness direction as a result of the manufacturing process.

The load factors for the rotations are chosen such that they amplify the forces. So that means that the for the x-force, the y-rotation should be positive and for the y-force, the x-rotation should be negative. That means that the worst case is considered, which is also required by the Class Guideline DNV-ST-N001 [16]. After the results for the single grillages were obtained, it became clear that a mistake was made in the calculation of the forces. For the first two loading conditions, the rotation around the y-axis was taken as working in the opposite direction to the force in x-direction. That means that the load on the grillage in that direction is smaller. For the full grillage, the load factors as described before are used.

The forces and moments are applied to the center of gravity of the tower. This location is represented by a distant node, which transfers the loads at this point to the top of the can, where in reality also the loads are applied. A schematic image (not to scale) of this is shown in Figure 4.9.

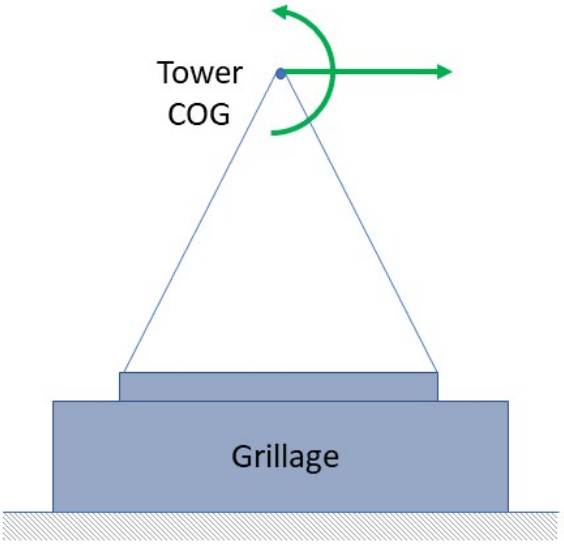

Figure 4.9: Schematic view of the application of the loads (not to scale).

The loads that are applied in this thesis are shown in Table 4.3. These forces are derived from the accelerations on the tower in the design of Vuyk Engineering.

Table 4.3: Loads that are used in the optimization

FX (kN)	FY (kN)	FZ (kN)	MX (MNm)	MY (MNm)	MZ (MNm)
973	1122	6361	29.4	25.1	0

4.5. Design variables

This model is built with the three groups of design variables: the thicknesses of the supports, the sides, the can and the flanges, and two angles describing the orientation of the radial supports. These angles are shown in Figure 4.10, where θ describes the angle with respect to the x-axis at which the radial support starts, and ψ describes the orientation of the support with respect to the normal of the can at the start location.

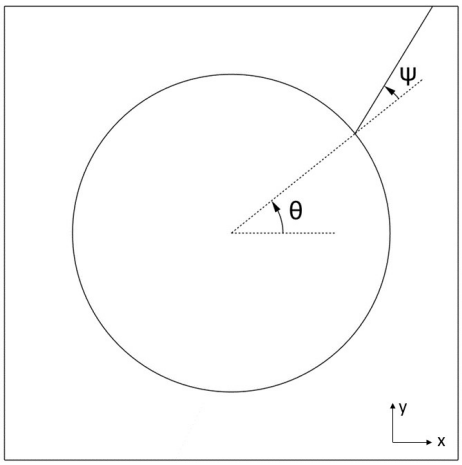

Figure 4.10: Figure showing the angles that are used to describe the orientation of the radial supports. θ describes the location of the start of the radial bracket and ψ describes the angle with respect to this line

For each of these values, a limit is chosen, both to improve the convergence and to improve the feasibility of the result. These limits are given in Table 4.4. The first parameter θ is different per radial support. This variation is described by the parameter $\theta_{initial}$, which is the angle of the considered support at the start of the optimization. In the first two steps, 10 supports are used, which results in initial angles that are 36° apart. For the last step, the full grillage, 16 supports are considered per layout, which means that the initial angles are 22.5° apart. This will be summarized in Table 4.5. The angles θ are constrained, to make sure that the radial supports cannot rotate around the whole can, but such that they stay in the same area.

Table 4.4: Limitations on the values that can be used in the optimization. The values for angle 1 describe the value with respect to the initial value.

Parameter	Type	Sign	Upper limit	Lower limit	Unit
Angle 1	Continuous	θ	-15 + $\theta_{initial}$	15 + $\theta_{initial}$	°
Angle 2	Continuous	ψ	-25	25	°
Thickness	Discrete	t	5	70	mm

The limits on the angle ψ are based on the assumption that larger angles are not likely to occur, because that means generally a longer, and thus heavier support. Also, larger angles mean that the supporting the loads is more difficult, which means larger stresses in these brackets. The limits for the thicknesses are based on manufacturability, but also on the freedom of the optimizer. The upper limit is chosen such that the thicknesses stay within reasonable manufacturable limits. Thicknesses above the given limit are not likely to be used, because these require a significant amount of welding effort and material. They are also based on some test runs, which show that the optimized thicknesses are generally not above 60 millimeter. Some extra room is added to make sure that the optimizer has enough design freedom. The lower limit is chosen such that the bracket is still able to support some load. It could have been beneficial to decrease this limit to zero, but that adds another layer of complexity to the implementation, because that means that the bracket needs to be removed in the FEA model. The limits for the thickness are the only discrete variables. This choice is made, because plate thicknesses are also only available in a discrete range. The other variables can well be continuous in reality, and they are therefore also kept as a continuous variable in the optimization.

The initial design vectors that are used in the optimization are described in Table 4.5. This table shows two different values for the initial values of angle 1, which each are specified for a different number of supports. The other values for the brackets, angle 2 and the thickness are specified once, because these are equal for all brackets in the optimization. The reason that the angles for 16 supports start at a value of 11.25 is that this distribution ensures that four supports connect to each side of the grillage. These angles are defined for one layout block, but they are equal for all four blocks.

Table 4.5: Start values of the optimization. The values for the supports that are defined once are equal for all supports.

Parameter	Value	Unit
Angle 1 (10 supports)	0, 36, 72, ..., 324	°
Angle 1 (16 supports)	11.25, 33.75, 56.25, ..., 348.75	°
Angle 2	0	°
Support thickness	45	mm
Can thickness	50	mm
Side thickness	50	mm
Flange thickness	50	mm

For the full grillage, four of the layout blocks as shown in Figure 4.3 are combined together. That means that the blocks share sides in the middle of the grillage. The brackets that are attached to these sides are considered to be symmetrical in the optimization, so they share their angles, as shown in the colored brackets in Figure 4.11. The same symmetry is applied to the other three shared boundaries. This reduces the number of design variables in the optimization, which is beneficial for the convergence of the algorithm. This symmetry is also present in the original design of Vuyk Engineering, which is at the basis of this design.

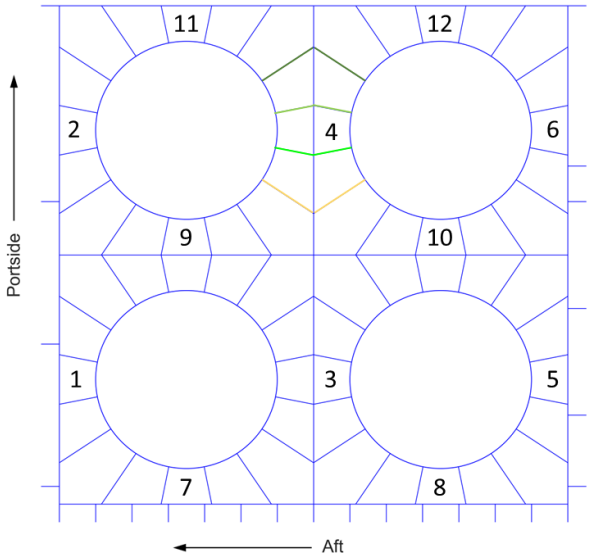

Figure 4.11: Example of the initial layout of the full grillage. The colored radial supports share their angles. This is the same for all other supports that share a side of the grillage in between. The numbers represent the different sides of the grillage

The sides of the grillage are split into 12 different parts with each their own thickness. The numbering of these elements is shown in the figure.

After defining the geometries, the boundary conditions, the loads and the important design parameters, the optimization can be performed. The results of this optimization will be shown in the next chapters.

5

Optimization results of the single grillage

This chapter will describe the results for the optimization with the single grillage. This will be explained in three steps. First, Section 5.1 will explain the outcomes for the single grillage on a rigid foundation. Next, Section 5.2 gives an overview of the results for the second step in the optimization, the single grillage with the ship underneath. After that, Section 5.3 analyzes the stress in a result from the first optimization with the ship as a boundary condition, to see the effect of including the ship as a boundary condition. Finally, the results will be concluded in Section 5.4.

5.1. Grillage on a rigid foundation

The first optimization step focuses on a single grillage where the ship is considered as a rigid foundation. That means that the only constraints on the optimization are the stresses in the grillage. This will give a better understanding of the optimization procedure, and it will give an indication of the results that can be expected in the next steps. The mass convergence and the corresponding layouts of this first optimization step are shown in Figure 5.1. The detailed numerical results per variable are shown in Table B.1 in Appendix B.

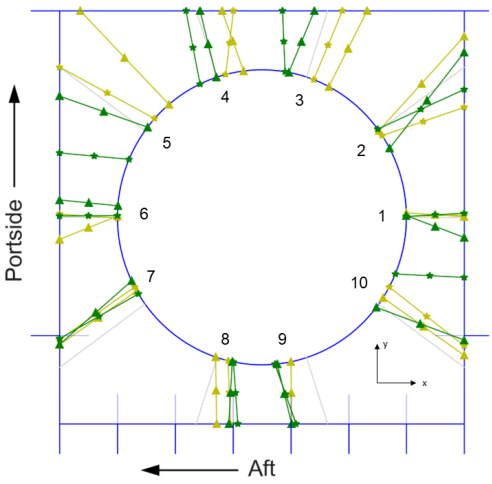

(a) Combination of the layouts of the different optimization runs. The grey lines are a reference for the initial layout of the grillage

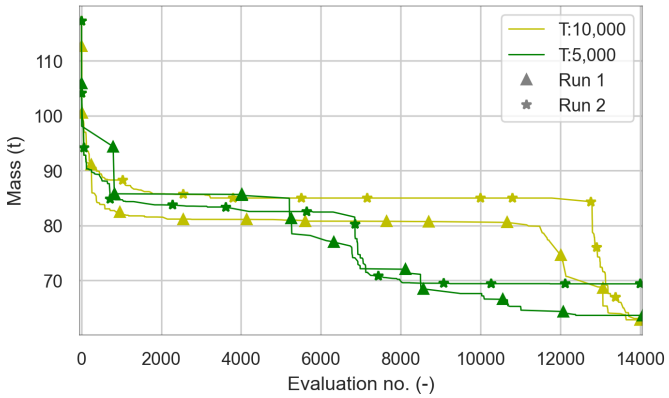

(b) Mass convergence for the different optimization runs

Figure 5.1: Optimization results for the single grillage on the rigid foundation

Figure 5.1a shows that only supports 1, 7, 8 and 9 have similar orientations, except one result for the first support. The other supports all have some kind of variation. This variation is mainly present for the supports in the upper half of the figure. This is the side of the grillage where the side shell of the ship is located in the next steps. Therefore, no outer brackets are placed on that side, which means that the stress is only transferred through the side of the grillage. However, on the other half of the grillage can be seen that the radial supports are optimized towards the outer brackets. That means that more load is distributed through these brackets and less through the side of the grillage. Both results have the effect that the stress in this plate is decreased, which means that its thickness, and thus the mass can be reduced.

As explained in Section 4.2, the bracket size changes when an intersection with a radial support is detected. This might also be a cause of the optimization of the radial supports towards these brackets, because that can cause the bracket to reduce in size, and a smaller bracket means a lower mass. This is however not in all cases true. For instance, the orientation of support 8 for the first run at a temperature of 10,000 is such that no intersection is detected, which means that the bracket is not removed. The same holds for support 10, where the orientation is also such that the bracket remains at that location. So, it is beneficial to optimize towards these brackets, regardless of they are removed or not, but an additional benefit is that the bracket is removed.

An interesting finding is that the results are approximately symmetrical around the y-axis, which is expected to be a result of the approximate symmetry in the load cases. The symmetry of the results is already seen in Figure 5.1a, but also the thicknesses of the radial supports as presented in Table 5.1 show this behaviour. For example, supports 3 and 4 show thicknesses in the same order of magnitude, again except the last run at a temperature of 5,000.

Table 5.1: Thicknesses in millimeter of the different elements in the optimized designs of the tower grillage on the rigid foundation. Also the mass per optimization run is shown.

	Support													
Run	**1**	**2**	**3**	**4**	**5**	**6**	**7**	**8**	**9**	**10**	**Can**	**Sides**	**Flanges**	**Mass (ton)**
Initial	*45*	*45*	*45*	*45*	*45*	*45*	*45*	*45*	*45*	*45*	*50*	*50*	*50*	*137.96*
T 10,000; run 1	8	10	16	18	10	9	11	23	22	11	25	12	26	62.82
T 10,000; run 2	8	8	19	18	12	6	20	15	23	13	24	12	31	63.06
T 5,000; run 1	7	14	18	20	16	10	11	25	18	15	20	12	34	63.62
T 5,000; run 2	15	6	20	13	10	5	15	17	20	16	32	13	34	69.37
Average	10	10	18	17	12	8	14	20	21	14	25	12	31	64.72
Difference	8	8	4	7	6	5	9	10	5	5	12	1	8	6.55

Figure 5.1b and Table 5.1 show that the mass converges to similar values for the different optimization runs. The difference between the three lowest values is only 1.27%. However, when the second run at a temperature of 5,000 is included, this difference is increased to 9.45%. This means that this is most likely an outlier, which shows that multiple runs are needed to verify if a result is indeed converged.

This last run is likely to be stuck in a local optimum, which might be caused by the lower temperature. The temperature determines how local the search is, as explained in Section 2.5. The runs for a temperature of 10,000 shows that the optimizer for other settings is able to escape from local optima. These runs seem converged early in the optimization (2,500 and 3,500 evaluations respectively), but that is only a local optimum. After a long time of not finding any significant improvement, suddenly a sharp decrease can be seen in the mass. This improvement may be a result of using a higher temperature, but more data is required to prove this.

It is also clear that especially for the runs at a temperature of 10,000, the mass is decreasing near the end of the optimization. That means that it is possible that these runs are not converged fully. Therefore, an extension to 17,420 function evaluations instead of 14,000 is done for the first run, but no further decrease in mass was found. That increases the certainty that these runs are converged.

Not only the mass is important, but also its composition from the thicknesses of the different elements in the optimization as presented in Table 5.1. This table shows that there is a large difference between

some of the thicknesses. When studying these values in more detail, it becomes clear that this is in most cases caused by only one variable that is different from the others. When, for instance, looking at the first support, we see that for the second run at a temperature of 5,000, the thickness is 15 millimeters, whereas the result for the other runs is 7 or 8 millimeters. This is however not the result of poor convergence of the considered support, because a sensitivity study of the results shows that the thicker supports cannot always be reduced in thickness without violating the stress constraint. That means that this is a result of the combination of the design variables. This can also be concluded from Table 5.1, which shows that most of the difference is caused by the second run at a temperature of 5,000, which also had the largest difference in mass, as shown in Figure 5.1b.

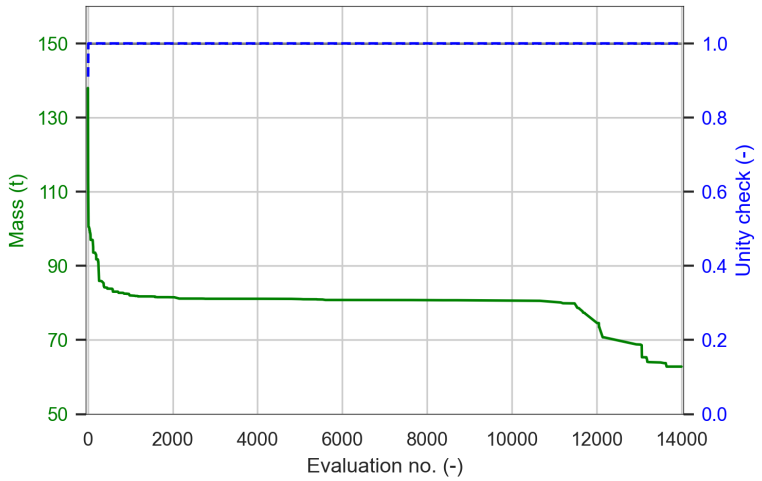

Figure 5.2: Mass convergence with the stress constraint for the first optimization run with a temperature of 10,000 of the single grillage on the rigid foundation. This figure is taken as an example for the other runs, which show similar behaviour.

Figure 5.2 shows the combination of the mass convergence and the unity check for the first run at a temperature of 10,000. This figure is representative for the constraint behaviour in the other runs, which are shown in Figure B.1 in Appendix B. This figure shows that there is only at the start a variation in the stress. This is because the stress in the initial layout is below the allowable level. After the first found optimum, the stress increases to the allowable stress level, after which it remains constant. This is caused by the peak stress function, which is explained in Section 3.5. The stress level in the grillage increases during the optimization, which means that peak stresses are also more likely to occur. As a result, the peak stress function is active for all the optimized grillages, resulting in a constant value for the constraint.

5.1.1. Variable analysis

Sensitivity study

Thusfar, only a visual inspection of the results is done. This does however not fully explain whether the results are really converged or not. Another way to look at the data is to do a small sensitivity check with the obtained results. That is done by decreasing the thicknesses one by one. This decrease is done in steps of 1 millimeter until the stress constraint is violated. So, after the lowest value for a given thickness is found, it is reset to its original optimized value, after which the same procedure repeats for the next thickness. The angles are only considered for the first run, but this showed that their influence on the mass is small compared to the thicknesses.

This study does not show the maximum improvement that can be made, because only a single variable is considered at a time. However, studying also the combinations of different design variables (for instance the thickness reduction of brackets 1 and 2 together) will make this study too large for its purpose: giving an idea of the possible improvements.

Table 5.2: Results of the sensitivity study of the different variables for the single grillage on the rigid foundation, showing the improvement that can be made manually.

Run	Optimized mass (t)	Improved mass (t)	Improvement (%)	Iterations (-)
T 10,000; Run 1	62.82	62.35	0.741	1
T 10,000; Run 2	63.06	62.85	0.331	6
T 5,000; Run 1	63.62	62.23	2.198	3
T 5,000; Run 2	69.37	69.32	0.079	2

The maximum mass decrease for each of the optimization runs that could be obtained with this study is shown in Table 5.2. The number of iterations describes the number of reductions to obtain the best improvement. This table shows that some improvement on the results can be made. An interesting result of this small study is that the results for the first run of temperature 5,000 can be improved quite easily. Figure 5.1b, however showed that the optimizer was not able to find improvements for a relatively long time. This is the result of the random nature of the optimizer, as explained in Section 2.5. On the other hand, the results for the second run of temperature 5,000 are converged well, although to a local optimum. Only little improvement can be made with this simple study, also when compared to the other runs.

The number of iterations shows that the improvement is dependent on the design variables that can be changed. For instance the second run at a temperature of 10,000 needs more iterations than the first run at a temperature of 5,000, while having a smaller improvement. This is caused by the thicknesses of the last three design variables, which have much more influence on the mass than the thicknesses of the radial supports.

Variable behaviour

Also the behaviour of the variables during the optimization is analyzed, to obtain a better understanding of the importance of these variables. First, the changes per variable (ψ, θ and t) are investigated by showing the change of each of the parameters per newly identified optimum. These changes are normalized with the maximum change for the considered variable that is made during the optimization. The result is shown in Figure 5.3. In this plot, only the results for the first runs at both temperatures are shown. The figures for the other two runs are similar to the figure at a temperature of 10,000. These figures are shown in Figure B.2 in Appendix B for reference.

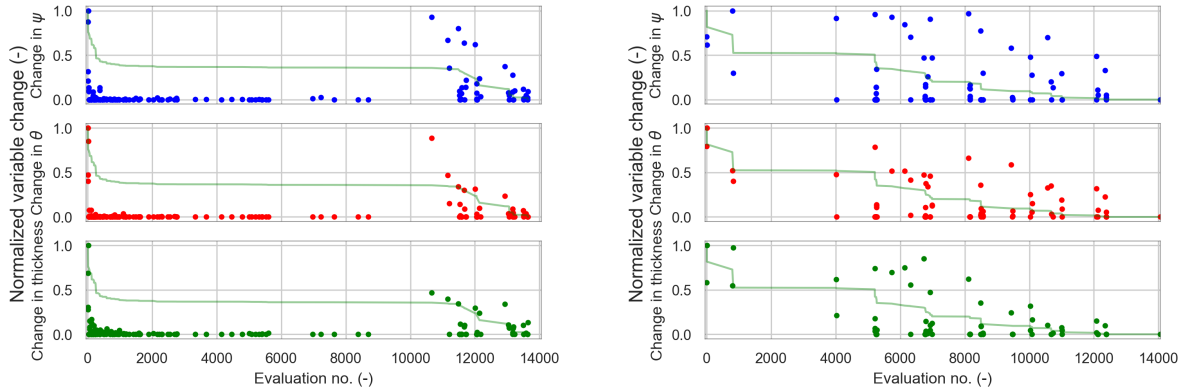

(a) Changes per variable type for the first run at an initial temperature of 10,000

(b) Changes per variable type for the first run at an initial temperature of 5,000

Figure 5.3: Changes per variable type for the convergence plots as shown in Figure 5.1b. The mass convergence graph is shown in the background for reference. The figures for the other results are similar to that of temperature 10,000

The results in this figure show a certain level of clustering in the results. That is especially clear in Figure 5.3b. The cause of this is that the optimizer has found an optimum at a different location, which means that it has found a new 'path'. The optimizer can find new optima around that point, resulting in the cluster that is observed. This is also caused by the switching between global (multi-variable) and local (single-variable) changes, as explained in Section 2.5. Every cluster is 'generated' in the local search part of the iteration, where the global search is responsible for finding the new search paths.

The runs at a temperature of 10,000 are escaping from a local optimum, as explained before. This is also visible in Figure 5.3a. During function evaluation 2,500 to 11,000, some changes are made, but no clear difference in the mass is observed. Also the relative size of the changes is small, which means that only local changes are made. However, after this period, the size of the changes is much larger, which means that a better optimum is found at a different location. That is also seen in the mass, which decreases substantially with these large changes.

The behaviour of the mass convergence graph for the second run at a temperature of 5,000 can also be better explained with Figure 5.3b. This figure shows that the relative change is large during the whole optimization. That also corresponds to the convergence line, which is decreasing much more gradually than the other figures. This difference between the runs is caused by the different random numbers, because the settings are kept the same for all the different runs.

5.1.2. Stress analysis

After the convergence and the behaviour of the variables is determined, the development of the stresses from the initial layout to the final result is studied. The expectation is that the stresses are globally at a higher level in the optimized layouts. To properly examine the results, the maximum stress over the four load cases for each of the elements is taken. The results in this section are presented for the first run at a temperature of 10,000, as the other ones are similar to this one. A global image of the stresses is shown in Figure 5.4. Elements with a red color show stresses that are above the allowable, but below the peak stress. So these elements are examined for peak stresses.

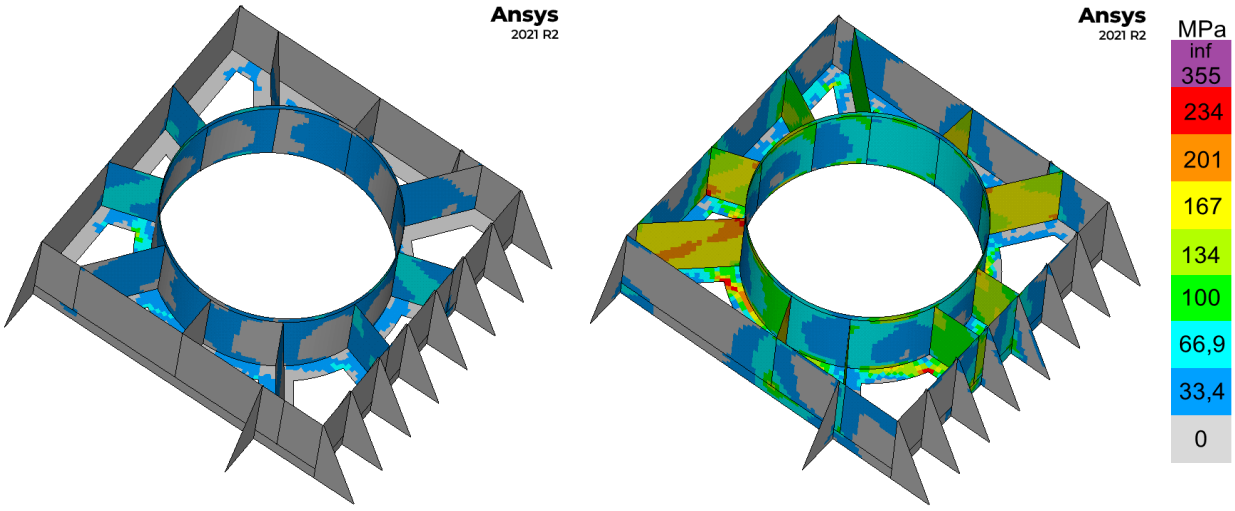

(a) Initial design **(b)** Optimized design

Figure 5.4: Comparison between the stress in the initial design of the grillage and the stress for an optimized design. The top flanges are deselected for a better view, but they are included in the calculation

Comparing the results of the initial grillage to the converged grillage indeed shows that the overall stress level is increased. However, the stress in some of the radial supports is still relatively low. That might give the impression that the mass can be decreased further, but that is only partially true. The sensitivity analysis showed that the radial supports with a low stress can indeed be decreased. But this decrease is small, because a decrease means a change in the stiffness of this support. That means that the load distribution in the grillage is different. That can have the effect that the stress in one of the other parts of the grillage is increasing above the allowable stress level. This is also shown in Table 5.2, where the number of iterations for the corresponding run is only 1. That means that the stress level will be higher if more changes are made.

This figure shows also that the stress in the sides of the tower grillage is generally low. This is caused by some small stress locations at the points where the radial supports attach. An example of this is shown in the left circle in Figure 5.5. This stress determines the thickness of the whole boundary, because such a stress location means that the thickness cannot be decreased without changing other parameters. These stresses will however increase in the real model, because manholes need

to be made in this boundary, which can be made at locations where the stress is low. These are not considered in the optimization, but in the final result, they need to be included.

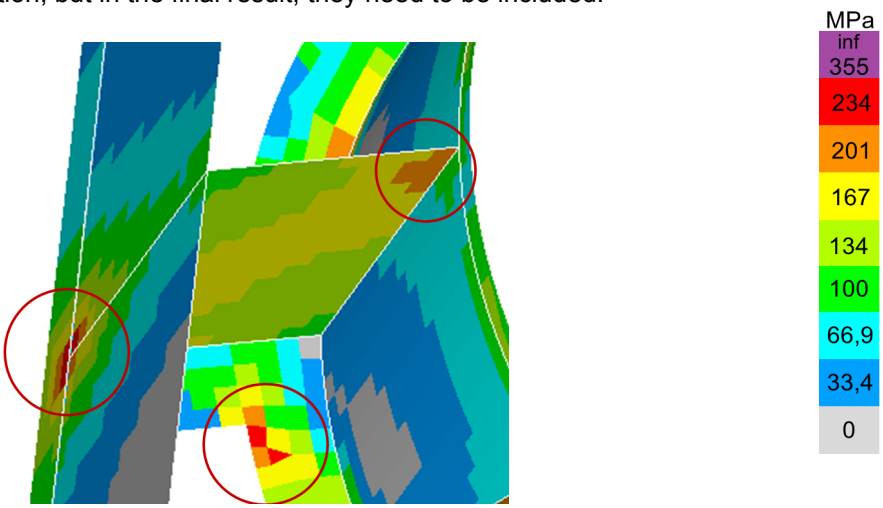

Figure 5.5: Example of typical locations with high stresses that occur in the optimized solution.

Two other typical locations where high stresses occur are identified: in the corners of the holes in the flange and at the corners of the radial supports. These are also shown in Figure 5.5. The stresses in the corners of the supports are mainly caused by the shear stress in that support. This shear stress also causes the stress pattern at the diagonal of the support, from the top of the can to the bottom of the boundary.

The stresses in the corners in the holes of the flanges are expected, because corners are typical stress locations. This is even increased because the corners are sharp. These are in reality rounded to have a better distribution of the stresses, but that would make the implementation much more complex, so that is not used in this thesis.

5.2. With ship

The second step is the optimization of the same grillage as explained in Section 5.1, but with the ship as the boundary condition. This will give more insight in the differences in behaviour of the optimization between the two different boundary conditions. The results of the mass convergence and the layouts for the different runs are shown in Figure 5.6. The numerical results per variable are shown in Table C.1 in Appendix C.

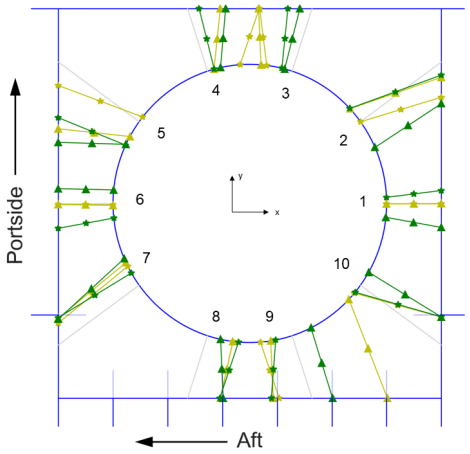

(a) Combination of the different layouts. The grey lines are a reference for the initial layout of the grillage

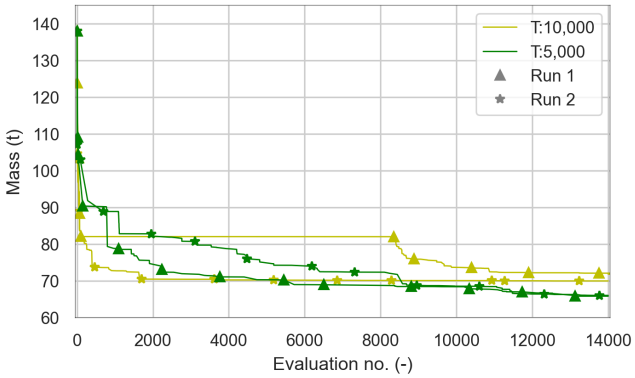

(b) Mass convergence for the different optimization runs

Figure 5.6: Optimization results for the single grillage with the ship as a foundation

One of the first things that is observed in Figure 5.6a is that the radial supports are overall more converged to the same location than the results without the ship. Also the gaps in the top left and right of the figure are larger than for the single grillage. These gaps are a result of the fact that a radial support that is located in this area has more length, and thus a higher mass. It is apparently more advantageous to place no radial supports at that location and to transfer the load to the ship further away.

For radial support 10, a remarkable difference is observed for the orientation of the support for the first run at a temperature of 10,000. It is not clear what is the cause of the orientation of this support, as the surrounding supports for this run are similar to the other runs. It is however interesting to see that this support is optimizing towards an outer bracket, although at a different location. Also on the other side of the grillage, supports 3 and 4, is shown that the supports for this optimization are behaving strangely, as they are close to each other. That might be a cause of the larger mass for this run.

The results for the optimization of the single grillage on the rigid foundation showed that the optimizer sometimes has supports that are relatively long. This is most clearly seen in supports 2 and 5. This behaviour is not present in the optimization of the full grillage. This is seen for each of the runs, so the conclusion can be drawn that including the ship is in this case beneficial for the consistency of the layouts.

Figure 5.6a shows the same symmetry about the y-axis as the single grillage on a rigid foundation, explained in Section 5.1. This is even more clear for the single grillage on the ship foundation, because the consistency of the layouts is larger. This symmetry is against the expectations, because the ship itself is not symmetric. That means that the ship is behaving differently at the front and aft of the grillage. That would mean that the interaction between the grillage and the ship is also different. This is however not the case, which means that the load on these grillages is not large enough to make this difference significant.

The results for the two runs at a temperature of 10,000 are higher than the results for the other optimization runs. That causes a difference in the mass results of 8.35%. The difference between the two runs at a temperature of 5,000 is however only 0.32%. This is particularly interesting, because their layouts are not the same. That suggests that there are many local optima that are close to each other. This suggests that the results at this temperature have a better performance for this particular optimization.

Table 5.3 shows that the thicknesses for the supports are generally in the same order of magnitude. However, the thicknesses for two large design elements, the can and the flanges, is different. The larger thickness of the flanges for the second run is a result of the orientation of brackets 3 and 4, which are very close to each other. That means that more force needs to be transferred via the flanges, so their thickness needs to be increased to deal with the higher stress.

Also the thickness for radial support 4 for the two runs at a temperature of 5,000 is higher than the others. Especially the thickness for the first runs is much higher than the others. It is not clear what the cause is of this behaviour, but the surrounding layout is similar to the other runs. Also the thicknesses of the surrounding supports is the same. In the sensitivity study, which will be presented later in this section, will be shown that this variable cannot be decreased to the value of the other thicknesses. That means that the thickness of this support is the result of the interaction between the different variables.

Table 5.3: Thicknesses in millimeter of the different parameters of the optimized design for the single grillage with the ship as a foundation. Also the mass per optimization run is shown.

	Support													
Run	**1**	**2**	**3**	**4**	**5**	**6**	**7**	**8**	**9**	**10**	**Can**	**Sides**	**Flanges**	**Mass (ton)**
Initial	*45*	*45*	*45*	*45*	*45*	*45*	*45*	*45*	*45*	*45*	*50*	*50*	*50*	*137.96*
T 10,000; run 1	8	22	17	12	15	6	12	14	8	6	43	11	33	71.80
T 10,000; run 2	5	13	16	11	9	5	12	17	12	9	15	15	48	69.95
T 5,000; run 1	6	18	14	39	12	6	15	19	13	5	21	12	39	65.80
T 5,000; run 2	11	11	17	20	6	7	16	15	11	9	22	9	44	66.01
Average	8	16	16	20	10	6	14	16	11	7	25	12	41	68.39
Difference	6	11	3	28	9	2	4	5	5	4	28	6	15	6.00

The average thicknesses for the radial supports in this optimization are generally lower than the results for the optimization with the rigid foundation. Only the thicknesses for supports 2 and 4 have a higher value. The higher value of the latter one is caused by the result of the first run at a temperature of 5,000, which has a large thickness for that support, compared to the other results. The largest differences are the thicknesses of the last two supports (9 and 10), which are 10 and 7 millimeters thinner, respectively. A cause of these differences is the interaction between the different variables, because these brackets do not violate the stress constraint if the grillage is placed on a rigid foundation.

The thicknesses for the can and the flanges have larger differences. These design variables describe the thickness of a larger surface than the radial brackets, which means that differences in these design variables are reflected more obvious in the total mass of the structure. The first difference is the mass of the can, which is generally lower, except the result of the first run at a temperature of 10,000. The thickness of the flanges is much higher. This is mostly caused by the larger stresses in the grillage due to the compliance of the ship, which will be shown in Section 5.3.

This table shows that a good general image of the required thicknesses can be obtained. This is also shown for the single grillage on the rigid foundation. The values should not be taken as an exact value, but they determine the order of magnitude that is required for the real grillage. There are some large differences between the results (for instance support 4), which shows that multiple runs are required to obtain this global image. One single run is not enough to explain if a thickness is an outlier or not.

The convergence plot for the first runs at both temperatures, combined with the constraints, are shown in Figure 5.7. Both figures are taken as an example for the results of that temperature, which shown similar behaviour. The figures for the other runs are shown in Figure C.1 in Appendix C. One similarity to the optimization of the grillage on the rigid foundation is that the stress in the grillage is again constant at the maximum value, caused by the peak stress evaluation function, as described in Section 3.5.

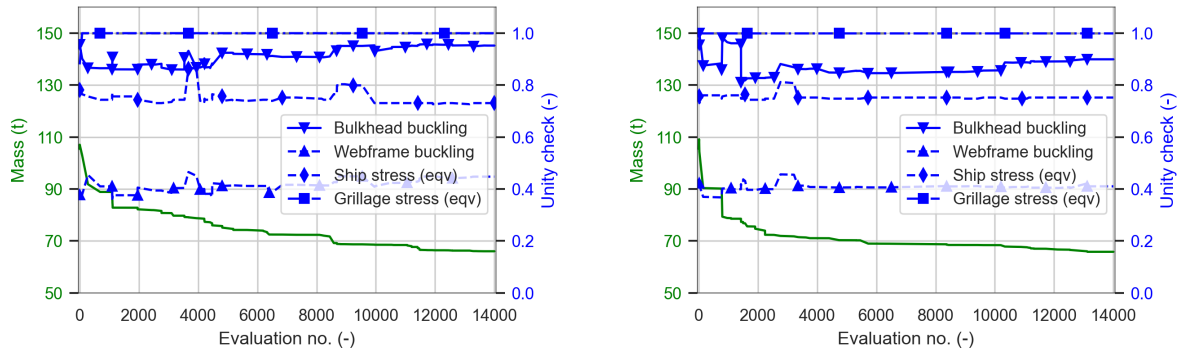

(a) Mass convergence with the constraints for the first run at an initial temperature of 10,000

(b) Mass convergence with the constraints for the first run at an initial temperature of 5,000

Figure 5.7: Mass convergence with the constraints for the convergence plots shown in Figure 5.6b.

An interesting finding is that the stress in the ship is not at the maximum allowable value. This might be caused by the fact that the loads in x-direction were smaller for this optimization, which means that the sensitive location in the ship experience less load, and thus has lower stresses.

Also the buckling usage factors are shown in this figure. These are clearly not active in the optimization. These low buckling factors have two causes. The first is that in this step, only one grillage is modelled. That means that the loads are different, especially at the locations where the different layouts connect in the full grillage. This is not implemented in this model, and the loads are therefore expected to be much different. The other reason is the low loads. These are especially small in x-direction, which is expected to be the most important direction, because there the gaps are located at the front of the grillage. So, based on these two reason can be concluded that the buckling is not representative for the full grillage. They do however show that there is some interaction between the stress and buckling constraints.

Buckling in the bulkheads is more important than buckling in the webframes for two reasons. The first reason is that the loads on the bulkheads are larger. These bulkheads experience a higher loading,

because the forces from the front and aft of the grillage and the webframe that is below these parts are transferred to this bulkhead, whereas the load on the sides is transferred to multiple webframes. The second reason is that the webframes are made from a material with a higher allowable stress. That means that these plates are able to carry a higher load before buckling becomes important.

5.2.1. Variable analysis

Sensitivity study

Also for this optimization, a sensitivity study is done. For this study, the same procedure is used as described in Section 5.1.1. The results for this study are shown in Table 5.4.

Table 5.4: Results of the sensitivity study of the different variables in the optimization of the single grillage with the ship as a foundation. This table shows that only small improvements can be made

Run	Optimized mass (t)	Improved mass (t)	Improvement (%)	Iterations (-)
T 10,000; Run 1	71.80	71.71	0.115	3
T 10,000; Run 2	69.95	69.89	0.079	2
T 5,000; Run 1	65.80	64.88	1.402	1
T 5,000; Run 2	66.01	65.96	0.068	1

This table shows that the results for this optimization step are more converged than for the optimization on the rigid foundation. Only a few iterations can be made to reduce the thickness. The largest possible improvement is the result for the first run at a temperature of 5,000. This is however the result of a decrease of only 1 millimeter in the thickness of the sides of the grillage. This has a larger impact, because of their relative weight compared to radial brackets.

The first run at a temperature of 10,000 requires the most iterations for the given improvement. This improvement is only 90 kilograms. This is caused by the fact that this optimization is in support 6, which is one of the shortest supports in the optimization. That means that a decrease of 3 millimeter has only little impact on the total mass of the structure.

Variable behaviour

To follow the same structure as for the single grillage, now the variable behaviour will be explained. The changes per variable type are shown in Figure 5.8. The figures for all four runs are shown in Figure C.2 in Appendix C.

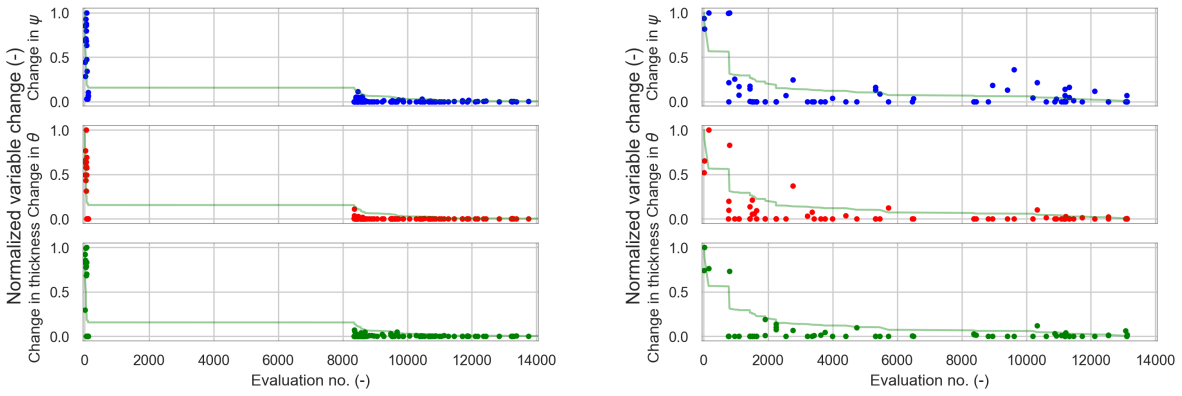

(a) Changes per variable type for the first run at an initial temperature of 10,000

(b) Changes per variable type for the second run at an initial temperature of 10,000

Figure 5.8: Changes per variable type for the convergence plots shown in Figure 5.6b. The line of the mass convergence is shown in the background for reference

This figure shows that the change is the largest at the start of the optimization, and smaller near the end. This is in accordance with Figure 5.6b, which shows a large decrease in the first steps, and a smaller decrease in later iterations. This also explains the difference to the convergence of the optimization

with the rigid boundary condition. There, the decrease was also large in the earlier iterations, but in later stages, again a decrease is found. That was also reflected in the relative changes of the variables, which were larger in later iterations.

Figure 5.8a shows some strange behaviour, because in the first iterations, the mass is decreasing very rapidly, while after that, no improvement is made for approximately 8,000 function evaluations. Similar behaviour was shown for the optimization of the grillage on a rigid foundation, where the runs at a temperature of 10,000 were also stuck on a local optimum for a long time. In that optimization however, the optimizer still found new optima during the iterations that no clear improvement was found. This is shown in Figure 5.3. It is not clear what the cause is of this behaviour, but it might be the cause of the higher mass for this run.

The results in Figure 5.8b show a much larger relative change and variability over the iterations. This is however not reflected in the mass convergence figure, which is nearly constant from halfway the optimization. That means that still new optima were found, but the improvement is much smaller.

5.2.2. Stress analysis

This section shows the stresses in both the ship and the grillage for the optimization result of the first run at a temperature of 5,000. The stress in the ship is shown in Figure 5.9. This is the maximum stress per element over the four load cases. This figure shows that the stress in the ship is overall quite low. That is also seen in Figure 5.7 where the unity check for this constraint was below 1.

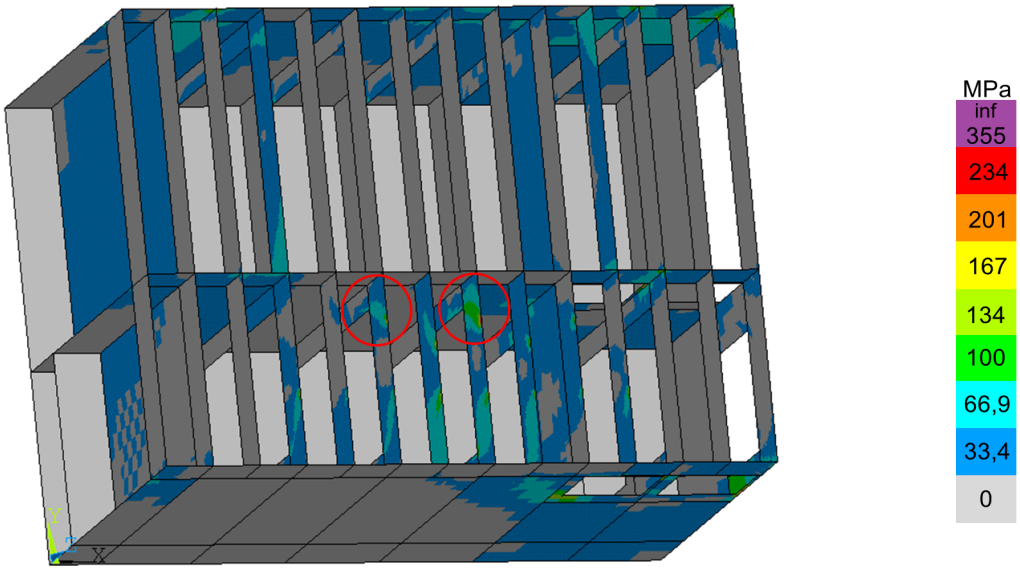

Figure 5.9: Finite element stress in the ship with the grillage and the decks deselected

This figure show clearly the interaction between the outer brackets and the ship. The two locations that are shown in the red circles are the locations where the radial supports are close to the outer brackets. This shows that the stress is indeed increased at these locations. Also the stresses in the fourth web frame from the aft and the front side of the model show higher stresses. That is the location where the boundary of the grillage attaches. The longitudinal bulkhead at these locations has also higher stresses, which is too a result of the outer brackets that attach at these locations and the radial supports that attach to these brackets.

The stress in the grillage is shown in Figure 5.10. This figure shows the same trend as for the optimization without ship. One important difference is that the stress in the initial grillage is lower for this setup, when compared to the optimization without ship, while the same thicknesses are used. That suggests that the mass could be decreased even more than the results as found without the ship. That is however not the case, as shown in Table 5.3.

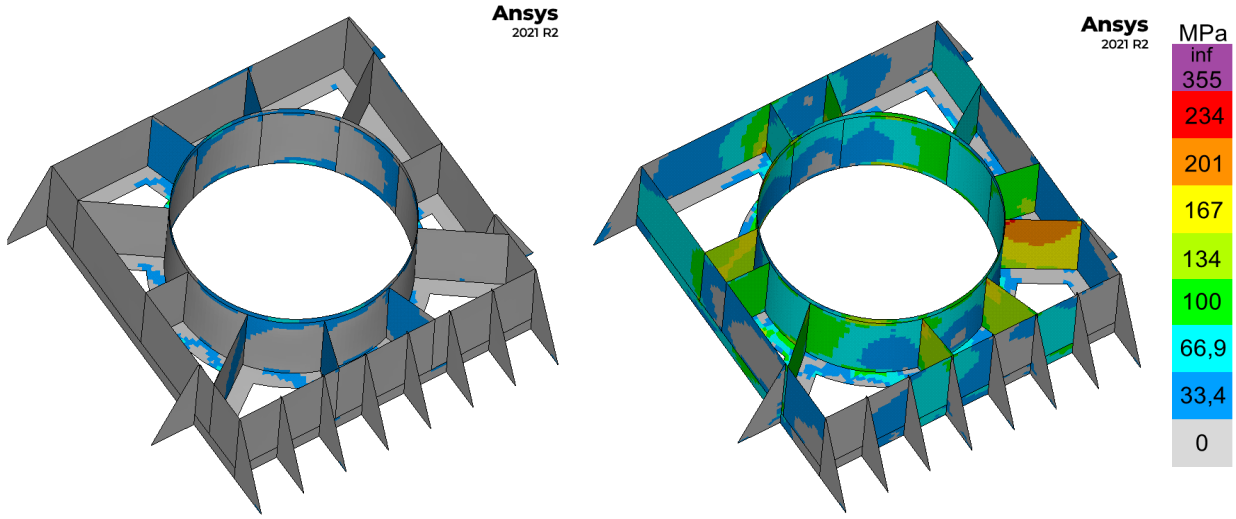

(a) Initial design **(b)** Optimized design

Figure 5.10: Comparison between the stresses in the initial design and the optimized design for the single grillage with ship

Further analysis of the differences in stress and stress patterns to the optimization on the rigid foundation will be shown in the next section.

5.3. Stress evaluation

This section describes the interaction between the ship and the grillage. For that purpose, the result of the first run at a temperature of 10,000 for the grillage on the rigid foundation is taken. This grillage is also analyzed with the ship as a boundary condition, to see how the stresses change. This showed that this grillage cannot be placed on the ship without violating the constraints. That is however not the stress or the buckling in the ship, but the stress in the grillage, as also found for the optimization with the ship. The causes of the changes are examined in more detail. First, a global image of the stress is presented in Figure 5.11.

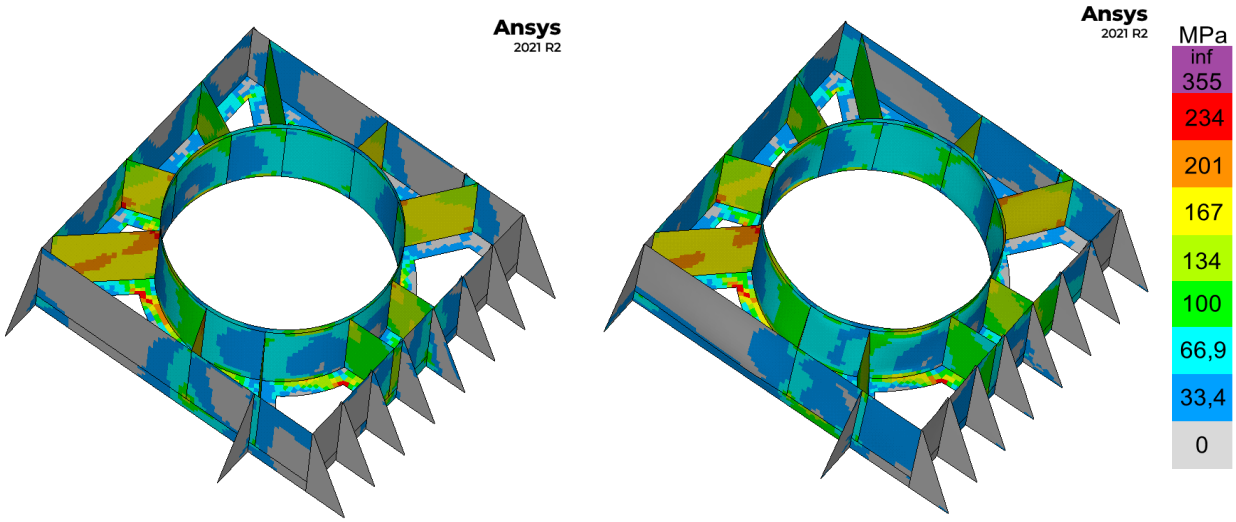

(a) Grillage on the rigid foundation **(b)** Grillage on the ship

Figure 5.11: Stress in the grillage that is optimized for the rigid foundation. This grillage is placed on the ship to show the differences in stress.

The stresses overall are similar, as shown in this figure. This is especially true for the stress in the

supports. These seem maybe different at first glance, but that is caused by stresses that are close to a step in the color legend. The differences that exist are caused by the compliance of the ship, which means a slightly different distribution of the stresses over the different supports. There are also three main regions where the stress is different: the sides of the grillage, the flanges and the can. That means that the parts that contribute most to the mass of the grillage experience the largest difference.

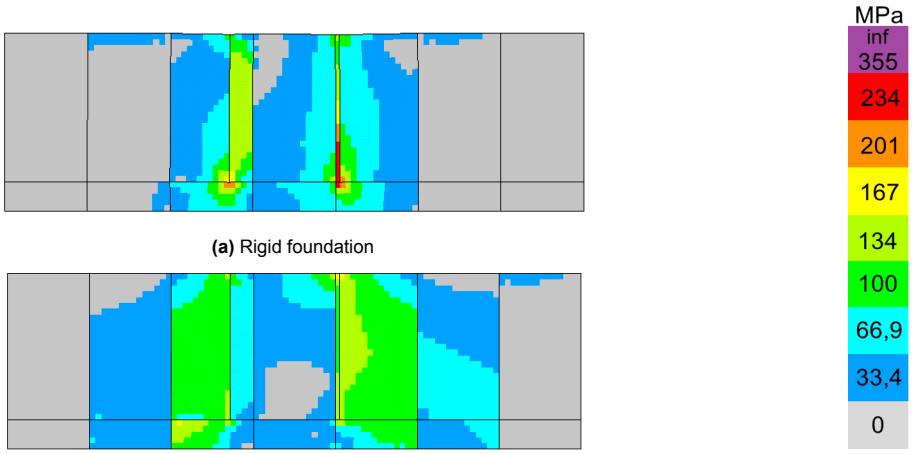

(a) Rigid foundation

(b) Ship foundation

Figure 5.12: Maximum stresses in the sides of the grillage. This figure shows how the stresses differ between the two different boundary conditions.

The first difference is the stress in the outside of the grillage. This stress is divided more equally when it is placed on the ship. This is caused by the difference in compliance between the two foundations. Figure 5.12 shows an example of this at the inside of the grillage. The equally spaced lines represent the locations of the outer brackets. The other two lines are the connection points of the radial supports. In Figure 5.12a, the stress is high around the radial supports, and also at the peak stress level. These stresses are however not present in Figure 5.12b. Also the distribution of the stress over the area is different. Figure 5.12a shows that the stress extends to the first available bracket, whereas the stress for the grillage on the ship shows that the stress extends to the the second bracket. This shows that the stress is divided more equally over the brackets, which means that peak stresses are lowered. That can have the result that the thickness can be reduced, or that the radial brackets can be placed closer to each other. The latter is indeed shown in Section 5.2.

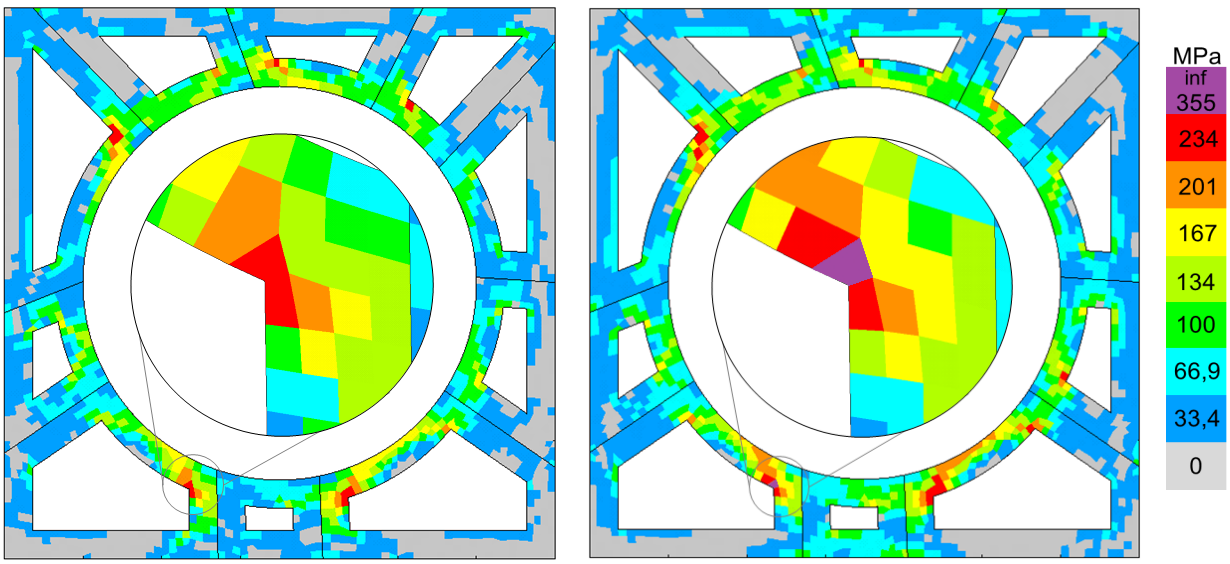

(a) Stress in the flange of the grillage on the rigid foudation

(b) Stress in the flange of the grillage on the ship

Figure 5.13: Maximum stresses in the flange of the grillage for both boundary conditions. The close-ups show how the peak stress differs between the solutions.

The second difference is the stress in the flanges, as shown in Figure 5.13. This figure shows two main differences. The first difference can be seen in the peak stresses. These increase above the peak stress, what is shown in the close-ups of Figure 5.13. This difference is small, but it does still mean that the stress constraint is violated, and this will thus not be accepted in the final solution. The other difference is the stress in the part of the flanges that is connected to the outside of the grillage. These parts are in the solution without the ship not that highly loaded, but on the ship, these parts become more important. This shows the interaction with the outside of the grillage, which is also a cause of the more distributed load.

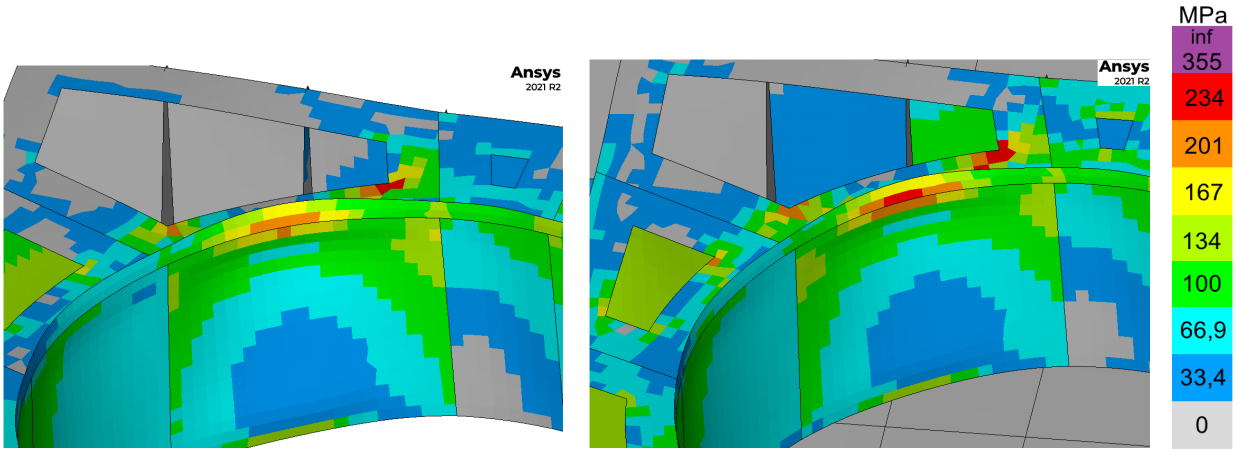

(a) Stress in the can of the grillage on the rigid foundation **(b)** Stress in the can of the grillage on the ship

Figure 5.14: Comparison of the stress in the can when a grillage is placed on the ship

The last difference is the stress in the can. The general pattern of the stress is similar, but at some locations, a considerable increase in the stress can be observed. This is generally in the corners of the grillage, where the optimizer did not place any radial supports. As a result, the negative z-displacement of the can is larger at that location, which results in a larger compressive stress at the top of the can. This effect is larger when the grillage is placed on the ship, resulting in a larger stress.

So the radial supports itself show little difference in stress. However, the items that have most influence on the mass, the sides of the grillage, the flanges and the can, are most different. The typical stress locations, as presented for the single grillage in Figure 5.5, remain the same, although the magnitude is different.

5.4. Conclusion

The results in this chapter gave more insight in the behaviour of the optimization, and they explained the influence of the ship on the results. Visual inspection of the layouts showed that there is variability between the results, but the overall picture is clear. The results with the rigid foundation have a larger difference than the results with the ship as a foundation, which might be caused by the differences in stress between the two different boundary conditions.

The optimal distribution of the radial supports in the grillage is dependent on the location of the outer brackets for both optimizations. That has the effect that the loads are more directly transferred through these brackets and less through the sides of the grillage. Also the part of the algorithm that reduces the bracket size at intersections has influence on this result.

For the optimization with the rigid foundation is shown that the difference in mass between the different results is 9.45%. However, when the largest mass of the runs is excluded, this difference drops to 1.27%. For the results with the ship as a foundation is shown that the results are 8.3% different between the different runs. When only the results for a temperature of 5,000 are taken, this difference decreases to 0.32%.

The average mass is different between the two optimizations. The mass for the grillage on the ship is 5.7% larger than for the optimization on the rigid foundation. This is mainly caused by differences

in the thicknesses of the flanges. These have a higher thickness in the optimization for the grillage on the ship, which increases their mass.

This is caused by the differences in stress in these elements. It is shown that the stress in the flanges and the can is increased when the grillage is placed on the ship. The sides, on the other hand, also experience an increased stress, but the peak stresses are lowered. The effects of stress and buckling in the ship are not important for the optimizations in this chapter, because their constraints were not active. The differences in the results show that the layouts cannot be interchanged without adapting the design. That means that including the ship is still important, even if it does not influence the optimization directly through the constraints of its own strength, but indirectly by the compliance of the structure.

Chosen temperature

Based on the results for this chapter can be concluded that the temperature did not have a large influence on the results of the optimization with the rigid constraint. However, the results at a temperature of 5,000 showed more variability and they had a higher mass. For the optimization of the grillage on the ship is however shown that the results for a temperature of 10,000 had higher masses. The layouts were however similar.

From that, the conclusion is drawn that no real advantage of one of the two temperatures could be observed. For that reason, the locality of the search was taken as the guiding aspect for the choice of the temperature. The expectation is that the search space for the full grillage will have more local optima, and therefore a more global search might be advantageous for the final result. That led to the choice of a temperature of 10,000 for the full grillage.

6

Optimization results of the full grillage

This chapter will explain the results for the full grillage. This result is divided in two steps: a first iteration with an initial design where the stress constraint was violated. This is shown in Section 6.1. During the optimization became clear that this optimization was not able to find a solution without constraint violations. Therefore, an adaptation is made to the design, which is explained in Section 6.2. After that, Section 6.3 will explain which manual step needs to be made to make the design more manufacturable and what the improvement of the optimized design is with respect to the original design by Vuyk Engineering. Section 6.4 will end with a discussion.

6.1. First iteration with initial bracket design

The results for the single grillage showed that the optimizer did not encounter problems with the external constraints. For the full grillage however, the stress constraints were violated severely, even in the initial solution. Two shorter optimizations of 7,000 iterations were run to see whether the optimizer was able to decrease the stress in the ship to allowable values, but it turned out that this is not the case.

The main finding of these runs is that the objective function decreases, but the maximum stresses remain at a similar level, as shown in Figure 6.1. The mass however increased at the initial stage, and it remained high during the optimization. The decrease in function value is mainly caused by a global decrease in stress. That means that the number of elements with a high stress and the height of that stress is decreasing. This does however not directly mean that the maximum stress is reduced. This will be shown in more detail later in this section.

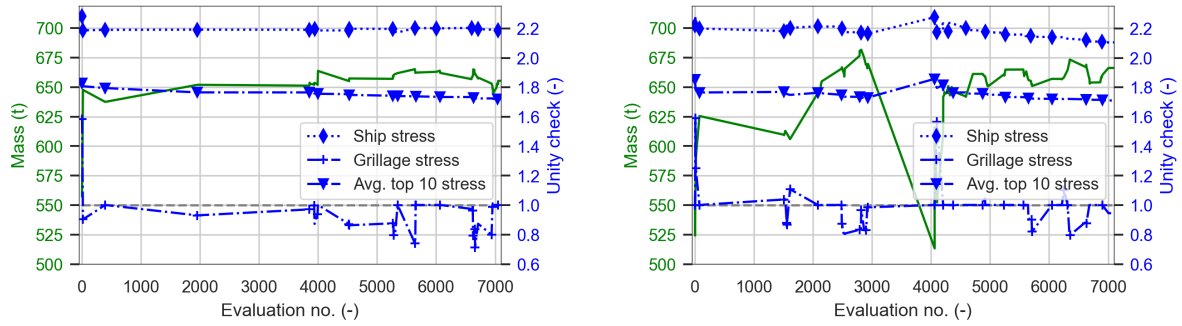

(a) Convergence for the first run

(b) Convergence for the second run

Figure 6.1: Convergence and objective for the first two optimization runs of the full grillage.

The increase in mass is caused by the settings of the penalty function. The violation of the mass is in the order of 1, but the stress has a much higher order of magnitude. First, because multiple elements violate the constraint, which all add a penalty to the objective function. The other reason are the factors that are used in the penalty function, as described in Section 3.4. The violation is squared and multiplied by 100, which means that this value is in the order of 100, for a unity check of 2.2 (which means a

violation of 1.2). This means that the stress is much more important than the mass when the constraints are violated severely. These settings are however necessary to keep the stresses acceptable when they are near the allowable stress.

Figure 6.1 shows three different lines for the stresses: the maximum values for the stresses in the ship and the grillage, and the average of the 10 elements with the highest stress. This average is shown to have a measure for the extent of the stresses. The mean is still close to the maximum stress, which shows that the extent is relatively large. This will also be shown in Figure 6.2. An interesting result is that the shapes of the maximum stress, which is the stress in the ship, and the top 10 average are similar. A more in-depth analysis of the values shows that overall, the mean of the stress is decreasing, although slowly. However, for the increase of the second run, between 3,000 and 4,000 function evaluations, all elements in the top 10 show an increase, which is most likely caused by the fact that these elements are all in the same area, what will be shown later in this section.

The line for the ship stress, which is also the maximum stress, is nearly constant at a value of 2.2, especially for the first run. That indicates that the optimizer is not able to make a significant decrease in this value. For the second run, some decrease is seen, but this is too small to conclude that the optimizer can find a solution without violation.

An interesting result is that the maximum in the grillage is generally below, or at least close to the allowable value. That indicates that the optimizer is able to keep a constraint allowable, even if other constraints are violated severely. This is not accounted for implicitly in the penalty function, and it gives therefore an indication that this function is working properly. For the second run, more violations are observed, but these are still very low. On top of that, these violations are present for only a small amount of time, which means that these are most likely not problematic.

The geometry of the most sensitive part of the structure was shown in Figure 4.5. This figure shows that a side of the grillage is located above the left hole, where a webframe is present in the ship. This already explains why the stress is high at this location, because the load from the webframe is transferred to the bulkhead. It was expected that the optimizer would be able to decrease the stress by placing the radial supports further away from this location, so that more load is transferred to other parts of the structure. This is however not the case, as shown in Figure 6.2. This figure shows two close-ups of the stress at this location in the initial design and the optimized design.

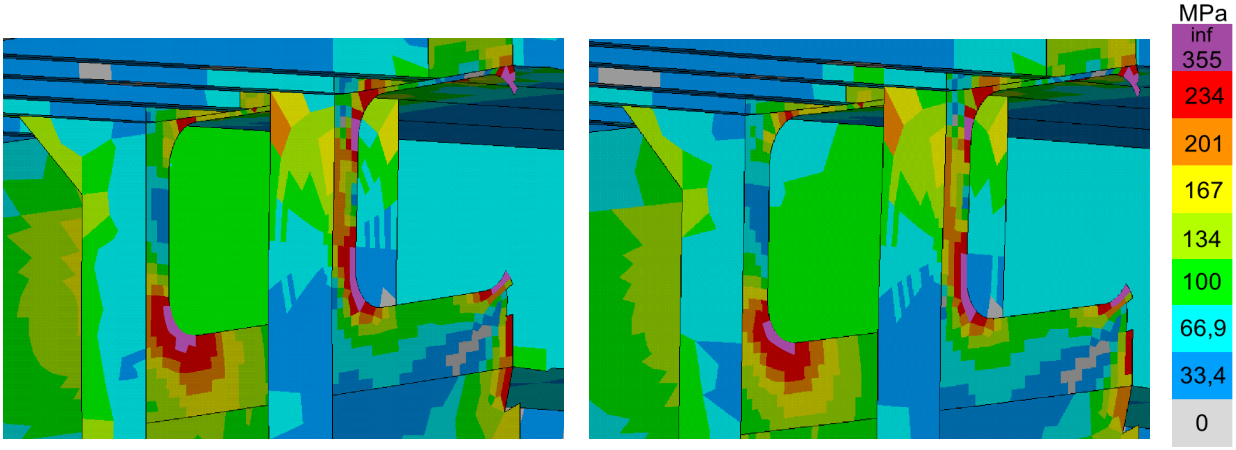

(a) Stress for the initial design of the grillage

(b) Stress for the optimized design of the grillage

Figure 6.2: Comparison of the stresses in the ship, with the full grillage on top. Optimized for the initial setting of the full grillage.

It is visible in this image that the extent of the stress is decreasing, which is the cause of the decrease of the objective function. The decrease is however clearly not large enough, particularly when considering the amount of iterations. The stresses are still above the peak stress level, and besides that, the stress locations are still too large accept it as a not important peak stress.

The layouts for the two optimization runs are shown in Figure 6.3. The red spots in the figure highlight the weakest bulkheads in the ship. The bulkhead with the light red color has no violations, but

only high stress. At the location of the darkest circle however, the stress constraint was violated. It was expected that the optimizer would place the radial supports away from this location, in order to transfer more load to other parts of the ship, and less to this location. This is visible in the result up to some extent, but it is not clear whether this is really an effect of the stress constraint or that it is caused by another effect, because the effect is much smaller for the second run.

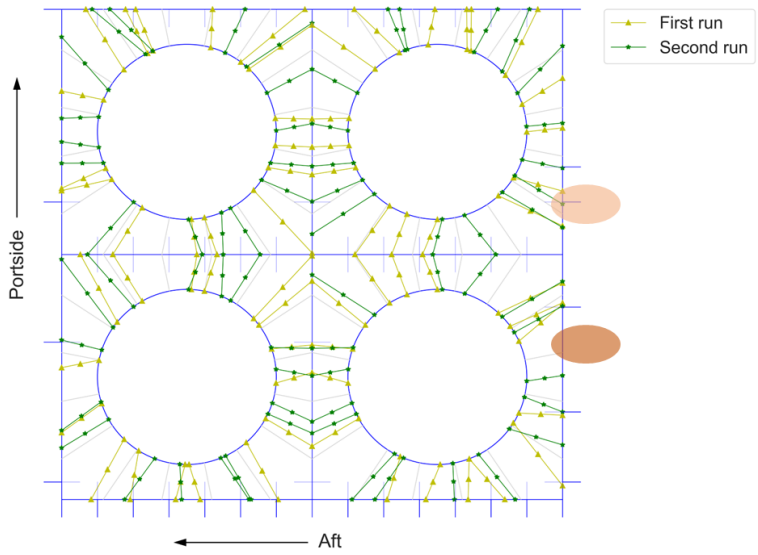

Figure 6.3: Comparison between the layouts of the two optimization runs for the full grillage. For these runs, the initial stress was higher than the allowable stress and the result contained still overstressed elements. The red parts highlight the most important weak parts in the ship.

This figure shows that there is no clear similarity between the two results. This is expected to be a result of the fact that the stresses could not be decreased substantially. That means that the optimizer was acting as an optimizer with two constraints, the mass and the stress. The mass can easily be related to the different design variables. For instance, the thickness directly influences the mass of the structure. This is however not true for the stress. A change in thickness can influence the stress in a certain element, but this is also dependent on the other design variables. It is therefore expected that it is harder to obtain a consistent result with the stress as objective.

A reason that the stress constraint is still violated in the bulkhead is the bracket shape. This is a triangular shape, as shown in Figure 4.4. The result of this shape is that the force is transferred to the next webframe, which is also connected to the weak points. That means that it is advantageous to transfer the stresses further forward in the ship. This is done in the second iteration for this grillage, what will be shown in the next section.

6.2. Optimization with new bracket design

Although the previous analysis showed that the stress level is decreased during the optimization, it is not enough to find a feasible solution. Also, the found decrease is coming at the cost of an increase in mass of around 50% compared to the design by Vuyk Engineering. To overcome the most important problem, a solution is sought in a new bracket design that decreases the stress in the bulkhead.

6.2.1. Model adaptation

Because the results of the first optimization runs were not satisfactory, enhancements need to be made to obtain a feasible initial result. The front side of the grillage is the most sensitive part, as explained in Section 6.1. For that reason, the brackets on the front side are adapted, such that they are similar to the brackets of the original design by Vuyk Engineering. The result is shown in Figure 6.4. This bracket shape ensures that that the load is partly transferred to the stronger parts that are further forward in the ship, which reduced the stress in the bulkhead to an acceptable level.

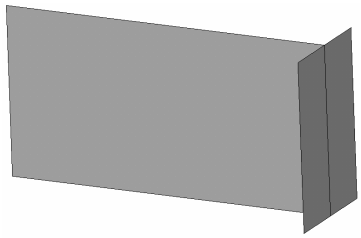

Figure 6.4: Updated bracket design on the front side of the grillage.

This bracket shape was not implemented in the initial model, because the intention of the optimization was that the optimizer should find a design that meets the requirements for a relatively simple input. This new bracket design means that more effort from the designer is required before the optimization is able to find a feasible outcome.

6.2.2. Results

After this design was made, another group of optimization runs is done to find out which reduction can be obtained and what the corresponding layouts are. The layouts are shown in Figure 6.5 and the corresponding thicknesses are shown later in this section in Table 6.1. Detailed numerical results per variable are shown in Appendix D. The stress results in this section will be compared to the stress in the original design of Vuyk Engineering, to get a better understanding of the improvement of the solution.

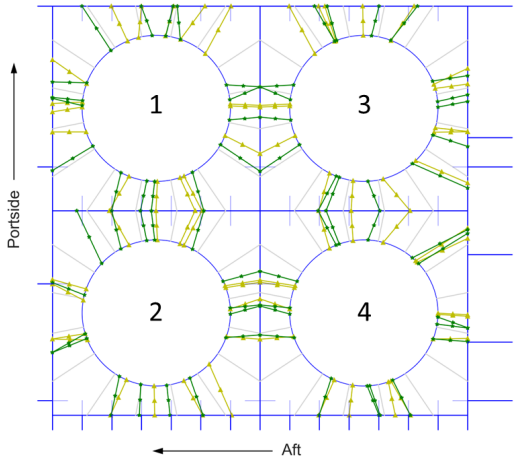

(a) Combination of the different layouts. The grey lines are a reference for the initial layout

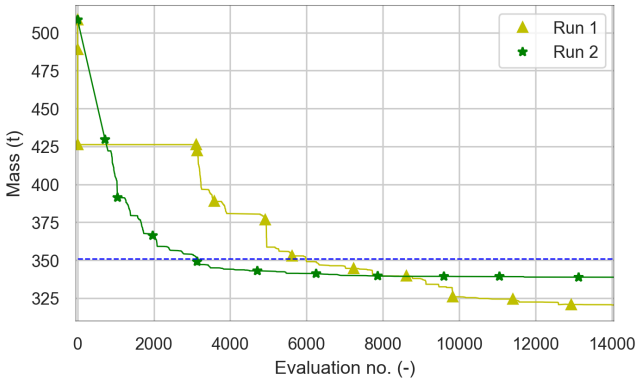

(b) Mass convergence for the different optimization runs of the full grillage with the ship. The blue line represents the mass of the original design by Vuyk Engineering

Figure 6.5: Optimization results for the full grillage with ship

This figure shows that some reduction of the mass in the grillage can be obtained with respect to the initial mass, but also to the mass of the original design of the grillage, which has a main steel weight of 351 tons, as shown by the blue line. The optimized masses are 319 and 339 tons. This means improvements of 9.1% and 3.5%, respectively. This is quite a large difference between the results, but it is promising to see that they are in the same order of magnitude, and that they are both below the original mass. A possibility for further reduction of the mass is decreasing the mass of the outer brackets. These have a slightly higher mass in the optimization than for the original design by Vuyk Engineering and they are not optimized. That means that these brackets might have a negative influence on the optimized mass.

Also the layouts are different between the runs. The radial supports are only in a few cases optimizing towards similar locations for both runs. That means that no clear pattern of the individual supports can be identified, what was the case for the optimizations of the single grillages. One of the causes of this is that this optimization has a larger number of design variables. That means that an optimizer has generally more difficulty with finding an optimum. This can both affect the convergence speed and the quality of the result.

Despite these differences, also some global similarities can be observed. The first is that near the corners, only few radial supports are placed, with the only difference the radial supports in the top right of grillage number 4. The reason that only few radial supports are placed at these locations is because the closer to the corner, the larger the support, and thus the larger the mass of that support. It was expected that the radial supports would be placed more in the direction of these corners, because the

vector of the combined load cases is pointing in the direction of these corners, as shown in Section 4.4. It is therefore interesting to see that it is not necessary to place supports at these locations, and that placing brackets at such a distance still results in a lighter solution.

The second similarity is that some supports within on solution are close, or even overlapping each other. This happens for both runs. It is however not in correspondence with the requirement of manufacturability, as connected to the research question in Section 1.4. This is resolved manually after the optimization by taking the average orientation of these supports and the sum of the thicknesses. The results of that will be presented in Section 6.3. This gives an indication that less radial supports can be used than the initial 16, which might be advantageous for welding lengths.

The last similarity is that the results of the for each of the layouts can be divided in four groups: one group on each side of a layout. The groups in y-direction contain generally more brackets, which is expected to be a result of the larger force in y-direction. That means that more load needs to be carried by the supports and the ship. These results suggest that it is more efficient to carry this by more supports than by thickening these supports. Another factor might be that at these locations, more radial brackets are located. It is shown for the single grillage that these brackets are one of the aspects that determine the layout of the radial supports.

Another interesting result is that the radial supports on the top right of grillage 4 are optimizing towards a similar point. Normally, when such a location is observed, either the supports are short, or an outer bracket is located at the point of convergence. It is however in this case not clear why these brackets are optimizing towards that point.

The thicknesses corresponding to the given layouts are shown in Table 6.1. The numbering of the supports has the same order as for the single grillage: starting from the right side of each grillage block and then counterclockwise around the can.

Table 6.1: Thicknesses of the different elements of the design in millimeters.

		Support															
Grillage number		**1**	**2**	**3**	**4**	**5**	**6**	**7**	**8**	**9**	**10**	**11**	**12**	**13**	**14**	**15**	**16**
	Initial	*45*	*45*	*45*	*45*	*45*	*45*	*45*	*45*	*45*	*45*	*45*	*45*	*45*	*45*	*45*	*45*
	Run 1	7	8	9	20	28	8	10	7	13	13	40	9	11	7	20	11
1	Run 2	7	13	14	10	14	10	14	6	8	14	7	13	19	15	15	8
	Difference	0	5	5	10	14	2	4	1	5	1	33	4	8	8	5	3
	Run 1	19	7	6	15	17	22	10	11	22	13	13	13	10	13	8	10
2	Run 2	14	7	15	27	13	7	12	16	12	6	14	6	9	15	9	36
	Difference	5	0	9	12	4	15	2	5	10	7	1	7	1	2	1	26
	Run 1	7	13	15	12	14	11	7	7	24	12	9	15	16	10	6	6
3	Run 2	6	11	9	38	6	13	24	9	8	11	15	21	16	6	32	18
	Difference	1	2	6	26	8	2	17	2	16	1	6	6	0	4	26	12
	Run 1	8	7	18	9	14	12	10	5	7	17	32	6	16	8	11	22
4	Run 2	8	13	15	15	8	15	9	15	7	12	18	8	8	12	14	9
	Difference	0	6	3	6	6	3	1	10	0	5	14	2	8	4	3	13

	Can	**Boundary**												**Flanges**
Initial	*50*	*50*	*50*	*50*	*50*	*50*	*50*	*50*	*50*	*50*	*50*	*50*	*50*	*50*
Run 1	45	38	38	35	35	20	52	37	30	50	24	25	9	32
Run 2	44	14	25	18	30	27	52	12	7	14	20	19	10	44
Difference	1	24	13	17	5	7	0	25	23	36	4	6	1	12

The thicknesses are converged overall to quite similar values. There are even supports that are optimized the same thickness, although they are not necessarily oriented in the same direction. There are however remarkable differences. An example is support 11 from the first grillage. There, a large difference in thickness is observed, while the radial brackets are optimized towards a similar orientation.

This might be a cause of a higher thickness for supports 12 and 13 for the second run, which are both close to this support. For the first run, there is only one support at that location, which also has a lower thickness.

The optimization as shown in Section 6.1 was not able to find a result that did not violate the stress constraints when the initial result was not free of violations. However, the new bracket design made sure that the initial design was free of violations. That remained during the optimization, as shown in Figure 6.6. The stress in both the ship and the grillage and the buckling unity checks remain at the allowable level.

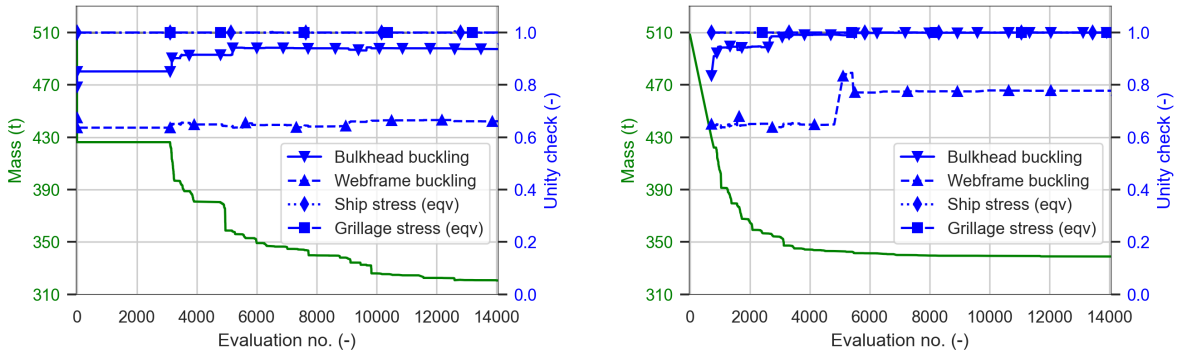

(a) Convergence and objectives

(b) Convergence and objectives for the second run

Figure 6.6: Convergence and objectives for the second optimization of the full grillage.

The unity checks for buckling in the webframes are below 1 for both optimization runs. The buckling for the bulkhead is however active for the last half of the second optimization run. Also for the first run is shown that the unity check for buckling is increasing over the iterations. This shows that buckling in the webframes is for this ship less important, what was also determined for the single grillage.

The stress in the ship for the optimized design is shown in Figure 6.7. This figure shows the interaction between the grillage and the stress in the ship. Especially the webframes in the middle of the section show a higher loading near the centerline of the ship. Also the webframes at the start and at the end of the grillage are loaded higher than the other webframes which is shown in the red circles.

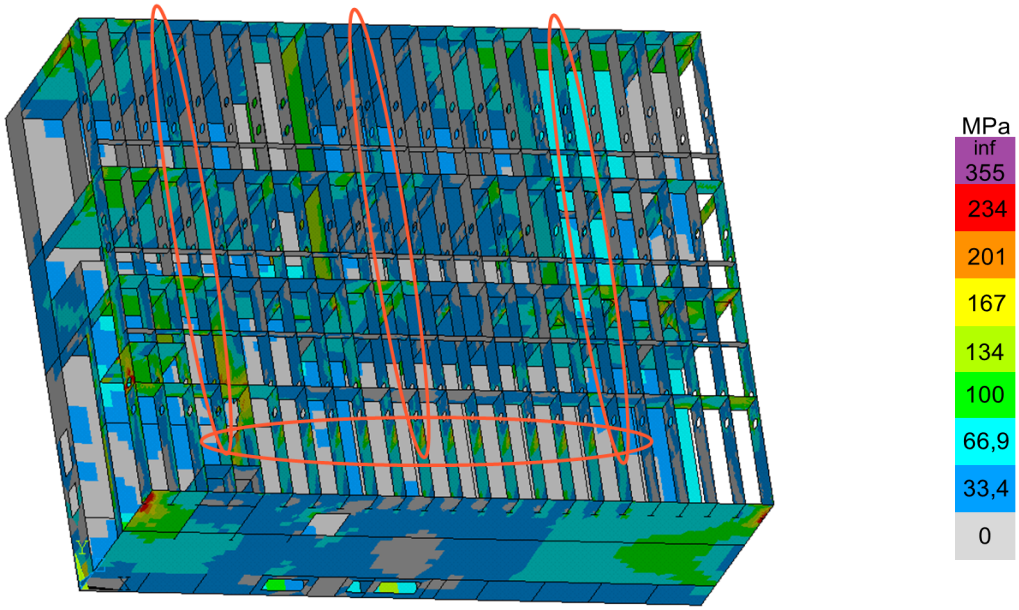

Figure 6.7: Stress in the ship for the optimized configuration.

This figure shows some high stresses at the ends of the modelled section. These are caused by the constraint, and they are therefore not considered in the optimization. The stress in the rest of the ship is overall at acceptable levels. However, still the stress in the sensitive locations as determined in Section 6.1 are important. These locations are shown in Figure 6.8. The stresses in this figure are clearly different from the results as shown in Figure 6.2. This shows the effect of the new bracket design on the height of the stress at these locations. The stress is still high, but this will remain, because still loads are transferred to the webframe below the boundary.

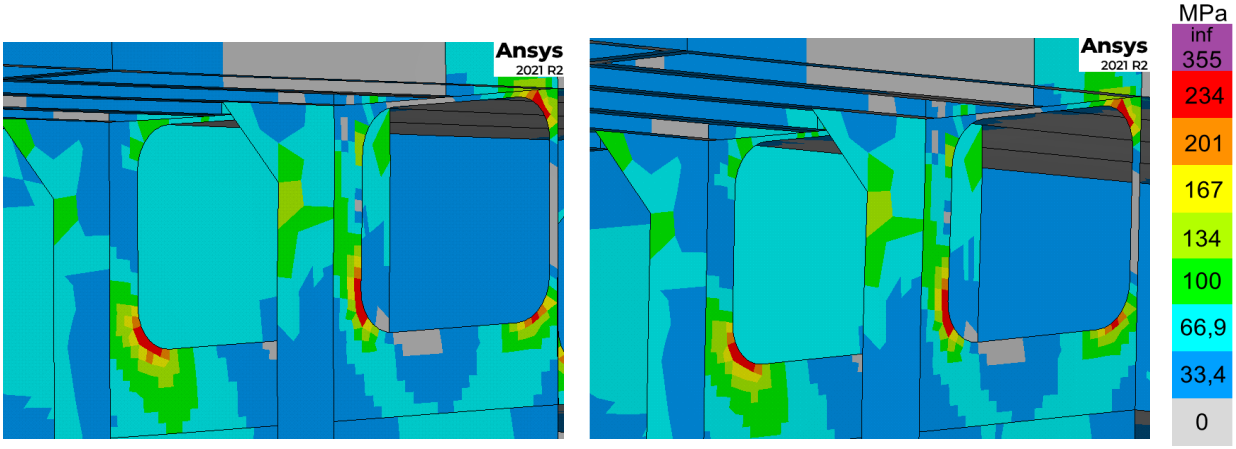

(a) Original design **(b)** Optimized design

Figure 6.8: Comparison of the stress at the most sensitive location in the ship. The difference is small, although the layout is different.

This figure shows that the difference in stress is small, what was also shown in Section 6.1. This raises the idea that the design and location of the outer brackets is more important for the stress in the ship than the layout of the radial supports. However, the mass can be reduced substantially, as shown in Figure 6.5.

Although this figure does show very little difference, one can still conclude that the stress in the ship is changing over the iterations. This is based on the behaviour of the buckling constraints, which do show difference over the iterations. It is not clear why this change is not present at this location, but that might be a result of the fact that less load is transferred to these locations due to the new bracket design, and thus less change can be observed.

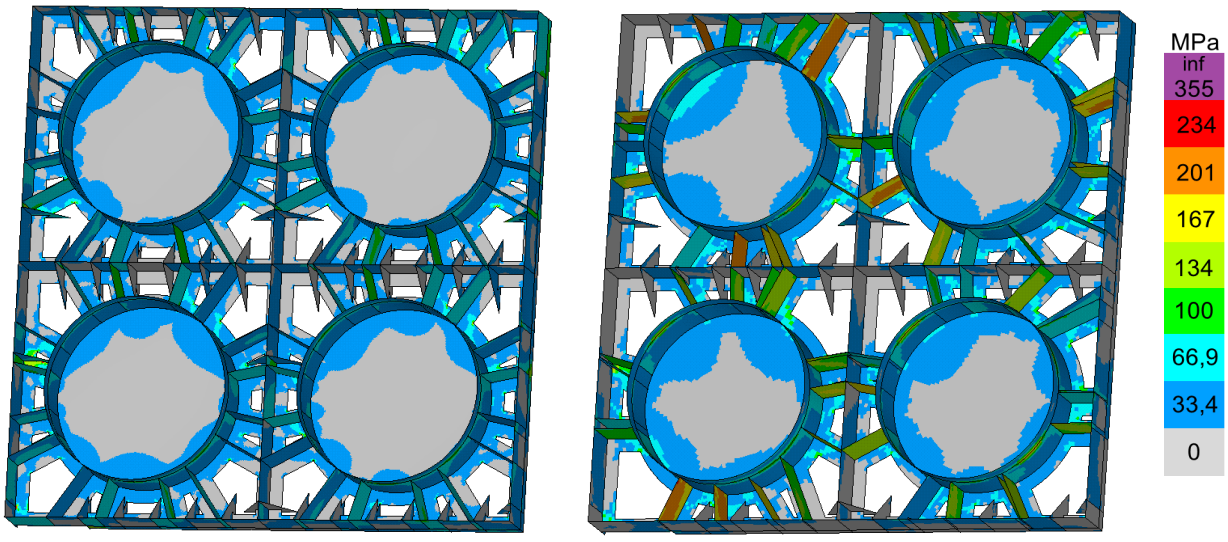

(a) Initial layout **(b)** Original layout

Figure 6.9: Comparison of the stress in the full grillage with the new design of outer brackets. The flanges and the outer brackets are deselected for a better visibility

The stress in the grillage is also an important aspect. The results for the initial design and the optimized design are shown in Figure 6.9. A remarkable difference to the single grillage is the stress pattern in the supports. This was diagonal from the top of the can to the bottom of the boundary, as explained in Section 5.1.2. For the full grillage however, there are two different patterns. The first is also a diagonal from the top of the can, but this ends near the flange at the boundary. An example of this is shown in at the left of the figure. The other is a stress concentration near the can. That is seen in the bottom of the figure. This stress concentration is caused by the outer bracket that connects to the flange of that support, which means that more stress is transferred through that bracket and less through the boundary.

The stress in the optimized design is clearly much higher than in the initial design. As explained earlier, the optimizer places the supports away from the corners, which is most likely to reduce the mass. It can be seen that the stress in the radial supports near the large openings in the flanges is higher than the stress in the other supports. That is according to the expectation, because the loads that are directed in those corners have to be carried by these supports.

6.3. Final result

6.3.1. Manual refinement

The result of the optimization showed to have some difficulties with manufacturing, because of radial supports that are close to each other. This problem is solved by a manual step, where two radial supports that are close are combined to one single support with the average orientation and the combined thickness. That means that less radial supports are used in the final solution. The obtained thicknesses are shown in Table 6.2 and the resulting layout is shown in Figure 6.10. The angles that are used for this layout are shown in Table D.4 in Appendix D.

Table 6.2: Thicknesses of the results after the manual improvement in millimeters

Grillage number	1	2	3	4	5	6	7	8	9	10	11	12	13
1	18	8	9	20	28	8	10	20	13	40	9	18	20
2	26	22	17	22	21	35	13	13	10	13	8	10	-
3	20	15	12	25	7	31	12	9	15	16	10	11	-
4	30	25	9	14	12	15	7	17	32	6	24	11	-

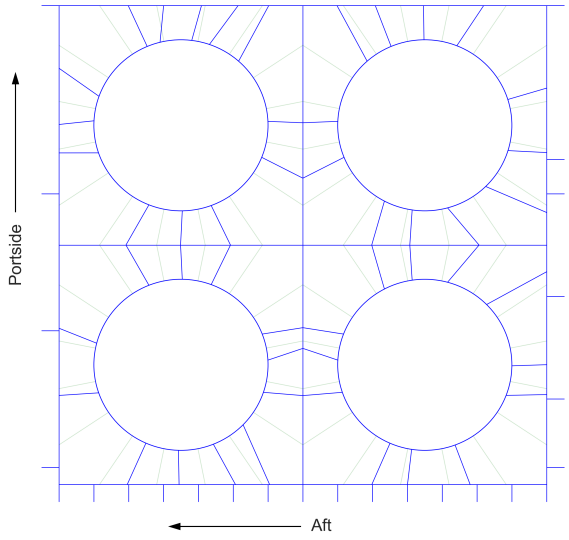

Figure 6.10: Layout of the full grillage after a manual design update where close supports are combined.

This figure shows that the number of radial supports is reduced significantly. The number of supports for

each of the grillages is reduced to 12, except grillage 1, which has 13 radial supports. This suggests that the number of supports in the real design can be reduced when no further requirements are posed to the result, such as different welding parameters for higher thicknesses. To check whether this solution is also feasible, a new finite element analysis is done. The result is shown in Figure 6.11.

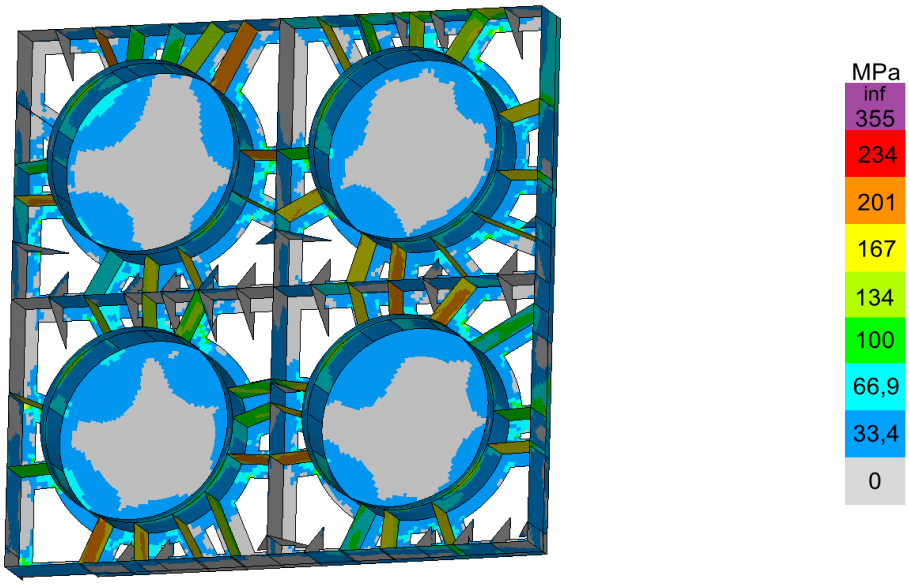

Figure 6.11: Stress in the full grillage after a manual design update where close supports are combined. The flanges and the outer brackets are deselected for a better visibility

It is clear that the stress in the grillage does not violate the stress constraints. That means that this is also a feasible result for the loads and constraints as used in this optimization. This shows that the optimizer does have some influence on the number of radial supports, although it is not explicitly accounted for in the optimization.

6.3.2. Improvement

The question that still remains is whether this result is indeed improved with respect to the initial design, and what extent this improvement has. The first improvement is the weight of the structure. The original design by Vuyk Engineering had a main steel weight of 351 ton. The most optimal weight of the structure found in this thesis is 319 ton, which is an improvement of 9.1%, as shown in Section 6.2.2. This mass decrease might be insignificant for the total mass of the ship, but for the cost of the structure it is not. The main steel weight is directly related to the total structural cost, which means that a decrease in weight affects the total cost of the structure.

Another improvement that is found in the optimization is the number of radial supports that is required. This number is decreased with 15, which means that the total length of the intersections is also reduced. That suggests that the welding length can also be decreased. This improvement is however hard to quantify, because many other parameters play a role. For example, the amount of filler material that is required depends on the thickness of the plate, but also on the accessibility. If a plate can only be accessed from one side, the weld is different than when it is welded from two sides. This are only two considerations, but more are involved. It is however outside the scope of this thesis to investigate these numbers, and it is therefore left as a point of further research what the improvement of this is. However, the expectation is that some improvement can be made, because of the significant reduction in the number of supports.

Only a part of the improvements can be quantified, so only a very rough estimate can be given of the cost reduction. This estimate is related to the mass of the structure. W.K. van der Leeden and H.W. Vuijk (personal communication, October 5, 2022) mentioned that a tower grillage has a price of 5 to 6 million euro. If the lowest of these values is related to the maximum mass decrease as found in this thesis, a decrease in cost of €450,000 is obtained. Although this number does not give an exact

answer, it does shows the potential of applying an optimization to such a structure.

6.4. Discussion

Engineering of the structure is also one of the aspects of a design of a tower grillage that contribute to the cost of the structure, although it is a relatively small part (in the order of 10% (W.K. van der Leeden and H.W. Vuijk, personal communication, October 12, 2022). This was also one of the focus points of this thesis, as the research question was how size and shape optimization can help in the design of a tower grillage. In this chapter is shown that the optimized layouts give a global image of layouts that can be used in the optimization. However, when the effort that is required to obtain the results and the amount of information that the results give -a global image- are compared, then it should be concluded that the current optimization results are not sufficient for their aim. They do however show that it is possible to find layouts with a lower mass, which is also shown for the single grillages.

The results in this chapter showed that the optimizer is able to find a new optimum, but it needs an initial design without constraint violations. From the results with the initial bracket design became clear that the optimizer is not able to optimize a structure that has constraint violations in the initial design. This is also the result of the fact that the optimizer is not tuned for such an optimization. The penalty function is tuned for small violations during the optimization, but the current optimization is actually an optimization with multiple constraints. This does however mean that already in the initial stage, input from the designer is required to ensure that the stress is at an allowable level. For this thesis, a change was made in the bracket design, which decreased the stress to below the allowable stress. This shows that the layout is not the only design aspect that is important for reducing the mass in the grillage. Also the design of the outer brackets is important, which can decrease the stress in the ship.

The optimizer is however able to reduce the mass if the stress is allowable in the initial solution. The maximum found mass reduction is 32 tons, which is an improvement of 9.1% when compared to the original design by Vuyk Engineering. There is some variability in the layouts, but still global patterns can be observed that can be used as a starting point of the design. The first pattern is that the optimization does not place supports near the corners. The second is that the optimization places the radial support in four different groups per grillage, and the last is that some supports are close, or even overlapping.

7

Conclusion

This research was focused on finding an answer to the question: *How can the combination of size and shape optimization help in the design of a tower grillage where buckling and stresses in the underlying compliant ship structure are implemented as constraints?* To answer this question, an existing tower grillage design is modelled and optimized.

The optimal distribution of radial supports is determined by the objective and constraint of the grillage: the mass and the stress. The mass should be decreased as much as possible, but the constraint should not be violated. As a result, the optimizer found two main factors that influence its behaviour: The length of the radial supports and the location of the outer brackets. The influence of the first factor, the length, is seen in all three the optimizations. The radial supports are optimizing away from the corners of the grillage, which means that their length, and thus their mass is reduced.

The other factor, the placement of the outer brackets, is shown by each of the three optimizations. The radial supports are in many cases connected to the outer brackets. The opposite is also shown for the single grillage, where no brackets were placed at the hull side of the grillage. It is shown that at that location, the placement of the supports is more variable between the different runs. Optimizing towards these outer brackets has the effect that less load needs to be transferred to the sides of the grillage, and thus a lower thickness for that element is required. Optimizing towards the brackets does also mean that in some cases, the bracket on the inside is removed, which has an additional advantage for the mass.

The behaviour of the ship influences the optimization in two different ways: by its stiffness and by its strength. The effects of the stiffness are shown by the optimizations of the single grillage. There, the stress constraint in the ship was not active, but the stress in the same grillage differs between the two boundary conditions. The observed differences are mainly present in the largest design elements of the grillage: the sides, the can and the flanges. The maximum stress in the first element is lowered, but for the other two, it is increased. That has the effect that the thickness of the flanges needs to be higher. This is shown for the optimization runs of the grillage on the ship, where this thickness is increased with respect to the grillage on the rigid foundation, which has an adverse effect on the mass. The lowest optimized mass for the grillage on the ship is 4.7 percent higher than the lowest mass of the grillage on the rigid foundation. Also the averages of the masses have a difference of 5.7 percent. On top of that, the results for the grillage on the ship did have less room for further improvement.

The effect of the ship strength is shown in the optimization of the full grillage. The ship that is used in the current optimization has some locations where peak stresses occur. In the first iteration step became clear that the optimizer is not able to reduce these stresses below the constraint. However, a small reduction in the stress could be made, which shows the influence of the layout on the stress in the ship. Another effect of the stress on the ship is that a new bracket design needed to be made to decrease the stress below the constraint value.

Buckling in the ship seems to be less important for the current ship. The constraint on buckling in the ship was active for only one optimization run of the full ship. The stress constraints were however active for all runs, which shows that stress is generally more important than buckling.

The optimization procedure in this thesis showed that the mass of the grillage can be decreased up to 32 tons, which is a decrease of 9.1 percent compared to the original grillage design by Vuyk Engineering. There is variability in the results, because another run shows a decrease of only 3.5 percent to the original grillage. Both results do however show a possible mass reduction.

The stress in the grillage is increased for the layouts of all optimizations, which means a more optimal use of the material. The stress in the ship is however less effected by changes in the layout. It does however change, as shown in the first iteration of the full ship. Also the behaviour of the buckling constraints, which are determined by the stress, changes over the iterations.

These observations lead to a final answer to the research question: The combination of size and shape optimization can help in the design of a tower grillage by providing a global image of lighter layouts which avoid stress and buckling constraint violations in the ship. A limitation of the applicability of the research in an engineering environment is that the results only provide a general image of the layout for the full grillage. It is therefore at this stage not worth the effort and time to use the current procedure in an engineering project. The results do however show that there is potential for mass reduction, and future enhancements can make the procedure suitable for engineering.

8

Discussion

In the conclusion is shown that the combination of size and shape optimization can help a designer by providing a global image of the layout of the grillage. However, the current implementation is not developed such that it will be used in a design process. The main reason for this statement is that the required effort and time do not weigh up against the obtained results, as the current implementation takes approximately two weeks to perform the optimization. This calculation time could be accepted if the result was more advanced, but it is too long to give a designer only a feeling for the design of the grillage. Moreover, the designer needs already to put effort in the initial design, because an input without constraint violations is required.

It is also important to notice that the optimizations in this thesis contain two runs for each problem, to check the consistency of the results, and to see what the most important locations from the optimization are. It is also shown that more runs are necessary if more certainty is desirable. That means that at least two optimization runs are needed before a conclusion can be drawn. As a result, the calculation time increases to four weeks, or two computers are needed to run the optimizations in parallel.

On top of these calculation times, the designer needs to keep an eye on the program when it is running. That is caused by some problems in the connection between Ansys and Python. One of these problems is that the connection is lost between the two instances, while Ansys keeps active. Another problem is that Ansys throws an error in its own base code (Fortran). The cause of both problems is unknown, but their effect is that Python cannot make a new connection. That means that a designer should resolve these problems, as soon as the optimizer detects the error.

Also for the geometrical model, different problems are encountered, as explained in Section 4.2. The solutions to this problem are coded such that they are applicable to other tower grillages with a similar layout, but for other structures, a new set of solutions needs to be written. This is very time consuming, which means that this is a limitation of the applicability to other structures. This is especially a limitation if this is only a one-of-a-kind structure.

Three settings in the optimization can change the problem from an engineering perspective. The first is that only four load cases are considered in the optimization, in order to reduce the calculation times. It is shown that the supports are optimized away from the corners of the grillage, but it is well possible that this will change if also other, such as quartering, load cases are implemented.

Another point is that the range of thicknesses in the current optimization consists of discrete values with each 1 millimeter apart. This choice was made to find a result that has a larger focus on decreasing the mass, rather than obtaining a structure that complies with given plate thicknesses. That means that for the current design, another translation needs to be made in order to have a design that is manufacturable. It also means that for a realistic design, the mass most likely increases.

The first of these two problems is the most difficult to overcome, because this is a trade-off between the calculation time and the feasibility of the result. The second point is however an easy adaptation, which only requires the input of available plate thicknesses. It is however dependent on the type of research one wants to do. More thicknesses means that a better view is obtained of the possibilities, but a range of real plate thicknesses is more functional in an engineering case.

An assumption at the start of the thesis was that changing the orientation of the radial supports had a significant influence on the stress in the ship. This influence is however smaller than expected. This was found in the optimization of the full grillage, where the stress constraint violation in the initial design of the ship could not be resolved by changing the layout. Therefore, a change of the outer brackets was made, which had a large impact on the stress. This shows that including these brackets in the optimization is expected to deliver a good improvement to the overall result.

This thesis was focused on optimizing a tower grillage on a ship, but the underlying principle, structural optimization on an external structure, can also be applied in other fields. In the maritime field alone, many possible applications can be thought of. Especially in the offshore industry, replacements of equipment, such as cranes, are made to ships. However, it should be noted that this thesis is only a first start in this type of optimization, which means that the existing problems need to be resolved, before in can actually be implemented in an engineering environment.

The largest problem with this type of optimization is the external structure itself. This structure increases the size of the underlying analysis, such as FEA (as used in this thesis) or CFD. That means that also the calculation times per function evaluation are increased with respect to an optimization without external structure. During this thesis, the calculation times were kept at a reasonable level, but other problems might very well be larger. That means that a reduction of these calculation times will be a leap forward in the applicability of optimization on an external structure.

When one considers to apply this optimization principle to other structures, he should be careful about the implementation of the underlying structure. If for instance the constraints are not likely to be violated, then the question appears if it is beneficial to use a full finite element model for it. It is shown that the compliance of the underlying structure influences the optimization, but that does not require such a computationally intensive finite element model. It might be worthwhile to consider other techniques, such as the use of a superelement, to reduce the computational time during the optimization.

So, three main factors are determined that significantly influence the usability of the optimization: Computational speed, quality of the result and the amount of human effort that is required to obtain a feasible result. That means that enhancements that can be made should be sought in these directions. More detailed recommendations will be given in the next chapter.

9

Recommendations

In the discussion, three main factors are determined that limit the usability of the optimization: Computational speed, quality of the result and the amount of human effort. That means that it is worthwhile to search for ways that improve at least one of these factors.

9.1. Scientific recommendations

The current algorithm has a number of parameters that needs to be defined. In Section 2.5 is explained that an initial artificial temperature T, an initial design vector and a specified number of iterations are required for a simulated annealing (SA) algorithm. For the generalized simulated annealing algorithm, also the visiting and acceptance parameters q_v and q_a need to be defined. For most of these parameters, except the temperature, only one single value is considered. It is possible to change the parameters that are specific for the SA algorithm (T, q_v and q_a). This can lead to a better convergence, but still, the number of required iterations remains in the same order of magnitude. That has the result that still the most important problem, the amount of computing time, is not resolved. On top of that, it is likely that these numbers need to be tuned for each individual problem, which means that the improvement in computational time is discounted by the extra amount of implementation time and human effort.

It might therefore be beneficial to look at a more advanced algorithm, where physics is also considered in the optimizer itself, and not only in the calculation of the stresses. In the current algorithm, only the magnitude of the constraints is considered, so the location is not used. That means that all parameters might be changed to react to a constraint violation, while changing only one parameter could have been sufficient when the location was known. It is possible that the current optimizer ends up with the same solution, but that requires more iterations, and thus more time. That shows that taking not only the magnitude, but also the location of a violation into account can enhance the results. This is not only an improvement of the required number of iterations, but also to the quality, because the process is based on physics, rather than (guided) randomness.

It might also be interesting to build a physics-based model that understands the interaction between the different design variables and the constraints. An example from the current optimization is a stress constraint violation in a radial support, which can be resolved by increasing the thickness of that support. Implementing the coupling between the different variables is another addition to this research. For a tower grillage, that would for instance mean a coupling between the angles and the thicknesses of one support.

Another parameter that needs to be defined at the start of every optimization is the initial design vector. This research has one design vector, but it will enhance the understanding of the result if more different starting points are used, such as different starting angles. This will show up to what extent the results are dependent on the initial values.

The last parameter that is needed for an algorithm is the number of function evaluations. This number is set to 14,000 in this thesis. It would enhance the understanding if a much longer run is done, to see if a larger decrease of the mass can be found. This is not a solution for the mentioned main

factors, as it increases the computational time, but it will give a better insight in the results.

A parameter that is not directly taken into account in this thesis is the number of radial supports. It is shown for the full grillage that some radial supports overlap, which were combined to one single support. It might however be interesting to see what happens if the number of supports is totally fixed, that is, that they are required to stay a certain distance apart, so that they cannot overlap. That will give a better insight in the effect of using different numbers of supports on the mass, but also on the layouts.

Another interesting point of research is using another optimization technique, to see if similar, or even better results can be obtained. This thesis made use of the combination of size and shape optimization, but layout optimization might as well be a solution to the problem. One should in that case however be careful about the quality of the result, regarding the manufacturability, which is generally harder to control with this technique, as explained in the literature study.

9.2. Practical recommendations

The optimization of the full grillage showed that the current procedure is not capable of handling stresses above the allowable value in the initial design. It will therefore be a useful addition to this research, regarding quality and human effort, if a procedure is found that makes sure that the stress can be decreased below the allowable stress. In this thesis is shown that the outer brackets can play a role in this, but future research should determine if this is the only important factor, or if also other aspects play a role.

Including these outer brackets can have the additional benefit that the mass of the grillage can be reduced even further, as shown for the full grillage. Also the fact that the radial supports are optimizing towards these supports shows the importance of these elements. That means that also for a stronger ship without stress constraint violations an improvement can be made.

For implementing the outer brackets, the shape, and not only the location and thickness of these brackets is important, as the new design for the bracket for the full grillage showed. One should however be careful with including this, because it increases the complexity of the optimization, which can have an adverse effect on the quality of the result.

In this thesis, a tower grillage for only one single ship is considered, and the results are therefore also focused on this ship. However, more investigation to different ships is desired to get an even better understanding of the optimization procedure and the behaviour to different ship models.

Another addition can be to include the manufacturability aspects direct into the optimization. It is shown that also the welding aspects are of importance for the design of a tower grillage. Including these aspects can not only enhance the quality of the results, it will also give a better insight in the real improvement that can be made.

It is also shown that many problems needed to be resolved in the current procedure, such as problems with intersections. This is also a limitation of the applicability of the procedure to structures other than tower grillages, because new rules need to be defined again for each type of structure. Defining new rules is necessary, because the variables for other structures are different, and thus other types of intersections can occur. This takes a considerable amount of time, which means that the procedure is not well-suited for a one-of-a-kind structure. That means that it it worthwhile to search for a general solution for this problem, which could be done by a more complex Python code, but possibly also another finite element code can improve the behaviour.

Bibliography

[1] Ansys®. *Theory Reference for the Mechanical APDL and Mechanical Applications*. Release 12.0. ANSYS, Inc., 2009.

[2] A. Antoniou and W.-S. Lu. *Practical optimization*. Ed. by D. Gries and O. Hazzan. 2nd ed. Springer, 2021. ISBN: 978-1-0716-0841-8. DOI: 10.1007/978-1-0716-0843-2.

[3] J. Bai and W. Zuo. "Hollow structural design in topology optimization via moving morphable component method". In: *Structural and Multidisciplinary Optimization* 61.1 (2020), pp. 187–205. ISSN: 1615-1488. DOI: 10.1007/s00158-019-02353-0.

[4] C. Bakker, L. Zhang, K. Higginson, and F. van Keulen. "Simultaneous optimization of topology and layout of modular stiffeners on shells and plates". In: *Structural and Multidisciplinary Optimization* 64.5 (2021), pp. 3147–3161. ISSN: 1615-1488. DOI: 10.1007/s00158-021-03081-0.

[5] M. P. Bendsøe and N. Kikuchi. "Generating optimal topologies in structural design using a homogenization method". In: *Computer Methods in Applied Mechanics and Engineering* 71.2 (1988), pp. 197–224. ISSN: 0045-7825. DOI: 10.1016/0045-7825(88)90086-2.

[6] M. P. Bendsøe and O. Sigmund. *Topology Optimization. Theory, Methods, and Applications*. 2nd ed. Springer, 2004. ISBN: 978-3-662-05086-6. DOI: 10.1007/978-3-662-05086-6.

[7] J. Błachut. "Optimal barreling of steel shells via simulated annealing algorithm". In: *Computers & Structures* 81.18 (2003), pp. 1941–1956. ISSN: 0045-7949. DOI: 10.1016/S0045-7949(03)00214-1.

[8] K. Bobrowski, E. Ferrer, E. Valero, and H. Barnewitz. "Aerodynamic Shape Optimization Using Geometry Surrogates and Adjoint Method". In: *AIAA Journal* 55.10 (2017), pp. 3304–3317. ISSN: 1533-385x. DOI: 10.2514/1.J055766.

[9] O. Bozorg-Haddad, M. Solgi, and H. A. Loiciga. *Meta-Heuristic and Evolutionary Algorithms for Engineering Optimization*. Hoboken, USA: John Wiley & Sons, Incorporated, 2017. ISBN: 9781119387077.

[10] T. Buhl. "Simultaneous topology optimization of structure and supports". In: *Structural and Multidisciplinary Optimization* 23.5 (2002), pp. 336–346. ISSN: 1615-1488. DOI: 10.1007/s00158-002-0194-2.

[11] H. Cao, X. Qian, Z. Chen, and H. Zhu. "Enhanced particle swarm optimization for size and shape optimization of truss structures". In: *Engineering Optimization* 49.11 (2017), pp. 1939–1956. ISSN: 0305-215X. DOI: 10.1080/0305215X.2016.1273912.

[12] X. Chen, M. Diez, M. Kandasamy, Z. Zhang, E. F. Campana, and F. Stern. "High-fidelity global optimization of shape design by dimensionality reduction, metamodels and deterministic particle swarm". In: *Engineering Optimization* 47.4 (2015), pp. 473–494. ISSN: 1029-0273. DOI: 10.1080/0305215X.2014.895340.

[13] DNV. *DNV-CG-0128: Buckling*. 2021.

[14] DNV. *DNV-GL Rules for classification: Ships*. 2018.

[15] DNV. *DNV-GL-OS-C201:Structural design of offshore units - WSD method*. 2017.

[16] DNV. *DNV-ST-001: Marine operations and marine warranty*. 2021.

[17] W. S. Dorn, R. E. Gomory, and H. J. Greenberg. "Automatic design of optimal structures". In: *J. de Mechanique* 3 (1964), pp. 25–52.

[18] "Fast simulated annealing". In: *Physics Letters A* 122.3 (1987), pp. 157–162. ISSN: 0375-9601. DOI: 10.1016/0375-9601(87)90796-1.

[19] A. I. J. Forrester and A. J. Keane. “Recent advances in surrogate-based optimization”. In: *Progress in Aerospace Sciences* 45.1 (2009), pp. 50–79. ISSN: 0376-0421. DOI: 10.1016/j.paerosci.2008.11.001.

[20] A. Francavilla, C. Ramakrishnan, and O. Zienkiewicz. “Optimization of shape to minimize stress concentration”. In: *Journal of strain analysis* 10.2 (1975), pp. 63–70. DOI: 10.1243/03093247V102063.

[21] M. Goalen. *Why sea fastening is critical to safe and efficient offshore wind installation*. 2020. URL: https://www.windpowerengineering.com/why-sea-fastening-is-critical-to-safe-and-efficient-offshore-wind-installation/ (visited on 10/09/2021).

[22] H. M. Gomes. “Truss optimization with dynamic constraints using a particle swarm algorithm”. In: *Expert Systems with Applications* 38.1 (2011), pp. 957–968. ISSN: 0957-4174. DOI: 10.1016/j.eswa.2010.07.086.

[23] S. Gubian. *SDAopt*. 2022. URL: https://github.com/sgubianpm/sdaopt (visited on 03/04/2022).

[24] S. Gubian. *Simulated Dual Annealing benchmark*. 2022. URL: https://gist.github.com/sgubianpm/7d55f8d3ba5c9de4e9f0f1ffff1aa6cf (visited on 03/03/2022).

[25] X. Guo, W. Zhang, and W. Zhong. “Doing topology optimization explicitly and geometrically-a new moving morphable components based framework”. In: *Journal of Applied Mechanics, Transactions ASME* 81.8 (2014). ISSN: 1528-9036. DOI: 10.1115/1.4027609.

[26] W. Hare, J. Nutini, and S. Tesfamariam. “A survey of non-gradient optimization methods in structural engineering”. In: *Advances in Engineering Software* 59 (2013), pp. 19–28. ISSN: 0965-9978. DOI: 10.1016/j.advengsoft.2013.03.001.

[27] B. Harl and M. Kegl. “Topology optimization course for mechanical engineering students”. In: *International Journal of Mechanical Engineering Education* (2020). ISSN: 2050-4586. DOI: 10.1177/0306419020967883.

[28] O. F. Hughes and J. K. Paik. *Ship Structural Analysis and Design*. Jersey City: Society of Naval Architects and Marine Engineers (SNAME), 2010. ISBN: 978-0-939773-82-4.

[29] iStock/janssenkruseproductions. *A large offshore vessel with a crane and a helipad is moored in the seaport of Rotterdam. A Jack-up vessel for use in the offshore wind industry*. 2022. URL: https://www.istockphoto.com/nl/foto/a-large-offshore-vessel-with-a-crane-and-a-helipad-is-moored-in-the-seaport-of-gm1417923722-464825338 (visited on 10/24/2020).

[30] K. A. James, J. S. Hansen, and J. R. Martins. “Structural topology optimization for multiple load cases using a dynamic aggregation technique”. In: *Engineering Optimization* 41.12 (2009), pp. 1103–1118. ISSN: 0305-215X. DOI: 10.1080/03052150902926827.

[31] F. K. J. Jawad, C. Ozturk, W. Dansheng, M. Mahmood, O. Al-Azzawi, and A. Al-Jemely. “Sizing and layout optimization of truss structures with artificial bee colony algorithm”. In: *Structures* 30 (2021), pp. 546–559. ISSN: 2352-0124. DOI: 10.1016/j.istruc.2021.01.016.

[32] P. Kang and S. K. Youn. “Isogeometric shape optimization of trimmed shell structures”. In: *Structural and Multidisciplinary Optimization* 53.4 (2016), pp. 825–845. ISSN: 1615-1488. DOI: 10.1007/s00158-015-1361-6.

[33] S. Katoch, S. S. Chauhan, and V. Kumar. “A review on genetic algorithm: past, present, and future”. In: *Multimedia Tools and Applications* 80.5 (2021), pp. 8091–8126. ISSN: 1573-7721. DOI: 10.1007/s11042-020-10139-6.

[34] S. Kirkpatrick, C. D. Gelatt, and M. P. Vecchi. “Optimization by Simulated Annealing”. In: *Science* 220.4598 (1983), pp. 671–680. DOI: 10.1126/science.220.4598.671.

[35] S. Kitayama, M. Arakawa, and K. Yamazaki. “Sequential Approximate Optimization using Radial Basis Function network for engineering optimization”. In: *Optimization and Engineering* 12.4 (2011), pp. 535–557. ISSN: 1573-2924. DOI: 10.1007/s11081-010-9118-y.

[36] M. Kociecki and H. Adeli. “Two-phase genetic algorithm for size optimization of free-form steel space-frame roof structures”. In: *Journal of Constructional Steel Research* 90 (2013), pp. 283–296. ISSN: 0143-974X. DOI: 10.1016/j.jcsr.2013.07.027.

[37] G. Kreisselmeier and R. Steinhauser. “Systematic Control Design by Optimizing a Vector Performance Index”. In: *IFAC Proceedings Volumes* 12.7 (1979), pp. 113–117. ISSN: 1474-6670. DOI: 10.1016/S1474-6670(17)65584-8.

[38] L. Krog, A. Tucker, M. Kemp, and R. Boyd. “Topology optimization of aircraft wing box ribs”. In: *10th AIAA/ISSMO Multidisciplinary Analysis and Optimization Conference* 10 (2004). DOI: 10.2514/6.2004-4481.

[39] L. Lamberti. “An efficient simulated annealing algorithm for design optimization of truss structures”. In: *Computers and Structures* 86.19-20 (2008), pp. 1936–1953. ISSN: 0045-7949. DOI: 10.1016/j.compstruc.2008.02.004.

[40] L. Lamberti and C. Pappalettere. “Move limits definition in structural optimization with sequential linear programming. Part II: Numerical examples”. In: *Computers & Structures* 81.4 (2003), pp. 215–238. ISSN: 0045-7949. DOI: 10.1016/S0045-7949(02)00443-1.

[41] T. U. Lee and Y. M. Xie. “Simultaneously optimizing supports and topology in structural design”. In: *Finite Elements in Analysis and Design* 197 (2021). ISSN: 0168-874X. DOI: 10.1016/j.finel.2021.103633.

[42] D. Leidenfrost. “Development of a Nature Inspired Hull Structure for a 46m Sailing Yacht”. Master’s thesis. Alfred Wegener Institute, 2015.

[43] C. Li, I. Y. Kim, and J. Jeswiet. “Conceptual and detailed design of an automotive engine cradle by using topology, shape, and size optimization”. In: *Structural and Multidisciplinary Optimization* 51.2 (2015), pp. 547–564. ISSN: 1615-1488. DOI: 10.1007/s00158-014-1151-6.

[44] J. G. Lin. “On min-norm and min-max methods of multi-objective optimization”. In: *Mathematical Programming* 103.1 (2005), pp. 1–33. ISSN: 1436-4646. DOI: 10.1007/s10107-003-0462-y.

[45] Y. Lin, Q. Yang, and G. Guan. “Scantling optimization of FPSO internal turret area structure using RBF model and evolutionary strategy”. In: *Ocean Engineering* 191 (2019). ISSN: 0029-8018. DOI: 10.1016/j.oceaneng.2019.106562.

[46] Z. Liu, S. Cho, A. Takezawa, X. Zhang, and M. Kitamura. “Two-stage layout–size optimization method for prow stiffeners”. In: *International Journal of Naval Architecture and Ocean Engineering* 11.1 (2019), pp. 44–51. ISSN: 2092-6782. DOI: 10.1016/j.ijnaoe.2018.01.001.

[47] I. Marinić-Kragić, D. Vučina, and M. Ćurković. “Efficient shape parameterization method for multidisciplinary global optimization and application to integrated ship hull shape optimization workflow”. In: *Computer-Aided Design* 80 (2016), pp. 61–75. ISSN: 0010-4485. DOI: 10.1016/j.cad.2016.08.001.

[48] A. G. M. Michell. “LVIII. The limits of economy of material in frame-structures”. In: *The London, Edinburgh, and Dublin Philosophical Magazine and Journal of Science* 8.47 (1904), pp. 589–597. ISSN: 1941-5982. DOI: 10.1080/14786440409463229.

[49] C. Millan-Paramo and J. E. A. Filho. “Size and Shape Optimization of Truss Structures with Natural Frequency Constraints Using Modified Simulated Annealing Algorithm”. In: *Arabian Journal for Science and Engineering* 45.5 (2020), pp. 3511–3525. ISSN: 2191-4281. DOI: 10.1007/s13369-019-04138-5.

[50] A. Mortazavi and V. Toğan. “Simultaneous size, shape, and topology optimization of truss structures using integrated particle swarm optimizer”. In: *Structural and Multidisciplinary Optimization* 54.4 (2016), pp. 715–736. ISSN: 1615-1488. DOI: 10.1007/s00158-016-1449-7.

[51] S. Nguyen-Van, K. T. Nguyen, V. H. Luong, S. Lee, and Q. X. Lieu. “A novel hybrid differential evolution and symbiotic organisms search algorithm for size and shape optimization of truss structures under multiple frequency constraints”. In: *Expert Systems with Applications* 184 (2021), p. 115534. ISSN: 0957-4174. DOI: 10.1016/j.eswa.2021.115534.

[52] S. Pajunen and O. Heinonen. “Automatic design of marine structures by using successive response surface method”. In: *Structural and Multidisciplinary Optimization* 49.5 (2014), pp. 863–871. ISSN: 1615-1488. DOI: 10.1007/s00158-013-1013-7.

[53] N. Pollini. “Gradient-based prestress and size optimization for the design of cable domes”. In: *International Journal of Solids and Structures* 222-223 (2021), p. 111028. ISSN: 0020-7683. DOI: 10.1016/j.ijsolstr.2021.03.015.

[54] N. M. K. Poon and J. R. R. A. Martins. “An adaptive approach to constraint aggregation using adjoint sensitivity analysis”. In: *Structural and Multidisciplinary Optimization* 34.1 (2007), pp. 61–73. ISSN: 1615-1488. DOI: 10.1007/s00158-006-0061-7.

[55] PyAnsys. *PyAnsys*. 2022. URL: https://docs.pyansys.com/ (visited on 08/30/2022).

[56] A. S. Ramos and G. H. Paulino. “Filtering structures out of ground structures – a discrete filtering tool for structural design optimization”. In: *Structural and Multidisciplinary Optimization* 54.1 (2016), pp. 95–116. ISSN: 1615-1488. DOI: 10.1007/s00158-015-1390-1.

[57] S. S. Rao. *Engineering Optimization - Theory and Practice*. 4th ed. John Wiley & Sons, 2009. ISBN: 978-0-470-18352-6.

[58] G. I. N. Rozvany. “A critical review of established methods of structural topology optimization”. In: *Structural and Multidisciplinary Optimization* 37.3 (2009), pp. 217–237. ISSN: 1615-1488. DOI: 10.1007/s00158-007-0217-0.

[59] M. P. Saka and Z. W. Geem. “Mathematical and Metaheuristic Applications in Design Optimization of Steel Frame Structures: An Extensive Review”. In: *Mathematical Problems in Engineering* (2013), p. 271031. ISSN: 1024-123X. DOI: 10.1155/2013/271031.

[60] E. D. Sanders, A. S. Ramos, and G. H. Paulino. “A maximum filter for the ground structure method: An optimization tool to harness multiple structural designs”. In: *Engineering Structures* 151 (2017), pp. 235–252. ISSN: 1873-7323. DOI: 10.1016/j.engstruct.2017.07.064.

[61] M. Sayebani, A. Mohammadrahimi, and H. K. Looyeh. “Weight and Cost Optimization of Midship Section Using Common Structural Rules”. In: *Journal of Ship Production and Design* 36.03 (2020), pp. 171–180. ISSN: 2158-2866. DOI: 10.5957/JSPD.01190002.

[62] J. Schwarz, T. Chen, K. Shea, and T. Stanković. “Efficient size and shape optimization of truss structures subject to stress and local buckling constraints using sequential linear programming”. In: *Structural and Multidisciplinary Optimization* 58.1 (2018), pp. 171–184. ISSN: 1615-1488. DOI: 10.1007/s00158-017-1885-z.

[63] SciPy. *scipy.optimize.dual_annealing*. 2022. URL: https://docs.scipy.org/doc/scipy/reference/generated/scipy.optimize.dual_annealing.html (visited on 03/30/2022).

[64] Z. Sekulski. “Least-weight topology and size optimization of high speed vehicle-passenger catamaran structure by genetic algorithm”. In: *Marine Structures* 22.4 (2009), pp. 691–711. ISSN: 0951-8339. DOI: 10.1016/j.marstruc.2009.06.003.

[65] Z. Sekulski. “Multi-objective topology and size optimization of high-speed vehicle-passenger catamaran structure by genetic algorithm”. In: *Marine Structures* 23.4 (2010), pp. 405–433. ISSN: 0951-8339. DOI: 10.1016/j.marstruc.2010.10.001.

[66] O. Sigmund and K. Maute. “Topology optimization approaches: A comparative review”. In: *Structural and Multidisciplinary Optimization* 48.6 (2013), pp. 1031–1055. ISSN: 1615-1488. DOI: 10.1007/s00158-013-0978-6.

[67] S. Sleesongsom and S. Bureerat. “New conceptual design of aeroelastic wing structures by multi-objective optimization”. In: *Engineering Optimization* 45.1 (2013), pp. 107–122. ISSN: 0305-215X. DOI: 10.1080/0305215X.2012.661728.

[68] C. Tsallis and D. A. Stariolo. “Generalized simulated annealing”. In: *Physica A: Statistical Mechanics and its Applications* 233.1 (1996), pp. 395–406. ISSN: 0378-4371. DOI: 10.1016/S0378-4371(96)00271-3.

[69] H. W. Vuijk. “Shape and Topology Optimized TSHD Midsection”. Master’s thesis. TU Delft, 2020.

[70] Q. Xia, M. Y. Wang, and T. Shi. “A level set method for shape and topology optimization of both structure and support of continuum structures”. In: *Computer Methods in Applied Mechanics and Engineering* 272 (2014), pp. 340–353. ISSN: 0045-7825. DOI: 10.1016/j.cma.2014.01.014.

[71] Y. Xiang and X. G. Gong. “Efficiency of generalized simulated annealing”. In: *Physical Review E* 62.3 (2000), pp. 4473–4476.

[72] Y. Xiang, D. Y. Sun, and X. G. Gong. “Generalized Simulated Annealing Studies on Structures and Properties of Nin (n = 2−55) Clusters”. In: *The Journal of Physical Chemistry A* 104.12 (2000), pp. 2746–2751. DOI: 10.1021/jp992923q.

[73] Y. Xiang, S. Gubian, B. Suomela, and J. Hoeng. “Generalized Simulated Annealing for Global Optimization: The GenSA Package for R”. In: *The R Journal* 5.1 (2013).

[74] B. Yang and Q. Zhang. “Parallelizing a modified Particle Swarm Optimizer (PSO)”. In: *Advanced Materials Research* 163-167 (2011), pp. 2404–2409. ISSN: 1022-6680. DOI: 10.4028/www.scientific.net/AMR.163-167.2404.

[75] Q. Yang and G. Guan. “A local mesh reconstruction method for layout and scantling optimization of FPSO internal turret area structure”. In: *Ocean Engineering* 208 (2020), p. 107429. ISSN: 0029-8018. DOI: 10.1016/j.oceaneng.2020.107429.

[76] R. J. Yang, N. Wang, C. H. Tho, J. P. Bobineau, and B. P. Wang. “Metamodeling development for vehicle frontal impact simulation”. In: *Journal of Mechanical Design, Transactions of the ASME* 127.5 (2005), pp. 1014–1020. ISSN: 1050-0472. DOI: 10.1115/1.1906264.

[77] W. Yang, Z. Yue, L. Li, and P. Wang. “Aircraft wing structural design optimization based on automated finite element modelling and ground structure approach”. In: *Engineering Optimization* 48.1 (2016), pp. 94–114. DOI: 10.1080/0305215X.2014.995175.

[78] T. Zegard and G. H. Paulino. “GRAND — Ground structure based topology optimization for arbitrary 2D domains using MATLAB”. In: *Structural and Multidisciplinary Optimization* 50.5 (2014), pp. 861–882. ISSN: 1615-1488. DOI: 10.1007/s00158-014-1085-z.

[79] T. Zegard and G. H. Paulino. “GRAND3 — Ground structure based topology optimization for arbitrary 3D domains using MATLAB”. In: *Structural and Multidisciplinary Optimization* 52.6 (2015), pp. 1161–1184. ISSN: 1615-1488. DOI: 10.1007/s00158-015-1284-2.

[80] W. Zhang, D. Li, J. Yuan, J. Song, and X. Guo. “A new three-dimensional topology optimization method based on moving morphable components (MMCs)”. In: *Computational Mechanics* 59.4 (2017), pp. 647–665. ISSN: 0178-7675. DOI: 10.1007/s00466-016-1365-0.

[81] J. Zhu and J. Wu. “Research on Topology Optimization of Transverse Web Frame in Midship Cargo Hold Region of VLCC Based on Variable Density Method”. In: *International Ocean and Polar Engineering Conference* (2020).

A

3D model of the large ship section

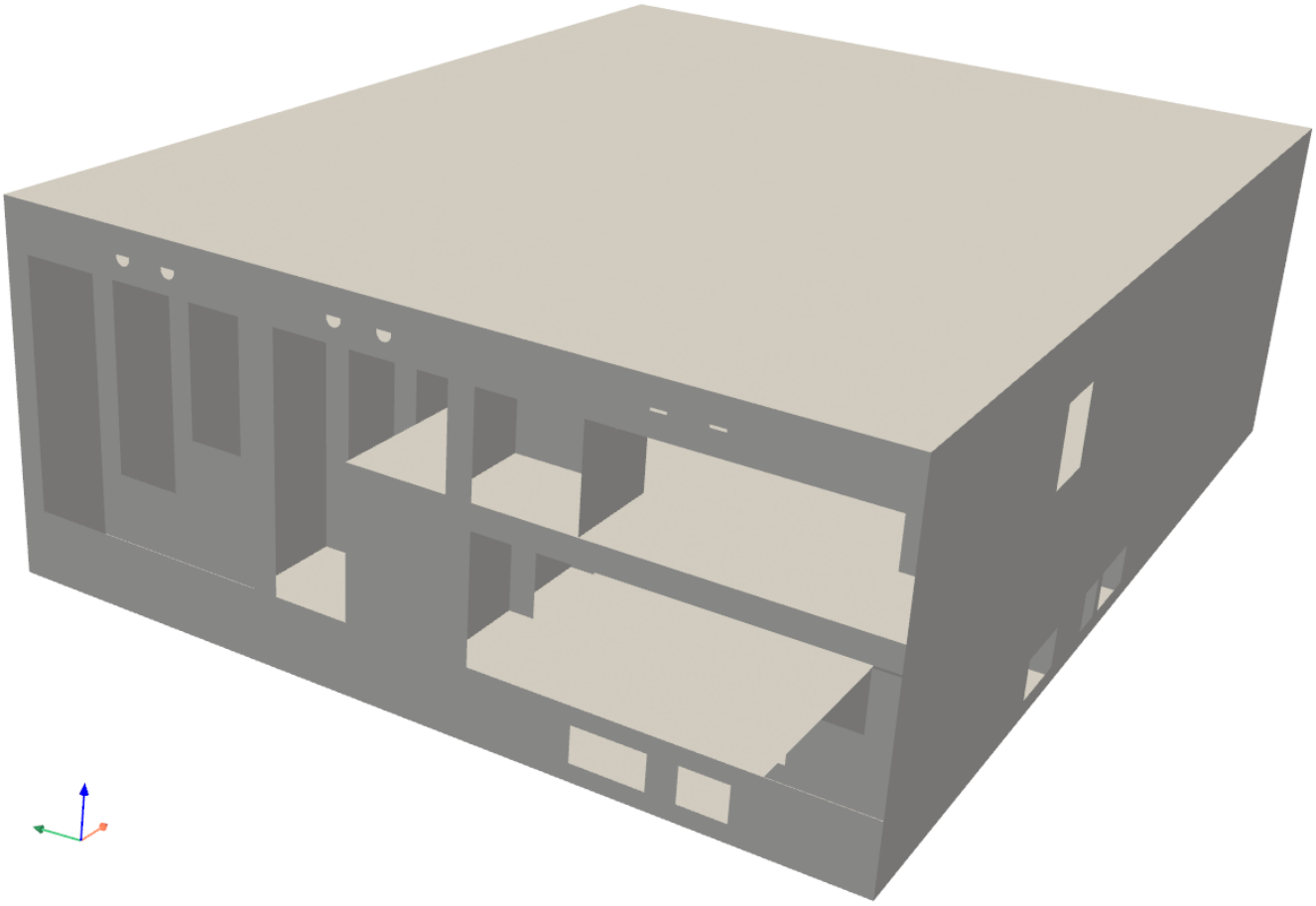

Figure A.1: 3D-view of the model of the large ship section, as used in the optimization of the full grillage.

B

Additional data for the optimization of the grillage on a rigid constraint

This appendix will give additional figures and numerical data for the optimization of the single grillage on the rigid constraint, as described in Section 5.1. Figure B.1 shows the combination of the mass and the stress constraint for the different optimization results. A general explanation about these figures is given in Section 5.1 for Figure 5.2.

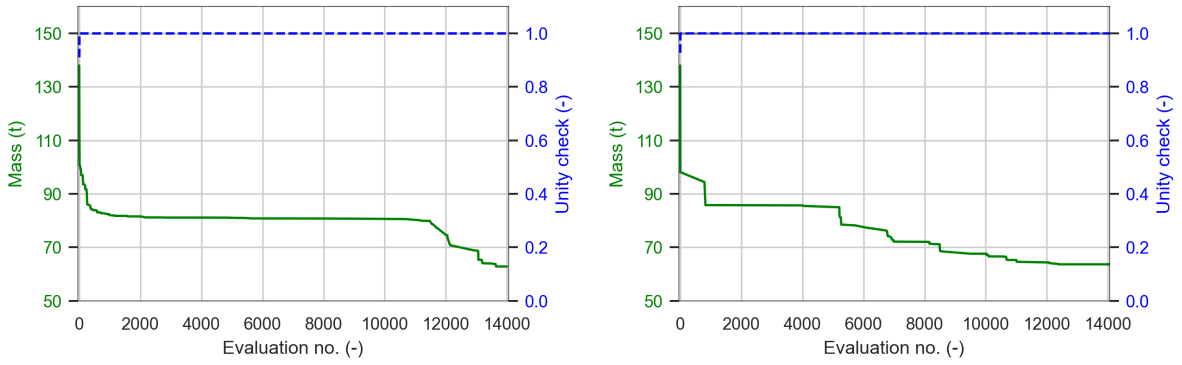

(a) Mass and stress constraint for the first run at an initial temperature of 10,000

(b) Mass and stress constraint for the first run at an initial temperature of 5,000

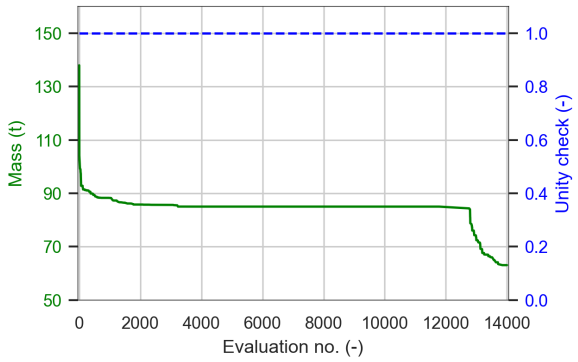

(c) Mass and stress constraint for the second run at an initial temperature of 10,000

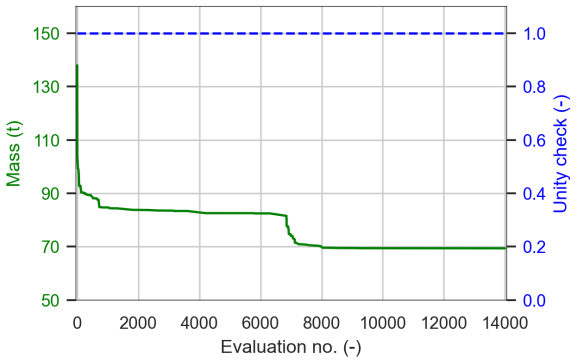

(d) Mass and stress constraint for the second run at an initial temperature of 5,000

Figure B.1: Combination of the mass and the stress constraint for the convergence plots shown in Figure 5.1b

Table B.1 shows the results for the different runs of the optimization of the single grillage on the rigid constraint. The results are grouped for each of the variable types. This data is used to construct the layouts as given in Figure 5.1a. The thicknesses were also shown in Table 5.1.

Table B.1: Numerical optimization results of the different runs in the optimi

		Run number						
		Initial	1	2	3	4	Average	Maximum difference
ψ (°)	1	0	-5.44	1.06	-20.91	2.82	-5.62	23.73
	2	0	11.36	-14.98	23.66	-12.62	1.86	38.64
	3	0	0.35	-2.07	-12.24	11.63	-0.58	23.87
	4	0	12.85	-21.66	-4.23	-14.19	-6.81	34.51
	5	0	3.95	14.07	18.57	18.05	13.66	14.62
	6	0	22.17	-4.29	-1.11	0.94	4.43	26.46
	7	0	4.53	6.34	15.26	-2.15	6.00	17.41
	8	0	19.55	15.55	8.56	15.53	14.80	10.99
	9	0	-11.10	13.89	7.58	14.84	6.30	25.94
	10	0	-1.62	-9.23	17.63	19.88	6.66	29.11
θ (°)	1	0	1.73	0.34	0.63	0.33	0.76	1.40
	2	36	35.94	33.64	27.89	36.75	33.56	8.86
	3	72	62.40	69.00	79.27	80.78	72.86	18.38
	4	108	97.26	104.52	108.35	115.34	106.37	18.08
	5	144	130.07	137.98	142.34	156.85	141.81	26.78
	6	180	179.49	180.34	175.52	179.36	178.68	4.82
	7	216	209.89	208.20	205.55	211.26	208.72	5.71
	8	252	251.32	256.51	258.17	258.62	256.15	7.30
	9	288	281.62	275.35	276.11	275.16	277.06	6.46
	10	324	326.92	331.77	322.36	337.38	329.61	15.02
t (mm)	1	45	8	8	7	15	10	8
	2	45	10	8	14	6	10	8
	3	45	16	19	18	20	18	4
	4	45	18	18	20	13	17	7
	5	45	10	12	16	10	12	6
	6	45	9	6	10	5	8	5
	7	45	11	20	11	15	14	9
	8	45	23	15	25	17	20	10
	9	45	22	23	18	20	21	5
	10	45	11	13	15	16	14	5
	Can	50	25	24	20	32	25	12
	Sides	50	12	12	12	13	12	1
	Flanges	50	26	31	34	34	31	8

The variable behaviour is shown in Figure B.2. This shows how the different variables behave during the optimization. More explanation about these figures is shown in Section 5.1.1 for Figure 5.3.

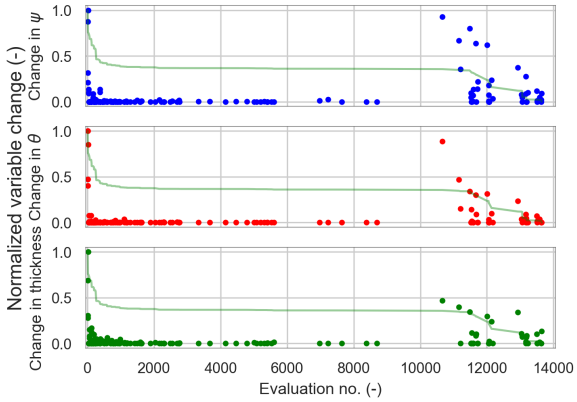

(a) Variable behaviour for the first run at an initial temperature of 10,000

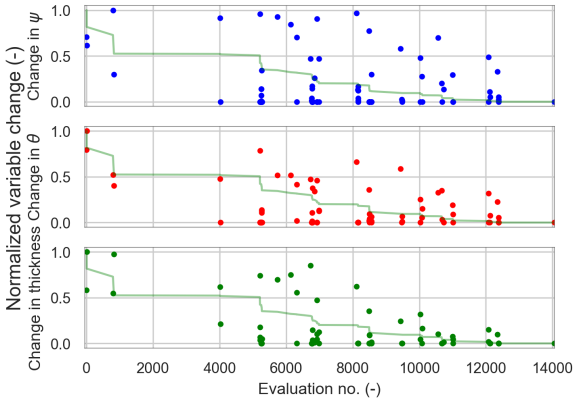

(b) Variable behaviour for the first run at an initial temperature of 5,000

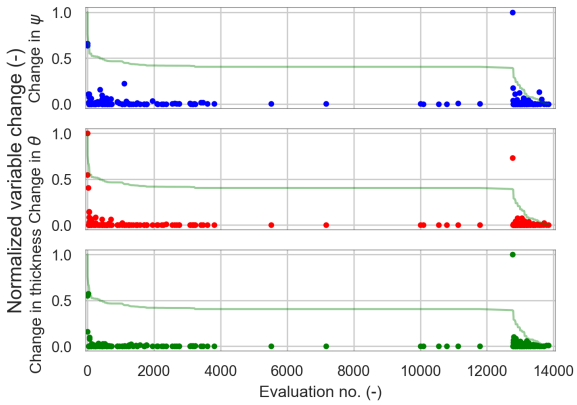

(c) Variable behaviour for the second run at an initial temperature of 10,000

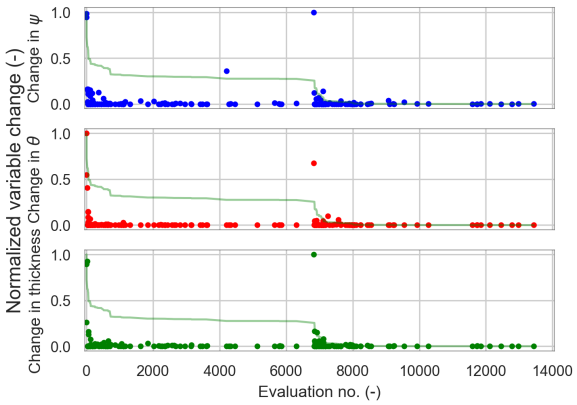

(d) Variable behaviour for the second run at an initial temperature of 5,000

Figure B.2: Variable behaviour corresponding to the convergence plots shown in Figure 5.1b.

C

Additional data for the single grillage with the ship as a foundation

This appendix gives some additional figures and numerical data for the optimizations of the single grillage with the ship as a foundation, as described in Section 5.2. Figure C.1 shows the behaviour of the different constraints during the optimization. Two figures were already shown in Figure 5.7 in Section 5.2. There, an explanation is given about these figures.

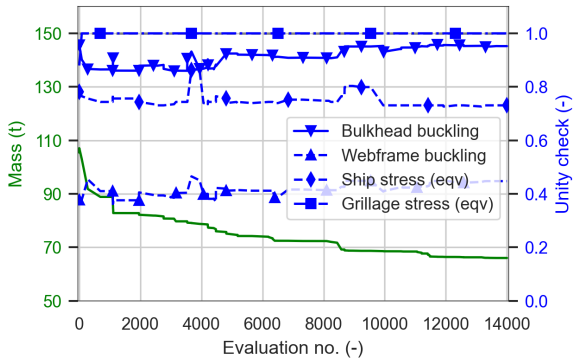

(a) Mass and unity checks for the first run at an initial temperature of 10,000

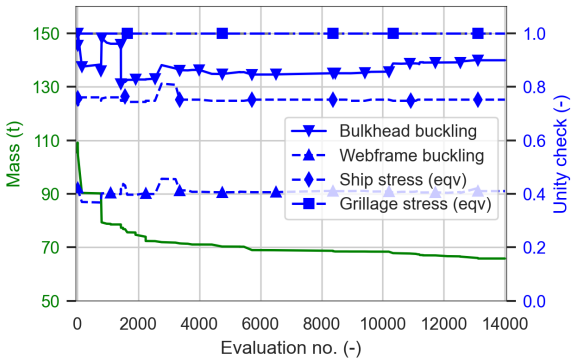

(b) Mass and unity checks for the first run at an initial temperature of 5,000

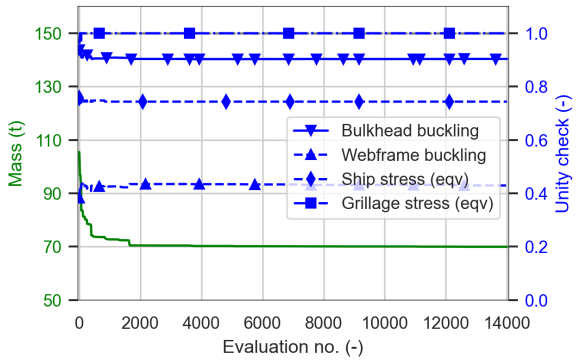

(c) Mass and unity checks for the second run at an initial temperature of 10,000

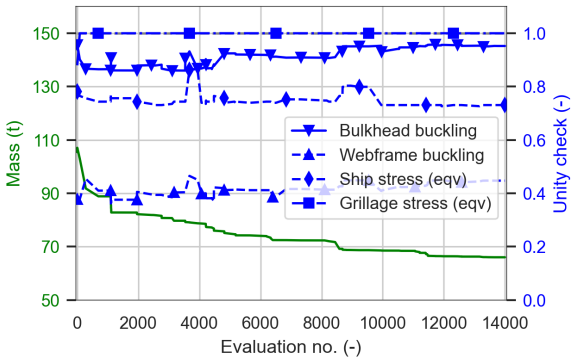

(d) Mass and unity checks for the second run at an initial temperature of 5,000

Figure C.1: Combination of the mass convergence line and the unity checks for the different constraints for the optimization of the single grillage with the ship as a boundary condition. The mass convergence lines correspond to the convergence plots shown in Figure 5.6b

Table C.1 shows the data of the results for the optimization of the single grillage with the ship as a foundation. These results are used to create Figure 5.6a. The thicknesses are also shown in Table 5.3. In Section 5.2, more information is given about the results.

Table C.1: Percentage of change of the different variable types compared to the total number of changes

		Run number						
		Initial	1	2	3	4	Average	Maximum difference
ψ (°)	1	0	0.50	0.07	-4.51	4.49	0.14	9.00
	2	0	-24.25	-19.32	9.22	-23.37	-14.43	33.47
	3	0	7.18	14.39	0.40	7.69	7.42	13.99
	4	0	-21.31	-23.22	-17.47	-0.77	-15.69	22.45
	5	0	22.71	18.24	23.48	2.91	16.84	20.57
	6	0	-1.53	-0.88	4.35	4.24	1.54	5.88
	7	0	13.81	11.94	18.73	1.00	11.37	17.73
	8	0	-5.54	-5.46	14.86	-14.00	-2.54	28.86
	9	0	-6.12	14.30	-9.28	-15.27	-4.09	29.57
	10	0	-24.84	24.98	-1.60	23.99	5.63	49.82
θ (°)	1	0	-0.19	-0.16	-5.71	2.51	-0.89	8.22
	2	36	42.93	35.95	23.76	43.07	36.43	19.31
	3	72	85.30	82.88	75.23	76.44	79.96	10.07
	4	108	105.18	94.08	102.38	105.07	101.68	11.10
	5	144	151.23	141.58	154.86	155.23	150.72	13.65
	6	180	180.77	180.55	174.40	186.04	180.44	11.64
	7	216	205.14	206.86	203.34	209.99	206.33	6.65
	8	252	262.92	262.88	257.67	265.27	262.18	7.60
	9	288	278.78	274.46	296.57	280.92	282.68	22.11
	10	324	316.43	319.86	330.37	320.33	321.75	13.94
t (mm)	1	45	8	5	6	11	8	6
	2	45	22	13	18	11	16	11
	3	45	17	16	14	17	16	3
	4	45	12	11	39	20	20	28
	5	45	15	9	12	6	10	9
	6	45	6	5	6	7	6	2
	7	45	12	12	15	16	14	4
	8	45	14	17	19	15	16	5
	9	45	8	12	13	11	11	5
	10	45	6	9	5	9	7	4
	Can	50	43	15	21	22	25	28
	Sides	50	11	15	12	9	12	6
	Flanges	50	33	48	38	44	41	15

The behaviour of the different variable types during the optimization is shown in Figure C.2. More explanation about these figures is shown in Section 5.2.1 for Figure 5.8.

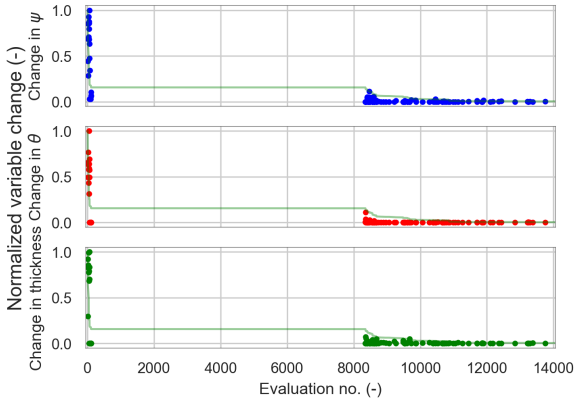

(a) Variable behaviour for the first run at an initial temperature of 10,000

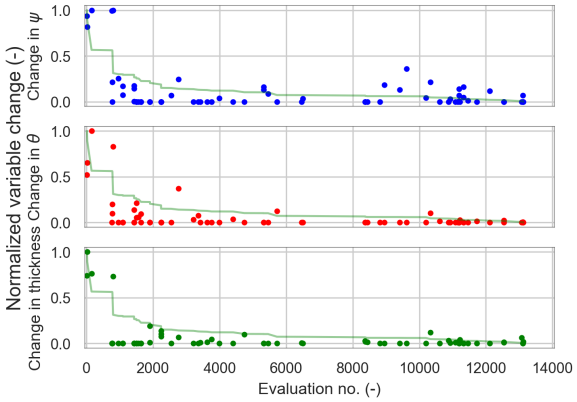

(b) Variable behaviour for the first run at an initial temperature of 5,000

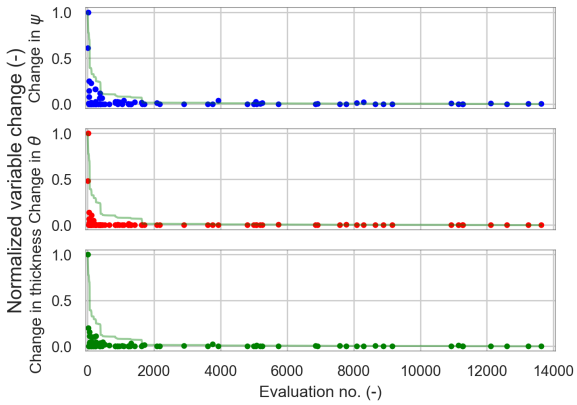

(c) Variable behaviour for the second run at an initial temperature of 10,000

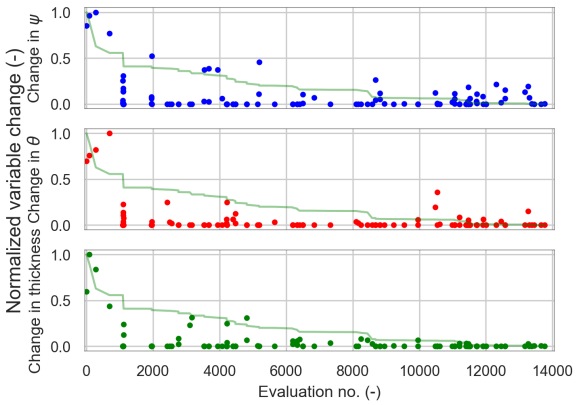

(d) Variable behaviour for the second run at an initial temperature of 5,000

Figure C.2: Variable behaviour corresponding to the convergence plots shown in Figure 5.6b

D

Additional data for the full grillage with the ship

This appendix gives additional data for the optimization of the full grillage with the ship as a foundation, which is explained in Chapter 6. Table D.1 gives the optimization results for the angles θ, which are used to construct Figure 6.5a. The numbering of the grillage is in accordance with the numbering in that figure. The numbering of the supports is counterclockwise, starting on the right of each figure, according to Figure 5.1a. The table is shown on the next page.

Table D.1: Angles θ of the different radial supports of the design of the full grillage in degree

		Grillage 1				Grillage 2			
Support number	*Initial*	Run 1	Run 2	Average	Difference	Run 1	Run 2	Average	Difference
1	*11.25*	3.39	6.93	5.16	3.54	21.85	3.96	12.90	17.89
2	*33.75*	48.54	18.78	33.66	29.76	20.27	25.66	22.96	5.39
3	*56.25*	70.93	71.09	71.01	0.16	67.99	60.85	64.42	7.14
4	*78.75*	82.89	82.61	82.75	0.28	71.38	91.24	81.31	19.86
5	*101.25*	103.90	93.11	98.50	10.79	89.13	97.37	93.25	8.24
6	*123.75*	112.82	127.63	120.22	14.81	111.59	118.44	115.02	6.85
7	*146.25*	160.20	159.51	159.85	0.69	160.87	137.38	149.12	23.49
8	*168.75*	174.99	173.83	174.41	1.16	169.90	165.76	167.83	4.14
9	*191.25*	178.97	177.82	178.40	1.15	196.49	196.56	196.52	0.07
10	*213.75*	198.80	211.14	204.97	12.34	201.76	200.49	201.12	1.27
11	*236.25*	248.41	241.56	244.98	6.85	246.28	240.13	243.20	6.15
12	*258.75*	270.87	262.63	266.75	8.24	268.34	257.88	263.11	10.46
13	*281.25*	288.62	268.76	278.69	19.86	291.85	278.17	285.01	13.68
14	*303.75*	292.01	299.15	295.58	7.14	315.52	297.09	306.30	18.43
15	*326.25*	338.02	330.13	334.08	7.89	341.24	340.29	340.76	0.95
16	*348.75*	361.91	350.94	356.42	10.97	363.13	359.16	361.14	3.97

		Grillage 3				Grillage 4			
Support number	*Initial*	Run 1	Run 2	Average	Difference	Run 1	Run 2	Average	Difference
1	*11.25*	15.89	5.42	10.66	10.47	-1.18	-3.29	-2.24	2.11
2	*33.75*	19.25	21.99	20.62	2.74	43.96	42.41	43.18	1.55
3	*56.25*	68.41	68.78	68.60	0.37	45.65	49.07	47.36	3.42
4	*78.75*	90.52	84.06	87.29	6.46	74.85	86.79	80.82	11.94
5	*101.25*	112.32	113.15	112.74	0.83	98.34	109.34	103.84	11.00
6	*123.75*	113.20	111.45	112.32	1.75	117.62	111.86	114.74	5.76
7	*146.25*	131.46	161.22	146.34	29.76	159.73	154.34	157.04	5.39
8	*168.75*	176.61	173.07	174.84	3.54	158.15	176.04	167.10	17.89
9	*191.25*	178.09	189.06	183.58	10.97	176.87	180.84	178.86	3.97
10	*213.75*	201.98	209.87	205.92	7.89	198.76	199.71	199.24	0.95
11	*236.25*	242.38	248.14	245.26	5.76	246.46	243.82	245.14	2.64
12	*258.75*	261.66	250.66	256.16	11.00	261.30	272.57	266.94	11.27
13	*281.25*	285.15	273.21	279.18	11.94	291.42	274.59	283.00	16.83
14	*303.75*	314.35	310.93	312.64	3.42	289.29	293.02	291.15	3.73
15	*326.25*	340.97	338.51	339.74	2.46	339.04	339.14	339.09	0.10
16	*348.75*	344.63	361.04	352.84	16.41	359.81	351.22	355.52	8.59

Table D.2 shows the optimization results of the angles ψ for the optimization of the full grillage.

Table D.2: Angles ψ of the different radial supports of the design of the full grillage in degree

		Grillage 1				**Grillage 2**			
Support number	*Initial*	Run 1	Run 2	Average	Difference	Run 1	Run 2	Average	Difference
1	*0*	-5.93	16.23	5.15	22.16	-16.02	-0.35	-8.18	15.67
2	*0*	13.43	-22.08	-4.32	35.51	-7.85	-10.28	-9.06	2.43
3	*0*	-16.89	24.00	3.56	40.89	4.58	12.80	8.69	8.22
4	*0*	-8.26	-6.06	-7.16	2.20	-14.57	5.11	-4.73	19.68
5	*0*	-19.35	17.16	-1.10	36.51	3.70	4.36	4.03	0.66
6	*0*	1.66	-4.84	-1.59	6.50	7.73	-15.02	-3.64	22.75
7	*0*	-15.73	19.05	1.66	34.78	10.41	-22.41	-6.00	32.82
8	*0*	7.95	2.09	5.02	5.86	-24.09	-7.21	-15.65	16.88
9	*0*	10.29	-13.48	-1.60	23.77	-7.04	13.61	3.28	20.65
10	*0*	-18.72	0.31	-9.20	19.03	-23.55	1.72	-10.92	25.27
11	*0*	-7.73	15.02	3.64	22.75	-0.22	18.05	8.92	18.27
12	*0*	-3.70	-4.36	-4.03	0.66	2.71	9.71	6.21	7.00
13	*0*	14.57	-5.11	4.73	19.68	6.43	-2.10	2.16	8.53
14	*0*	-4.58	-12.80	-8.69	8.22	-21.98	-8.09	-15.04	13.89
15	*0*	-5.33	-4.39	-4.86	0.94	13.92	24.24	19.08	10.32
16	*0*	-4.06	14.19	5.06	18.25	15.76	18.06	16.91	2.30

		Grillage 3				**Grillage 4**			
Support number	*Initial*	Run 1	Run 2	Average	Difference	Run 1	Run 2	Average	Difference
1	*0*	16.09	-5.29	5.40	21.38	0.59	-17.15	-8.28	17.74
2	*0*	-18.83	-13.12	-15.97	5.71	-9.40	-7.27	-8.34	2.13
3	*0*	-11.67	-16.46	-14.07	4.79	-22.16	-24.92	-23.54	2.76
4	*0*	0.36	-8.09	-3.86	8.45	-24.62	-18.38	-21.50	6.24
5	*0*	3.75	6.54	5.14	2.79	-4.57	12.64	4.04	17.21
6	*0*	-7.72	-6.03	-6.88	1.69	-11.77	-5.66	-8.72	6.11
7	*0*	-13.43	22.08	4.32	35.51	7.85	10.28	9.06	2.43
8	*0*	5.93	-16.23	-5.15	22.16	16.02	0.35	8.18	15.67
9	*0*	4.06	-14.19	-5.06	18.25	-15.76	-18.06	-16.91	2.30
10	*0*	5.33	4.39	4.86	0.94	-13.92	-24.24	-19.08	10.32
11	*0*	11.77	5.66	8.72	6.11	0.15	8.31	4.23	8.16
12	*0*	4.57	-12.64	-4.04	17.21	2.11	20.92	11.52	18.81
13	*0*	24.62	18.38	21.50	6.24	8.03	12.53	10.28	4.50
14	*0*	22.16	24.92	23.54	2.76	-7.70	3.17	-2.26	10.87
15	*0*	19.73	3.34	11.54	16.39	22.16	16.48	19.32	5.68
16	*0*	8.74	21.87	15.30	13.13	-5.76	1.86	-1.95	7.62

Table D.3 shows the thicknesses of the optimized designs of the full grillage. These optimized thicknesses were also shown in Table 6.1.

Table D.3: Thicknesses of the different radial supports of the design of the full grillage in degree

		Grillage 1				**Grillage 2**			
Support number	*Initial*	Run 1	Run 2	Average	Difference	Run 1	Run 2	Average	Difference
1	*45*	7	7	7	0	19	14	16.5	5
2	*45*	8	13	10.5	5	7	7	7	0
3	*45*	9	14	11.5	5	6	15	10.5	9
4	*45*	20	10	15	10	15	27	21	12
5	*45*	28	14	21	14	17	13	15	4
6	*45*	8	10	9	2	22	7	14.5	15
7	*45*	10	14	12	4	10	12	11	2
8	*45*	7	6	6.5	1	11	16	13.5	5
9	*45*	13	8	10.5	5	22	12	17	10
10	*45*	13	14	13.5	1	13	6	9.5	7
11	*45*	40	7	23.5	33	13	14	13.5	1
12	*45*	9	13	11	4	13	6	9.5	7
13	*45*	11	19	15	8	10	9	9.5	1
14	*45*	7	15	11	8	13	15	14	2
15	*45*	20	15	17.5	5	8	9	8.5	1
16	*45*	11	8	9.5	3	10	36	23	26

		Grillage 3				**Grillage 4**			
Support number	*Initial*	Run 1	Run 2	Average	Difference	Run 1	Run 2	Average	Difference
1	*45*	7	6	6.5	1	8	8	8	0
2	*45*	13	11	12	2	7	13	10	6
3	*45*	15	9	12	6	18	15	16.5	3
4	*45*	12	38	25	26	9	15	12	6
5	*45*	14	6	10	8	14	8	11	6
6	*45*	11	13	12	2	12	15	13.5	3
7	*45*	7	24	15.5	17	10	9	9.5	1
8	*45*	7	9	8	2	5	15	10	10
9	*45*	24	8	16	16	7	7	7	0
10	*45*	12	11	11.5	1	17	12	14.5	5
11	*45*	9	15	12	6	32	18	25	14
12	*45*	15	21	18	6	6	8	7	2
13	*45*	16	16	16	0	16	8	12	8
14	*45*	10	6	8	4	8	12	10	4
15	*45*	6	32	19	26	11	14	12.5	3
16	*45*	6	18	12	12	22	9	15.5	13

Table D.3 continued

	Initial	Run 1	Run 2	Average	Difference
Can	*50*	45	44	44.5	1
	50	38	14	26	24
	50	38	25	31.5	13
	50	35	18	26.5	17
	50	35	30	32.5	5
	50	20	27	23.5	7
Sides	*50*	52	52	52	0
	50	37	12	24.5	25
	50	30	7	18.5	23
	50	50	14	32	36
	50	24	20	22	4
	50	25	19	22	6
	50	9	10	9.5	1
Flanges	*50*	32	44	38	12

Table D.4 describes the values for the different radial supports in the new manual design of the grillage, as described in Section 6.3

Table D.4: Parameters of the different radial supports for the manual design of the full grillage

Support number	**Grillage 1**			**Grillage 2**			**Grillage 3**			**Grillage 4**		
	θ (°)	ψ (°)	t (mm)	θ (°)	ψ (°)	t (mm)	θ (°)	ψ (°)	t (mm)	θ (°)	ψ (°)	t (mm)
1	2.65	-4.99	18	21.06	-11.94	26	17.57	-0.96	20	-0.68	-2.59	30
2	48.54	13.43	8	69.68	-5.29	22	68.41	-11.67	15	44.80	-15.74	25
3	70.93	-16.89	9	89.13	3.70	17	90.52	0.36	12	74.85	-24.62	9
4	82.89	-8.26	20	111.59	7.73	22	112.76	-1.94	25	98.34	-4.57	14
5	103.90	-19.35	28	165.38	-7.42	21	131.46	-13.43	7	117.62	-11.77	12
6	112.82	1.66	8	199.13	-15.30	35	177.35	4.99	31	158.94	11.94	15
7	160.20	-15.73	10	246.28	-0.22	13	201.98	5.33	12	176.87	-15.76	7
8	176.98	9.12	20	268.34	2.71	13	242.38	11.77	9	198.76	-13.92	17
9	198.80	-18.72	13	291.85	6.43	10	261.66	4.57	15	246.46	0.15	32
10	248.41	-7.73	40	315.52	-21.98	13	285.15	24.62	16	261.30	2.11	6
11	270.87	-3.70	9	341.24	13.92	8	314.35	22.16	10	290.36	0.16	24
12	290.32	5.29	18	363.13	15.76	10	342.80	14.24	11	339.04	22.16	11
13	338.02	-5.33	20	-	-	-	-	-	-	-	-	-